

ASSESSMENT OF THE EFFECT OF NON-STRUCTURAL WALLS ON THE DYNAMIC
PROPERTIES AND ENGINEERING DEMAND PARAMETERS OF A CASE STUDY
BUILDING

by

Ayman RAMADAN

THESIS PRESENTED TO ÉCOLE DE TECHNOLOGIE SUPÉRIEURE
IN PARTIAL FULFILLMENT FOR A MASTER'S DEGREE
WITH THESIS IN CONSTRUCTION ENGINEERING
M.A.Sc.

MONTREAL, APRIL 27, 2022

ÉCOLE DE TECHNOLOGIE SUPÉRIEURE
UNIVERSITÉ DU QUÉBEC



Ayman RAMADAN, 2022



This Creative Commons licence allows readers to download this work and share it with others as long as the author is credited. The content of this work can't be modified in any way or used commercially.

BOARD OF EXAMINERS (THESIS M.Sc.A. OR THESIS PH.D.)

THIS THESIS HAS BEEN EVALUATED

BY THE FOLLOWING BOARD OF EXAMINERS

Prof. Rola Assi, Thesis Supervisor
Department of Construction Engineering, École de Technologie Supérieure

Prof. Ali Motamedi, President of the Board of Examiners
Department of Construction Engineering, École de Technologie Supérieure

Prof. Ahmad Abo El Ezz, Member of the jury
Department of Construction Engineering, École de Technologie Supérieure

THIS THESIS WAS PRESENTED AND DEFENDED

IN THE PRESENCE OF A BOARD OF EXAMINERS AND PUBLIC

APRIL 20, 2022

AT ÉCOLE DE TECHNOLOGIE SUPÉRIEURE

ACKNOWLEDGMENT

First, it is with great pleasure that I thank all the people who supported and encouraged me during this master's degree. I want to express my sincere gratitude to them.

I would like to thank my supervisor, Ms. Rola Assi, for her availability, her wise advice, her rigor, and her financial support. This allowed me to devote myself to my master's degree in research and to improve myself from every point of view.

Thanks to the École de technologie supérieure for allowing me to perform ambient vibration measurements in their premises.

Many thanks to Suze Youance, Azarm Farzam, Ghaleb Damaj, Mohammad El Chamaa, and Bilal Yassine for helping me during the ambient vibration measurements of the building.

On a more personal note, I would like to thank my parents for their support, encouragement and listening during my stay in Canada. They passed on to me the taste for a job well done and the strength needed to overcome hardships.

ÉVALUATION DE L'EFFET DES MURS NON STRUCTURAUX SUR LES PROPRIÉTÉS DYNAMIQUES ET LES PARAMÈTRES DE DEMANDE D'INGÉNIERIE DANS UN BÂTIMENT ÉTUDIÉ

Ayman RAMADAN

RÉSUMÉ

Lorsqu'un tremblement de terre se produit, la plupart des approches de conception internationales ignorent la contribution des composants non structuraux (CNSs) aux propriétés dynamiques du bâtiment. Ce mémoire évalue les effets des composants architecturaux, à savoir les murs rideaux et les murs de maçonnerie, sur les différents modes de déformation, les périodes fondamentales, l'amortissement et la rigidité latérale du bâtiment MDE situé sur le campus de l'école de technologie supérieure. De plus, les paramètres de demande d'ingénierie en termes de déplacement inter-étages et d'accélération absolue des planchers ont été évalués sous l'effet des séismes sélectionnés et calibrés, correspondant au spectre de risque sismique uniforme de Montréal avec une période de retour de 2500 ans.

Tout d'abord, des mesures de vibrations ambiantes (MVAs) ont été effectuées au niveau du cadre nu composé des éléments structuraux. Ensuite, une autre série de MVAs a été réalisée au cadre complet lorsque les murs non-structuraux (MNSs) ont été ajoutées à la structure. Les paramètres modaux (fréquences naturelles, modes de déformation et l'amortissement) ont été obtenus en utilisant la méthode « *Stochastic Subspace Identification (SSI)* » implémentée dans le logiciel ARTeMIS®. Les paramètres modaux de la MDE ont été obtenus pour le premier mode seulement du cadre nu à cause d'un nombre insuffisant d'enregistrements, et pour les trois premiers modes du cadre complet. De plus, les amplifications de l'accélération du plancher (AAP) ont été calculées au toit pour le cadre nu, et à tous les planchers pour le cadre complet.

Deux modèles d'éléments finis linéaires du bâtiment aux deux stades de construction ont été développés dans le logiciel ETABS® (CSI, 2017) et calibrés selon les résultats des MVAs.

Dans cette analyse, seulement la masse des autres CNSs et le contenu du bâtiment ont été pris en considération.

Il a été constaté que la période fondamentale du bâtiment a subi une diminution de -12,4% lorsque les MNSs étaient ajoutés. Les modes de déformation sont demeurés les mêmes aux deux stades de la construction en raison de la présence de murs en maçonnerie uniquement au rez-de-chaussée. L'amortissement a subi une augmentation allant de +1.98% (cadre nu) à +3.03% (cadre complet). De plus, il a été observé que les MNSs ont contribué à la réduction des déplacements inter-étages à tous les étages dans les deux directions (de -20,5% à -41,6% dans la direction longitudinale, et de -25,8% à -67,6% dans la direction transversale). En addition, il a été démontré que les AAP du cadre complet sont supérieures à celles du cadre nu dans tous les étages dans la direction transversale. Dans la direction longitudinale, les AAP du cadre complet sont supérieures à celles du cadre nu dans les étages intermédiaires (2^{ème}, et 3^{ème}), et inférieures à celles du cadre nu dans la mezzanine, et les étages supérieurs (4^{ème}, 5^{ème}, et toiture). En effet, il a été démontré que les AAP ne sont pas linéaires, et qu'elles sont sous-estimées par le CNB2015 ce qui pourrait entraîner une sous-estimation de la force sismique latérale des CNSs en sous-estimant l'amplification de l'accélération du plancher.

Enfin, pour évaluer l'effet de chacun des MNSs séparément sur la rigidité du bâtiment, deux modèles d'éléments finis ont été pris : un modèle du cadre complet et un autre modèle sans le MNS (murs de maçonnerie ou murs rideaux), puis l'effet de ce MNS a été quantifié. Il a été observé que les murs de maçonnerie et les murs rideaux apportaient respectivement une rigidité supplémentaire de +20% et +5% dans la direction transversale. Tandis que dans la direction longitudinale, les murs de maçonnerie apportaient une rigidité supplémentaire de +16%, et les murs rideaux diminuaient la rigidité de -4% à cause de leurs déconnexions des dalles dans les étages supérieurs.

Mots clés : composants non structurels, mesures des vibrations ambiantes, modèles à éléments finis, analyse modale, calibration, amplifications de l'accélération du plancher, déplacements inter-étage.

ASSESSMENT OF THE EFFECT OF NON-STRUCTURAL WALLS ON THE DYNAMIC PROPERTIES AND ENGINEERING DEMAND PARAMETERS OF A CASE STUDY BUILDING

Ayman RAMADAN

ABSTRACT

When an earthquake occurs, most international design approaches ignore the contribution of non-structural components (NSCs) to the building dynamic properties. This thesis evaluates the effects of the architectural components, namely curtain walls, and masonry walls, on the mode shapes, fundamental periods, damping ratios, and lateral stiffness of a case study building as well as the engineering demand parameters in terms of inter-story drifts and peak floor accelerations under the effect of selected and scaled earthquake records matching Montreal's uniform hazard spectrum with a return period of 2500 years.

First, ambient vibration measurements (AVMs) were conducted on the bare frame composed of the structural components. Then, another series of AVMs were conducted on the full frame when the NSWs were added to the structure. Modal parameters (natural frequencies, mode shapes and damping ratios) were extracted using the *Stochastic Subspace Identification (SSI)* implemented in the software ARTEMIS®. The modal parameters of the MDE were obtained for the first mode only at the bare frame stage due to lack of sufficient records, and for the first three modes of the full frame stage. Moreover, the floor acceleration amplifications (FAA) were computed for the roof at bare frame stage, and all floors at full frame stage.

Two linear-finite element models of the building at both construction stages were developed in the software ETABS® (CSI, 2017) and calibrated according to the AVMs results. Only the mass of the other NSCs and building content was considered in the analysis.

It was found that the building fundamental period decreased by -12.4% when the NSWs were added. The mode shapes remained the same at both stages of construction due to the presence of masonry walls only on the ground floor. Damping has been increased from +1.98% (bare frame) to +3.03% (full frame). Moreover, it was observed that NSWs contributed to the reduction of inter-story drifts at all floors in both directions (from -20.5% to -41.6% in the longitudinal direction, and from -25.8% to -67.6% in the transversal direction). In addition, the FAA of the full frame have been shown to be superior to those of the bare frame in all stages in the transversal direction. In the longitudinal direction, the FAA of the full frame are higher than those of the bare frame in the intermediate floors (2nd, and 3rd), and lower than those of the bare frame in the mezzanine, and the upper floors (4th, 5th, and roof). Indeed, it has been demonstrated that the FAA are not linear, and that they are underestimated by the NBC 2015 which may leads to an underestimation of the lateral seismic force of the NSCs by underestimating the amplification of the floor acceleration.

Finally, to evaluate the effect of the NSWs separately on the stiffness of the building, two finite element models were taken: the full frame model, and another model without the NSC (masonry walls or curtain walls), then the effect of this NSW was quantified. It was also observed that masonry walls and curtain walls provided an additional stiffness of +20% and +5% respectively in the transversal direction. While in the longitudinal direction, the masonry walls brought an additional stiffness of +16%, and the curtain walls decreased the stiffness of -4% due to their disconnections from the slabs in the upper floors.

Keywords: non-structural components, ambient vibration measurements, finite element models, modal analysis, calibration, floor acceleration amplification, inter-story drifts.

TABLE OF CONTENTS

	Page
INTRODUCTION	1
CHAPTER 1 LITERATURE REVIEW	6
1.1 Introduction.....	6
1.2 Effect of masonry walls and curtain walls on dynamic response of buildings.....	6
1.2.1 Effect on lateral stiffness	7
1.2.2 Effect on Natural Frequencies, and Mode Shapes	8
1.2.3 Effect on damping ratio	8
1.3 Engineering demand parameters (EDP) for NSCs.....	11
1.3.1 Lateral seismic demand in NBC 2015	11
1.3.2 Floor acceleration amplification in previous studies	12
1.4 Modelling of NSWs	14
1.4.1 Masonry infill walls	14
1.4.1.1 Equivalent diagonal compression struts.....	14
1.4.1.2 Continuous model	18
1.4.1.3 Choice of the simplified model of infill walls	20
1.4.2 Curtain walls	21
1.5 Conclusion	23
CHAPTER 2 DESCRIPTION OF THE MDE, AVMs, AND CALIBRATION OF THE FINITE ELEMENT MODELS	24
2.1 Description of the case study building MDE.....	24
2.2 Description of NSWs selected in this study.....	26
2.3 Description of ambient vibration measurements (AVMs) of the MDE.....	29
2.3.1 Principles of AVMs	29
2.3.2 Experimental apparatus and data acquisition.....	33
2.3.3 Extraction and pretreatment of data	36
2.3.4 Experimental results and their validation	37
2.3.5 Comparison of periods and damping ratios between AVMs at different stages of construction.....	38
2.3.6 Comparison of fundamental periods using NBC equations and AVMs ...	39
2.4 Finite element Modelling and calibration of the MDE models	42
2.4.1 Modelling assumption of SCs.....	42
2.4.2 Modelling assumption of NSWs.....	45
2.4.2.1 Modelling of masonry infill walls and connections with the surrounding reinforced concrete structure	45
2.4.2.2 Modelling of curtain walls and connections	46
2.5 Calibration of FEM.....	48
2.5.1 Generalities concerning the calibration process	48
2.5.2 Manual calibration	50
2.5.3 Automated calibration.....	50

2.5.4	Modifying the modulus of elasticity	51
2.5.5	Calibration of the bare frame	52
2.5.6	Calibration of the full-frame model	53
2.5.7	Comparison of mode shapes of calibrated FE models.....	55
2.6	Conclusion	55
CHAPTER 3 EVALUATION OF THE STIFFNESS AND MASS CONTRIBUTION OF NSWs.....57		
3.1	Stiffness and mass contribution of NSWs	57
3.2	Parametric study of the effect of masonry infill walls on the fundamental period, and mass and stiffness contribution.....	61
3.3	Conclusion	65
CHAPTER 4 PEAK FLOOR ACCELERATIONS AND INTER-STORY DRIFTS OF THE MDE WHEN SUBJECTED TO EARTHQUAKES COMPATIBLE WITH THE UHS FOR MONTREAL.....67		
4.1	Selection and scaling of earthquakes	67
4.1.1	Period range	68
4.1.2	Selection of earthquake records	69
4.1.3	Calculation of the scaling factors.....	70
4.2	Seismic response of the MDE.....	72
4.2.1	Inter-story drift computed with finite element models	72
4.3	Floor acceleration amplification (FAA).....	75
4.3.1	At full frame stage using AVMs and FEM in the transversal direction ...	75
4.3.2	Comparison of the FAA at full frame stage using AVMs and FEM in the longitudinal direction.....	77
4.3.3	Comparison of FAA of bare frame and full frame using FEM.....	78
4.4	Conclusion	80
CONCLUSION.....		81
RECOMMENDATIONS.....		84
ANNEX I DEFINITION OF MATERIALS, STRUCTURAL COMPONENTS, AND NON-STRUCTURAL WALLS.....		86
ANNEX II AMBIENT VIBRATION MEASUREMENTS		92
ANNEX III FINITE ELEMENT MODELLING		97
ANNEX IV CALIBRATION OF FINITE ELEMENT MODELS OF THE MDE.....		101
ANNEX V FLOOR ACCELERATION AMPLIFICATION.....		104
ANNEX VI SELECTION AND SCALING OF GROUND MOTION TIME HISTORIES		112
REFERENCES		114

LIST OF TABLES

	Page
Table 1.1	Effect of masonry walls on fundamental period and lateral stiffness.....10
Table 1.2	Effect of curtain walls on fundamental period and lateral stiffness.....10
Table 2.1	Total surface of NSWs and floors.....27
Table 2.2	Composition of the glass panels28
Table 2.3	Date and details of AVMs in the MDE.....35
Table 2.4	Modal parameters of the MDE at the bare frame stage37
Table 2.5	Modal parameters of the MDE at the full frame stage.....38
Table 2.6	Comparison of the periods obtained by AVMs at different stages of construction.....38
Table 2.7	Properties of the masonry infill walls gap element.....46
Table 2.8	Uncertainties on the parameters of a numerical model.....49
Table 2.9	Comparison of the period obtained by AVMs at bare frame stage with that of calibrated and non-calibrated models52
Table 2.10	Calibration of the bare frame model52
Table 2.11	Comparison of the period obtained by AVMs at full-frame stage with that of calibrated and non-calibrated models53
Table 2.12	Calibration of the full frame model53
Table 2.13	Correlation between the mode shapes obtained by AVMs at full-frame stage and that of calibrated and non-calibrated models54
Table 3.1	Stiffness and mass contribution of masonry infill walls in the transversal direction58
Table 3.2	Stiffness and mass contribution of masonry infill walls in the longitudinal direction58
Table 3.3	Stiffness and mass contribution of curtain walls in the transversal direction60

Table 3.4	Stiffness and mass contribution of curtain walls in the longitudinal direction	60
Table 3.5	The surface of masonry walls in each floor for each case	62
Table 3.6	Results of the parametric study of masonry walls in the ground and second floors	64
Table 3.7	Results of the parametric study of masonry walls in the ground, second, and third floors.....	64
Table 3.8	Results of the parametric study of masonry walls in all floors.....	65
Table 4.1	Modal periods and ranges for ground motion scaling for the MDE	68
Table 4.2	Selected earthquakes	70
Table 4.3	Comparison of the inter-story drifts in longitudinal direction in both stages of construction.....	73
Table 4.4	Comparison of the inter-story drifts in transversal direction in both stages of construction.....	74

LIST OF FIGURES

	Page
Figure 1.1	Equivalent diagonal compression struts.....15
Figure 1.2	Continuous model19
Figure 2.1	Photos for the MDE24
Figure 2.2	Elevation view of the MDE25
Figure 2.3	Plan view of the ground floor of the MDE26
Figure 2.4	Masonry walls location on the ground floor27
Figure 2.5	Masonry gap element.....28
Figure 2.6	Details of the MDE curtain walls.....29
Figure 2.7	Stabilization diagram of estimated state space models.....33
Figure 2.8	Trominos sensors a) with radio antennas b) with radio amplifiers.....34
Figure 2.9	Configuration of the sensors on the 5th floor36
Figure 2.10	MAC matrix between SSI and EFDD methods37
Figure 2.11	Fundamental periods of the MDE obtained by the NBC equation, AVMs (bare frame and full frame), and the equation of Gilles and McClure (2012).....40
Figure 2.12	Spectral acceleration of the MDE according to different periods (the NBC equation, AVMs at both stages of construction, and the equation of Gilles and McClure 2012).....41
Figure 2.13	3-D FEM of the bare frame of MDE43
Figure 2.14	FEM of the full frame of MDE44
Figure 2.15	Gap element of the masonry wall45
Figure 2.16	Connection between the aluminium frame and the glass panel47
Figure 2.17	Elasto-plastic Wen link48
Figure 2.18	Normalized mode shapes for the MDE (modes 1 and 2).....55

Figure 3.1	Masonry walls in the ground and 2 nd floors	62
Figure 3.2	Masonry walls in the ground, 2nd, and 3rd floors	63
Figure 3.3	Masonry walls in all floors	63
Figure 4.1	Mean acceleration spectra for scenarios 1 et 2	71
Figure 4.2	Difference between the mean $S_g(T)$ of the scaled records and $ST(T)$	72
Figure 4.3	Inter-story drifts in the longitudinal direction at both stages of construction.....	73
Figure 4.4	Inter-story drifts in the transversal direction in both stages of construction.....	74
Figure 4.5	FAA of the full frame based on AVMs, the numerical model and NBC 2015 provisions in the transversal direction	76
Figure 4.6	FAA of the full frame based on AVMs, the numerical model and NBC 2015 provisions in the longitudinal direction	77
Figure 4.7	Comparison of the FAA of bare frame and full frame in the longitudinal direction.....	78
Figure 4.8	Comparison of the FAA of bare frame and full frame in the transversal direction.....	79

LIST OF ABBREVIATIONS

AAP	Amplification de l'accélération du plancher
ACNOR	Association canadienne de normalisation
ASTM	American Society for Testing and Materials
AVMs	Ambient vibration measurements
BF	Bare frame
CNB	Code national du bâtiment
CNSs	Composants non structuraux
CSA	Canadian Standards Association
DOF	Degree of freedom
EDP	Engineering demand parameters
EFDD	Enhance frequency domain decomposition
ÉTS	École de technologie supérieure
FAA	Floor acceleration amplification
FDD	Frequency domain decomposition
FEM	Finite element modelling
FEMA	Federal Emergency Management Agency
FF	Full frame
FVMs	Forced vibration measurements
IO	Immediate occupancy
LFRS	Lateral force resisting system
LS	Life safety
MAC	Modal assurance criterion

MDE	Maison des étudiants
MNSs	Murs non-structuraux
MVAs	Mesures de vibrations ambiantes
NBC	National building code
NSCs	Non-structural components
NSWs	Non-structural walls
OFCs	Operational and functional components
OMA	Operational modal analysis
PFA	Peak floor acceleration
PGA	Peak ground acceleration
RC	Reinforced concrete
SDOF	Single degree of freedom
SCs	Structural components
SSI	Stochastic subspace identification

LIST OF SYMBOLS

Greek alphabet

θ	Angle between the equivalent diagonal compression strut and the horizontal
ζ	Damping ratio
λ_l	Coefficient used to determine the equivalent width of the equivalent diagonal compression strut
λ_h	Relative stiffness of infill wall to the column
Φ	Mode shape vector
ω	Angular frequency

Lowercase Latin alphabet

a	Effective width of the equivalent diagonal compression strut
f	Frequency of vibration
h_n	Building height
h'	Masonry infill wall height
h_{col}	Height of column
h_x	Height above the base to level x of NSCs or floor
m	Mass of the building
r	Mode shape correlation coefficient
r_{inf}	Diagonal length of the masonry infill wall
t, t_w	Thickness of the masonry infill wall
t_i, t_{inf}	Thickness of infill wall
\bar{x}	Mean value of the x -variables

x_i	Displacement of the joint representing the tromino in the numerical model
\bar{y}	Mean value of the y-variables
y_i	Displacement of the tromino in ARTeMIS

Uppercase Latin alphabet

A_r	Element of force amplification factor as per NBC 2015
A_x	Height factor
C_p	The component factor
E	Elastic modulus of the surrounding structural element
E_b	Elastic modulus of the beam
E_c, E_i, E_w	Elastic modulus of masonry infill wall
E_{col}	Elastic modulus of the column
E_{fe}	Expected modulus of elasticity of the material of the structure
E_{me}	Expected modulus of elasticity of the filling material
F_a	The acceleration-based site coefficient
H_{in}, H_{inf}	Net height of infill panel
I	Moment of inertia of the surrounding structural element
I_b	Moment of inertia of the beam
I_{col}	Moment of inertia of the column
I_E	Importance factor for the building as per NBC 2015
K	Stiffness of the building
K_i	Stiffness of the masonry infill wall
K_g	Stiffness of the gap element
L	Structure span length

L_{inf}	Masonry infill wall Length
M	Moment magnitude of an earthquake event
R	Fault distance
R_d	Ductility-related force modification factor
R_o	Overstrength-related force modification factor
R_p	Component response modification factor
$S_a(0.2)$	The spectral response acceleration value at a period of 0.2 s
$S(T)$	The spectral acceleration value for a period of T
S_p	Horizontal force factor for part or portion of the building
$S_T(T)$	Target response spectrum
T_a	Building period defined by code expression
T_{Bldg1}	The fundamental period of the building
T_{max}	The upper limit of the period range T_R
T_{min}	The lower limit of the period range T_R
T_R	Period range of interest for selection and scaling ground motion
$T_{90\%}$	The period of the highest mode of vibration required to achieve 90% mass participation
V	Lateral earthquake design force at the base of the structure
V_p	Lateral force on a part of the structure
W	Seismic weight of the building

W_{eff}	Effective width of the equivalent diagonal compression strut
W_p	Weight of the non-structural component

INTRODUCTION

Problem definition

A building is composed of structural components (SCs), and non-structural components (NSCs). NSCs are not intended to take over the main loads of the building. Like SCs, NSCs are subject to significant seismic forces, and displacements and must be designed to withstand these forces.

According to the Canadian Standards Association (CSA-S832-14, 2014), NSCs are named by a different designation: Operational and Functional Components (OFCs), and divided into three categories:

a) Architectural components (functional):

- External: cladding, glazing, roofing, balconies...
- Internal: partitions, ceilings...

b) The technical (operational) components:

- Mechanics: elevators, ventilation apparatus, boilers, tanks...
- Plumbing: pipes, sprinklers, fire extinguishing systems, faucets...
- Electricity: electrical control panels, lighting, generator, telecommunication, telephone system, cables...

c) Components related to the contents of the building (operational):

- General: removable partitions, office equipment, storage lockers...
- Specialized: antiques, works of art, hazardous materials, medical supplies...

When an earthquake occurs, all components of a building, whether structural components (SCs) or non-structural components (NSCs), are subjected to significant forces, and displacements propagating in all directions. However, structural engineers model only the primary structure (columns, beams, slabs, shear walls and rigid cores) which takes up the loads while neglecting all the NSCs (masonry infill walls, prefabricated panels, facades, windows, equipment, and furniture), and choose to account for NSCs by adding mass at floors in the model. In such an examination, the NSCs participate only to the increase in the mass of the building and their contribution to lateral stiffness is totally ignored. Neglecting the NSCs in the modelling of a building may lead to an overestimation of the natural period of the building (Li et al., 2011; Sofi et al., 2017; Su et al., 2005).

On the other hand, the seismic design of NSCs is done using an empirical equation specified in the National Building Code of Canada (NRC, 2015) and the Canadian Standards Association (CSA-S832-14, 2014). This equation is primarily intended for use in regular buildings, where floor acceleration amplification (FAA) is calculated as the ratio of peak floor acceleration (PFA) to peak ground acceleration (PGA) and is assumed to vary linearly along the building height, with a maximum value of three at the rooftop. Several factors, however, such as the influence of higher modes of the building, the effect of torsion, and the dynamic interaction between the structural system and NSCs, are ignored (Aldeka et al., 2014; Asgarian et McClure, 2014; Asgarian et McClure, 2017; Qu et al., 2014; Singh et al., 2006).

Recent research has demonstrated that the presence of NSWs such as masonry infill walls, curtain walls, and façades has an effect on building dynamic properties (Asgarian, 2012; Li et al., 2011; Orumiyehi et al., 2017; Su et al., 2005). According to Asgarian (2012), the presence of infill walls reduces the building period, increases the floor accelerations experienced by NSWs, and decreases the drift demand. Orumiyehi et al. (2017) studied the influence of masonry infill walls on the seismic response of five regular and one irregular reinforced concrete (RC) buildings and found out that adding infill walls increased PFAs due to the increase in stiffness.

Hence, the behavior of these NSWs under dynamic loads must be considered to assess their effect on the mode shapes, fundamental periods, damping ratios, lateral stiffness of the supporting structure as well as the engineering demand parameters in terms of inter-story drifts and absolute floor accelerations.

Research objectives

The main objective of this research is to gain a better understanding of the effect of curtain walls, and masonry walls on the elastic response of buildings during earthquakes. This objective will be achieved through a case study building located on the campus of École de technologie supérieure (ÉTS) in Montreal. The specific research objectives are:

- Assess the effects of NSWs, namely masonry walls, and curtain walls, on mode shapes, fundamental periods, damping ratios, and lateral stiffness of the building.
- Evaluate the engineering demand parameters (absolute floor accelerations, and inter-story drifts) with and without NSWs in elastic domain.

Methodology

The methodology adopted for this research is to gain an understanding of the literature relevant to the contribution of NSWs to the dynamic response of structures (mode shapes, fundamental periods, damping ratios, and lateral stiffness). Then develop numerical models for the building studied in both phases of construction (bare, and full frame) calibrated with conducted AVMs. Having the calibrated models, the study can be further advanced towards the second specific objective. Therefore, this research can be divided into two main phases:

1. Experimental Study: in which AVMs have been conducted in multi-floor level of the MDE at the full frame stage of construction and in roof at the bare frame stage. Then, the dominant dynamic properties of both buildings including the lowest natural

frequencies, corresponding mode shapes, and damping ratios were extracted using operational modal analysis techniques.

2. Numerical Study: in which two 3D linear elastic finite element models of the studied building in both stages of construction (bare frame and full frame) were developed and calibrated with AVMs.

Finally, the effect of NSWs on the dynamic characteristics of the building (mode shapes, fundamental periods, damping ratios, and lateral stiffness) is studied by comparing the different models (bare frame and full-frame model). In addition, the engineering demand parameters (absolute floor accelerations, and inter-story drifts) are evaluated with and without NSWs in the elastic domain under the effect of selected and scaled earthquake records matching Montreal's seismic uniform hazard spectrum with a return period of 2475 years and compared to results obtained from AVMs.

Organization of the Thesis

Chapter 1 presents a literature review describing the importance of NSWs and covers studies about the importance of their effect on the dynamic behavior of buildings, and engineering demand parameters. Chapter 2 presents a description of the MDE, AVMs, the modelling assumptions of the MDE at two construction stages (bare frame stage and full frame), and the calibration of numerical models. Chapter 3 presents the mass and stiffness contribution of NSWs (masonry infill walls, and curtain walls) on the dynamic properties (fundamental period, mass, and stiffness contribution) of the MDE. In addition, it presents a parametric study to assess the effect of masonry infill walls on the dynamic properties of the MDE. Chapter 4 estimates the effect of NSWs of the MDE on engineering demand parameters (absolute floor accelerations and inter-story drifts) under the effect of selected and scaled earthquake records matching Montreal's uniform hazard spectrum with a return period of 2475 years and based on AVMs. Finally, conclusions and recommendations for future work are suggested.

CHAPTER 1

LITERATURE REVIEW

A detailed literature review of previous research carried out by incorporating the NSWs into buildings numerical models, using ambient vibration measurements (AVMs) and laboratory tests are presented. In addition, the engineering demand parameters, and the simplified numerical models used to simulate the behavior of NSWs are shown in this chapter.

1.1 Introduction

NSWs are often connected to the principal structural system via connections designed to prevent the transmission of vertical loads, such as superimposed live loads on floors, or lateral loads, such as wind or seismic excitation on entire buildings. As a result, it is thought that NSWs are separate from the bare frame and have no effect on the building lateral stiffness and its dynamic properties and response. However, many researchers (Asgarian et McClure, 2014; Bonne, 2018; Devin et Fanning, 2012a; Li et al., 2011; Su et al., 2005) have pointed the contribution of NSWs to the lateral stiffness and dynamic properties of buildings.

1.2 Effect of masonry walls and curtain walls on dynamic response of buildings

In the following, previous studies on the effect of masonry walls, and curtain walls on the lateral stiffness, natural frequencies, mode shapes, and damping ratios of buildings will be presented.

1.2.1 Effect on lateral stiffness

Su et al. (2005) were interested in the effect of infill walls on the lateral stiffness of buildings and their data reveal that the linear analysis of the numerical model with these NSWs contribute to the lateral stiffness of the building, they observe an increase of the order of +61% in the longitudinal direction and +82% in the transversal direction. This difference results from a larger quantity of NSWs in the Y direction. In addition, Amanat et Hoque (2006) analyzed the fundamental period by modal analysis of a 35 m reinforced concrete moment resisting building. The building was modelled using finite elements. The masonry infill walls were modelled as equivalent diagonal compression struts. The results obtained show that in the absence of NSWs in the model, an overestimation of the period in the range of +40% to +160% was obtained depending on the quantity of masonry infill walls present in the building. This study shows that the presence and the number of infill walls contribute to increasing the stiffness of the building. Subsequently, Li et al. (2011) came to the same conclusion by comparing curves representing the force as a function of the displacement of a floor between a bare frame model and a model with structure and masonry infill walls. In linear analysis with the same loading conditions, they notice an increase of about +60% in structural stiffness including the masonry infill walls. Bonne (2018) has studied the effect of masonry infill walls on the stiffness, and he has found that these masonry infill walls contribute to the stiffness of the building by +20.8%. This contribution is lower than those found by (Li et al., 2011; Su et al., 2005); this can be explained by the presence of masonry infill walls only in the ground floor.

There are few studies to quantify the overall stiffness contribution of curtain walls to an entire building. Li et al. (2011) considered glass panels in numerical models to represent windows. The results indicate that these make a slight contribution (around +1.2%) to the lateral stiffness of the building, which is far less significant than the effect of masonry infill walls. However, Bonne (2018) has found that curtain walls contribute to the stiffness of a fully building by +11%.

1.2.2 Effect on Natural Frequencies, and Mode Shapes

Devin et Fanning (2012a) did an operational modal analysis on a reinforced concrete frame structure under construction and discovered that adding cladding panels to the structure increased the fundamental frequency of the floor slab by +9%. The explanation for this increase is because these partitions were connected at their top and bottom to floor slabs, and this connectivity finally engaged both slabs during vibration. Asgarian et McClure (2014) have developed numerical models of two blocks of a hospital, they found that adding the masonry infill walls to the models decreased the fundamental period of the two blocks by nearly -200% and -40%, respectively. In addition, Kechidi et Bourahla (2014) have developed numerical model of RC commercial building, they discovered that adding interior and exterior masonry walls reduced the fundamental period by -20%. Bonne (2018) has found that masonry infill wall decrease the fundamental period by -8%, and the curtain walls decrease it by -6%. Fiorino et al. (2019) performed shake table tests on different building prototypes made of NSCs (partition walls, outdoor façade walls and suspended continuous ceilings). They found that the presence of the NSCs altered the response of the bare structure, by increasing the fundamental frequency up to about 5 times. As a result, disregarding this effect in seismic design as commonly done by engineers will result in underestimated earthquake load (i.e., selecting a lower acceleration on Design Spectrum).

When these studies are compared, it can be concluded that the influence of NSCs on dynamic response is dependent on a variety of parameters, including structural system, structural type, and density (presence) of non-structural elements.

1.2.3 Effect on damping ratio

Estimating damping ratio within a structure during the design stage is a difficult task, especially because there are multiple sources that contribute to the overall energy dissipation capability, such as primary structural elements, secondary structural elements, and energy dissipation between interfaces or joints in the structure. Several experimental

studies on the damping ratio of in-situ constructions have been carried out. Kim et You (2002) investigated the dynamic properties of a tall residential building and concluded that damping could be significantly underestimated during the design stage, and that the only way to accurately estimate damping was to consider additional factors that are commonly overlooked, such as NSCs. Devin et Fanning (2012b) studied the modal damping of a reinforced concrete floor building throughout three stages of construction. This analysis indicated that damping ratios of a floor system change throughout construction stages and that suggested values in the literature that range from 2% to 3% for a bare frame floor and from 4% to 8% for a finished structure would appear to be reasonable.

Tables 1.1 and 1.2 present a summary of the percentage change in the dynamic properties of buildings (fundamental period, lateral stiffness) when non-structural walls are included in the models.

Table 1.1 Effect of masonry walls on fundamental period and lateral stiffness

Year	Authors	Research	Contribution
2005	Su et al.	Studied the influence of masonry walls on lateral stiffness of tall buildings	Increase of the lateral stiffness by +60%
2006	Amanat et Hoque	Studied the effect of masonry walls on the fundamental period	Overestimation of the fundamental period (absence of masonry walls) by a range of +40% to +160%
2011	Li et al.	Studied the influence of NSCs on tall building stiffness	Increase of the structural stiffness by +60%
2014	Asgarian et McClure	Studied the impact of unreinforced masonry (URM) infill walls on the dynamic characteristics of a hospital building in Montreal	Decrease of the fundamental period by -40%
2014	Kechidi et Bourahla	Developed RC commercial building and added interior and exterior masonry walls	Decrease of the fundamental period by -20%
2018	Bonne	Characterization of the effect of non-structural components on the dynamic properties of a building in Montreal	<ul style="list-style-type: none"> • Decrease the fundamental period by -8% • Stiffness contribution of +21%

Table 1.2 Effect of curtain walls on fundamental period and lateral stiffness

Year	Authors	Research	Comments
2011	Li et al.	Studied the influence of NSCs on tall building stiffness	Increase of the lateral stiffness by +1.2%
2018	Bonne	Characterization of the effect of non-structural components on the dynamic properties of a building in Montreal	<ul style="list-style-type: none"> • Decrease the fundamental period by -6% • Stiffness contribution of +11%

1.3 Engineering demand parameters (EDP) for NSCs

In this section, previous studies on the engineering demand parameters namely floor acceleration amplification will be presented.

According to the 2015 edition of the NBC, the NSCs should be designed to:

- Resist deformation of the building.
- Resist deformation of other elements or components.
- Resist a lateral seismic force V_p given by Equation (1.1).

FEMA 356 (2000) limits the interstory drift ratio of curtain walls and masonry walls to:

- 0.01h for Immediate Occupancy (IO) Non-structural Performance Level
- 0.02h for Life Safety (LS) Non-structural Performance Level

Where h is the height of the story.

The lateral displacements multiplied by $R_d \cdot R_o / I_E$ give realistic values of anticipated displacements: $R_d = 1.5$ (the energy dissipation capacity of the element or its connections),

$R_o = 1.3$ (the force overstrength factor), $I_E = 1$ (the importance factor for the building).

1.3.1 Lateral seismic demand in NBC 2015

The lateral seismic force of NSCs is presented in the followed equation:

$$V_p = 0,3 F_a * S_a(0.2) * I_E * S_p * W_p \quad (1.1)$$

Where F_a is the acceleration-based site coefficient, corresponding to the value $F(0.2)$ which varies from 0.69 to 1.64 depending on the type of soil. $S_a(0.2)$ is the spectral response

acceleration value at 0.2 s. I_E is the importance factor for the building varying from 0.8 to 1.5. W_p (KN) is the weight of the NSCs or the equipment. $S_p = C_p A_r A_x / R_p$ is the horizontal force coefficient of a part of a building and its anchorage varying from 0.7 to 4.0; Where C_p is the seismic coefficient of the element or component, A_r is the force amplification coefficient of the element or component, R_p is the response modification coefficient of the element or component and A_x is the height factor defined in Equation (1.2), with h_x the height of the level x of the NSCs or equipment and h_n is the height of the building. This coefficient varies linearly over the entire height of the building, its minimum value is 1 at the ground level and its maximum value is 3 at the roof level.

$$A_x = 1 + 2 \frac{h_x}{h_n} \quad (1.2)$$

This coefficient is referred to as the floor acceleration amplification (FAA), which is the ratio between the peak floor acceleration of this floor and the peak ground acceleration (PFA/PGA).

1.3.2 Floor acceleration amplification in previous studies

The accelerations of the NSCs are amplified by two phenomena: 1- the amplification of the peak ground accelerations by the structural system resulting in amplified accelerations at the level of the floors supporting the NSCs, 2- the amplification of the floor accelerations caused by the dynamic characteristics of the NSCs resulting in accelerations amplified at the level of the latter (Cunha et al., 2014). In this research, the AVMs, and the earthquake records have made it possible to determine the first phenomena.

Singh et al. (2006) conducted a numerical study in which they compared the floor acceleration amplification of several buildings with the code equation and dynamic analysis. The comparison demonstrates that the code equation overestimates the amplification factor for tall buildings (more than 4 floors) and underestimates this factor for low-rise buildings (4 floors and less). Cunha et al (2014) evaluated the seismic forces

applied to NSCs in different buildings (5,10, and 15 floors) and they also concluded that the code equation leads to an overestimation of the seismic force in buildings of great height.

Surana et al. (2017) conducted linear and non-linear analysis on 4, 8, and 12 floor building models and determined that for low-rise buildings (4 floors) the variation in floor acceleration amplification is approximately linear since the response of the structure is dominated by the fundamental mode of vibration. For tall buildings (8 and 12 floors) the variation of this amplification is approximately linear up to 25% of the height of the building, remains constant between 25 and 75% of the height and increases very significantly from 75% of the height of the building, up to the roof. This large increase in the amplification factor of floors at roof level is caused by higher modes (Singh et al., 2006). Petrone et al. (2015) also demonstrated that in buildings of 1 to 5 floors, the variation of the floor acceleration amplification is linear, but not for a 10-floor building due to the participation of higher modes.

Asgarian et McClure (2020) conducted linear seismic analysis on 27 reinforced concrete buildings with 2 types of LFRS (reinforced concrete shear walls system and reinforced concrete moment-resisting frame system) located in Montreal, Canada, for which AVMs are used to determine their in-situ 3D dynamic characteristics. They observed a considerable dispersion of the PFA results obtained in all building categories: at roof level, the amplification factors vary between 1.5 and 3.5 for low-rise buildings, between 2.3 and 4.1 for medium-rise buildings, and 1.3 to 3.1 for high-rise buildings. In addition, they observed that the linear variation assumption is adequate for low-rise structures (one, two, or three floors), but it is not completely correct for medium and high-rise buildings because higher mode effects are important, particularly for high-rise buildings. The codes underestimate the PFA/PGA ratios on every level and roof of low-rise buildings, as well as in the top half of mid-rise buildings, while overestimate the ratio in the top half of high-rise buildings.

1.4 Modelling of NSWs

Simplified modelling approaches used to model the NSWs considered in the building studied are explained.

1.4.1 Masonry infill walls

Two techniques are commonly adopted in the literature to model infill walls: the first one consists of a simplified model aiming to translate the behavior of the wall by a braced frame with an equivalent compression diagonal strut, the second one aims to represent the wall by a shell element connected to the structure.

1.4.1.1 Equivalent diagonal compression struts

This subsection presents equations taken from the literature on equivalent diagonal struts to compare their relevance with a second technique which is detailed in the following subsection. The first research on infill walls was carried out by Polyakov (1960). He was the first to study the effects of NSWs on reinforced concrete structures. Several full-scale tests were carried out on square and rectangular structures. This work demonstrated that the masonry infill walls and the frames behave monolithically until cracks between the infill wall and the frames develop around the perimeter of the infill, except for small regions at the two diagonally opposite corners. As the load increases during the experiment, a compression strut forms in the wall and this diagonal compression begins to shorten the filler as the diagonal tension tends to stretch it. As a result, the masonry cracks along the diagonal. The structure continues to withstand the increasing load despite the new diagonal cracks which appear, and which continue to spread. System failure is defined as the moment when substantial cracks appear in the element. Observing this type of behavior, it was concluded that the infilled frame system is equivalent to a braced frame with a compression diagonal strut replacing the masonry infill wall (Figure 1.1). Subsequently, researchers attempted to refine this model. Holmes (1961) proposed a method to predict

deformations and strength of infill walls, based on Polyakov's model. His hypothesis was that the infill wall acted as a diagonal compression strut of the same thickness and modulus of elasticity as the infill wall with a width equal to one third of the diagonal length.

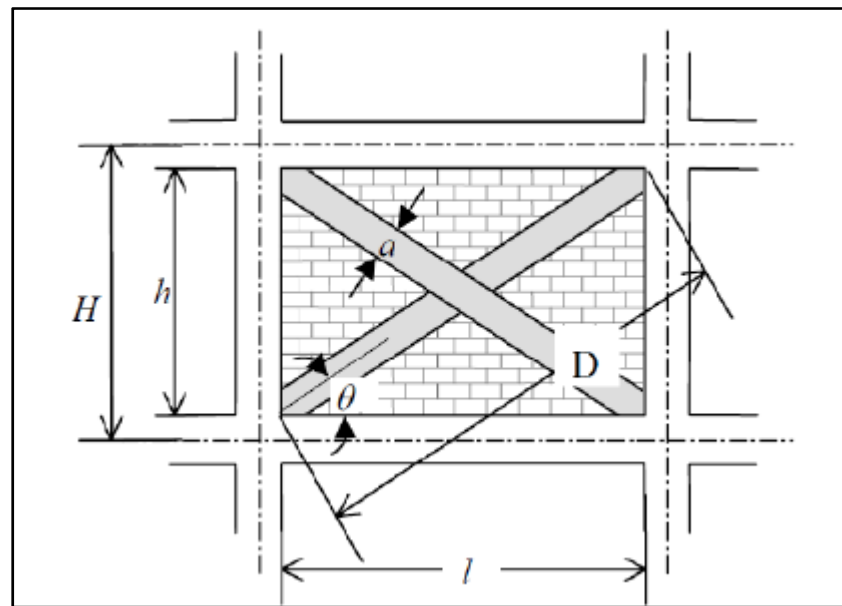


Figure 1.1 Equivalent diagonal compression struts

Smith (1967) carried out a series of tests in which double-storey model infilled frames were laterally loaded to failure. The study shows that the masonry infill walls can be modelled by an equivalent diagonal compression strut connecting to the loaded corners. This means that the masonry infill walls bounded by the beams and columns can be replaced with an equivalent diagonal compression strut connecting the four corners of the frame. The equivalent diagonal compression strut should be equal in length to the diagonal of the wall, so its thickness and modulus of elasticity are the same as that of the wall. He endorsed Holmes' (1961) model by suggesting that the effective width of the equivalent diagonal compression strut should not be a fixed value, but rather a function of the ratio (height / thickness) of the wall and the relative stiffness of the column and filling. λ_h is the relative stiffness of the infill wall with respect to the column defined by Equation (1.3).

$$\lambda_h = \sqrt[4]{\left(\frac{E_c * t * \sin 2\theta}{4EIh'}\right)} * h_{col} \quad (1.3)$$

Where E_c is the elastic modulus of the brick infill masonry (ksi), t is the thickness of the brick infill masonry (in), h' is the height of the brick infill masonry (in). E is the elastic modulus of the surrounding structural element (ksi), I is the moment of inertia of the surrounding structural element (in^4), h_{col} is the height of the column (in), θ (radians) is the angle between the equivalent diagonal compression strut and the horizontal direction. Having λ_h , the ratio of the effective width to the length of the diagonal of the infill wall, W_{eff}/d can be read from the experimental curves provided by Smith (1967) .

Subsequently, Durrani et Luo (1994) analyzed a series of numerical models comprising masonry infill walls. Their research led to the development of Equations (1.4) to (1.6) which make it possible to calculate the effective width of the equivalent diagonal compression strut. Where W_{eff} is the effective width of the equivalent diagonal compression strut (in) defined by equation (1.4). Then γ and m are determined from the coefficients defined in Equations (1.5) and (1.6) which are used to determine the effective width of the equivalent diagonal compression strut. Unlike the other proposed formulations which neglected the stiffness of the upper and lower beams connected to the strut in the calculation of the effective width, they do take this parameter into account and indicate that the section of the beams has only a slight effect on the effective width of the equivalent diagonal compression strut.

$$W_{eff} = \gamma * \sqrt{L^2 + H^2} * \sin 2\theta \quad (1.4)$$

$$\gamma = 0.32 * \sqrt{\sin 2\theta} \left(\frac{H^4 * E_w * t_w}{m * E_{col} * I_{col} * H_{in}} \right)^{-0.1} \quad (1.5)$$

$$m = \left(1 + \frac{6E_b * I_b * H}{\pi * E_{col} * I_{col} * L} \right) \quad (1.6)$$

Where H is the height of the storey (in), H_{in} is the net height of the infill panel (in), L is the span length of the structure (in), t_w is the thickness of the infill wall (in), E_w is the elastic modulus of the infill wall (ksi), E_{col} is the elastic modulus of the column (ksi) and E_b is the elastic modulus of the beam (ksi). I_{col} is the moment of inertia of the column (in⁴), I_b is the moment of inertia of the beam (in⁴) and θ is the angle between the equivalent diagonal compression strut and the horizontal (radians). FEMA (2000) has suggested that the elastic stiffness of an unreinforced masonry infill wall before cracking can be represented by an equivalent diagonal compression strut having the same thickness and modulus of elasticity as the infill wall. The only difference with previous research comes from calculating the effective width "a" of the equivalent diagonal compression strut (in) defined by Equation (1.7) and λ_1 a coefficient defined by Equation (1.8) which is used to determine the effective width of the equivalent diagonal compression strut.

$$a = 0.175(\lambda_1 * h_{col})^{-0.4} * r_{inf} \quad (1.7)$$

$$\lambda_1 = \sqrt[4]{\left(\frac{E_{me} * t_{inf} * \sin 2\theta}{4E_{fe} * I_{col} * H_{inf}}\right) * h_{col}} \quad (1.8)$$

Where h_{col} is the height of the column between the beams (in), r_{inf} is the diagonal length of infill panel (in), H_{inf} is the height of the infill panel (in), E_{fe} is the expected modulus of elasticity of the material of the structure (ksi), E_{me} is the modulus of expected elasticity of the filling material (ksi) and I_{col} is the moment of inertia of the column (in⁴). L_{inf} is the length of the infill panel (in), T_{inf} is the thickness of the infill panel (in) and θ is the angle between the equivalent diagonal compression strut and horizontal (radians).

The equivalent diagonal compression strut model is widely accepted as a simple and rational tool for describing the influence of masonry panels on the infill structure.

However, the model with a single equivalent diagonal compression strut does not describe the local effect resulting from the interaction between the infill walls and the structure surrounding the panel. As a result, the bending moment, and the shear forces of the SCs are not realistic and the location of the plastic hinges cannot be precise. In addition,

achieving equivalent nonlinear stiffness is not straightforward when there are openings in masonry walls. It is also difficult to predict the damaged area of the masonry and the behavior under severe deformation. This is not surprising given the following assumptions:

- The horizontal shear and the deformation of the structure are large enough to cause a loss of contact between the panel and the columns in the two diagonally opposite corners.
- The state of stress in the masonry panel causes the appearance of cracks in the bricks or mortar, defining a diagonal between the other two angles. The strength and boundary conditions of an isolated panel are different from those of a panel in a complete structure.

Finally, by carrying out a quantitative evaluation on the seismic performance and the vulnerability of masonry walls, (Lefebvre, 2012) modelled masonry walls by compression struts with plastic hinges. The use of this method is based on the work of FEMA 356 (2000) and Al-Chaar (2002) , it makes it possible to consider the modes of rupture of the walls and to consider the presence of openings.

1.4.1.2 Continuous model

Another way to model masonry infill walls is to consider them as a flat panel made of homogeneous material (Figure 1.2). In the literature, this type of material is commonly referred to as a continuous, homogeneous, and isotropic material.

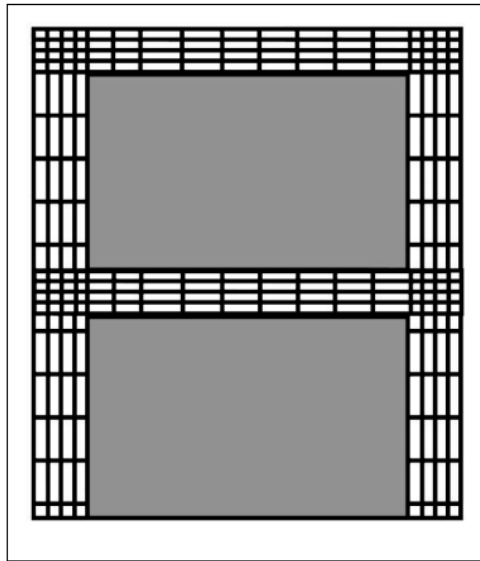


Figure 1.2 Continuous model
Asgarian et McClure (2014)

By adopting this technique, the masonry infill wall is simulated by shell elements. An essential part of this process is to define the equivalent properties of the material so that the panel element correctly represents the behavior of the wall. Some researchers (Asgarian et McClure, 2014; Li et al., 2011; Sofi et al., 2017) have defined shell elements for masonry walls and their characteristics (compressive strength, modulus of elasticity, Poisson's ratio, density and shear modulus). In addition, it is necessary to define the interaction between the infill walls and the surrounding structure. In practice, infill walls are connected to the structure using elastic infill between the wall and the frame. Here, the weakness of the connection arises from the susceptible contact between the infill wall and the surrounding frame, which induces a change in the path of the load.

To date, there are no requirements or guidelines that deal with modelling the interface between the infill wall and the surrounding structure. However, there are some studies that focus on this subject. Lefebvre (2012) modelled masonry infill walls with shell elements and used contact elements to connect the infill wall with the surrounding structure (El-Dakhakhni et al., 2003; Li et al., 2009; Li et al., 2010). In these studies, the out-of-plane behavior of shell elements is not considered since researchers claim that infill walls

improve strength, stiffness, and energy-absorbing capacity in the plane. In addition, the risk of wall buckling under these conditions is low.

The contact element, also called the *gap element*, can withstand only compression in the direction normal to the surfaces and shear in the tangential direction. Dorji et Thambiratnam (2009) proposed Equation (1.9) to calculate the stiffness of the contact element K_g by a trial-and-error procedure based on the results of Doudoumis et al. (1995). The advantage of using the contact element is its simplicity in modelling and its ability to transfer stiffness from the wall to the frame without transmitting building loads.

$$K_g = 0.0378 * K_i + 347 \quad (1.9)$$

$$K_i = E_i * t_i \quad (1.10)$$

Where K_g , is the axial stiffness of the contact element (N/mm); K_i (Equation 1.10), is the stiffness of the infill wall in (N/mm); E_i is the young elastic modulus of the infill wall (Mpa); t_i , is the thickness of the infill wall (mm).

1.4.1.3 Choice of the simplified model of infill walls

The use of a continuous model is more complex but allows a better representation of the infill walls. Indeed, the continuous model presents results of fundamental period closer to AVMs than that of the equivalent diagonal compression strut as reported in studies carried out by researchers (Asgarian et McClure, 2014; Chaker et Cherifati, 1999; Sofi et al., 2017; Su et al., 2005). The results of Asgarian et McClure (2014) reveal a 9-96% difference between AVMs and models using equivalent diagonal compression struts. The continuous model shows a difference of 3 to 37% with the AVMs (Asgarian et McClure, 2014; Chaker et Cherifati, 1999; Sofi et al., 2017; Su et al., 2005). Therefore, the best technique among the methods adopted to model masonry infill walls is the continuous model. The use of shell and contact elements to represent masonry infill walls is therefore recommended for this research project.

1.4.2 Curtain walls

Curtain walls are considered secondary elements since they do not support the main loads of the building and are simply attached to the slabs of each floor. Their modelling in numerical models is a relatively complex. One of the first problems arises from the space between the glass panel and the aluminum structure which is often insufficient for moderate earthquakes. This has the effect of causing contact between the two parts and thus subjecting the glass panel to compression along its diagonal. Usually, the contact between the glass panel and the aluminum structure occurs at the corner of the panel or near the corners where the first cracks appear.

Researchers (Caterino et al., 2017b; Memari et al., 2011; Shirazi, 2005) have carried out tests in the inelastic domain where they apply an increasing force on a curtain wall to record its displacement. Subsequently, they developed numerical models of the curtain walls based on data obtained during tests. The results obtained classify the stresses undergone by the curtain wall into two categories (Shirazi, 2005):

- The friction of the seal on the edge of the glass panel; this gasket pressure generates a stress which is almost constant as the displacement applied to the panel increases
- The contact between the corner of the glass panel and the edge of the frame; this stress does not only depend on the force applied to the panel, but also on the boundary conditions of the corners of the glass panel, on the initial gap between the glass panel and the fasteners of the aluminum structure, on the thickness of the panel, the bending stiffness of the structure, the connection at the transom and the mullion and the torsional stiffness of the structure.

In his study, Shirazi (2005) observed that the displacement of the panel increases throughout the test and the boundary conditions change during the test (no contact, contact and friction). They noticed a reduction in the gap between the aluminum structure and the

glass, followed by contact between these two parts, and the whole ends with friction of the seal. The numerical model must be able to reflect these effects, and to simulate the initial gap between the glass panel and the frame. Initially, there is a space between the glass panel and the frame around the glass panel (except where the edges meet the laying blocks and side blocks). The stress experienced by a glass panel results from the contact between the frame and the glass and depends on the applied displacement, the conditions at the corner of the glass panel, the initial gap between the glass panel and the edge of the glazing, the thickness of the glass, the mullion-transom connection, and the torsional stiffness of the structure. The difficulties of modelling are summarized as follows (Caterino et al., 2017b; Memari et al., 2011):

- Connections and torsional stiffness between mullions and transoms
- The space between the glass panel and the aluminum structure
- The stiffness of the frame during contact
- Modelling the friction effect of the joint

To respond to these difficulties, Caterino et al. (2017b) modelled the glass panels using shell elements and the aluminum mullions / transoms using beam elements. In addition, they chose to use a gap element to model the contact between the glass panel and the gaskets of the aluminum structure to simulate the boundary conditions of the glass panel. By assigning stiffness to the contact elements, they simulate the local deformations of the frame. These researchers chose a rigid link between the transoms and the mullions to represent the fixed connection. In addition, they used an elastoplastic link (Wen's model) to model the effect of friction. Finally, buckling of the glass panels was not considered because such a failure mode did not occur during testing.

In this research, the model proposed by Caterino et al. (2017b) was adopted since the properties of gap elements are well defined.

1.5 Conclusion

This chapter presents a literature review on the contribution of NSWs on the dynamic response (natural frequencies, mode shapes, damping ratios, and lateral stiffness) of buildings, the engineering demand parameters (floor acceleration amplification, and inter-story drift) in the NBC 2015 and FEMA 356, and the simplified methods used for the modelling of masonry infill walls and curtain walls. From all the studies carried out, it is deduced that these components have an impact on the natural frequencies of the buildings and contribute to the stiffness. In addition, many researchers are developing simplified models of NSWs to better represent the behavior of numerical models. These components do not only affect the stiffness, but also the modal properties (damping, mode shapes, and frequencies) of a building.

In conclusion, when designing a building, it is essential to not overlook all the NSWs and to consider their effect in building code equations.

The following chapter examined the building used in this study (MDE) in detail: description, AVMs, FEM, and calibration of earthquakes records.

CHAPTER 2

DESCRIPTION OF THE MDE, AVMs, AND CALIBRATION OF THE FINITE ELEMENT MODELS

In this chapter, the selected building and its NSWs are described. In addition, the ambient vibration measurements, and the calibration of the building finite element models are presented.

2.1 Description of the case study building MDE

The building *La maison des étudiants* (MDE) selected in this study forms part of the campus of École de technologie supérieure in Montreal and was constructed between 2017 and 2020 (Figure 2.1).



Figure 2.1 Photos for the MDE
(Imtl.org)

The MDE measures 23.2 m in height. It has one level in the basement, followed by five floors composed essentially of offices, classrooms, and workspaces, then a top floor consisting of a mechanical room for water treatment, electricity, and mechanical ventilation of the building with an extension of lifts and stairs (Figure 2.2). This building has an almost

rectangular trapezoidal shape at the base with dimensions of 40.8 m in the small side and 45.6 m in the big side for the transversal direction and 66.3 m for the longitudinal direction. The architectural plans were transmitted by "SDK et associés inc."

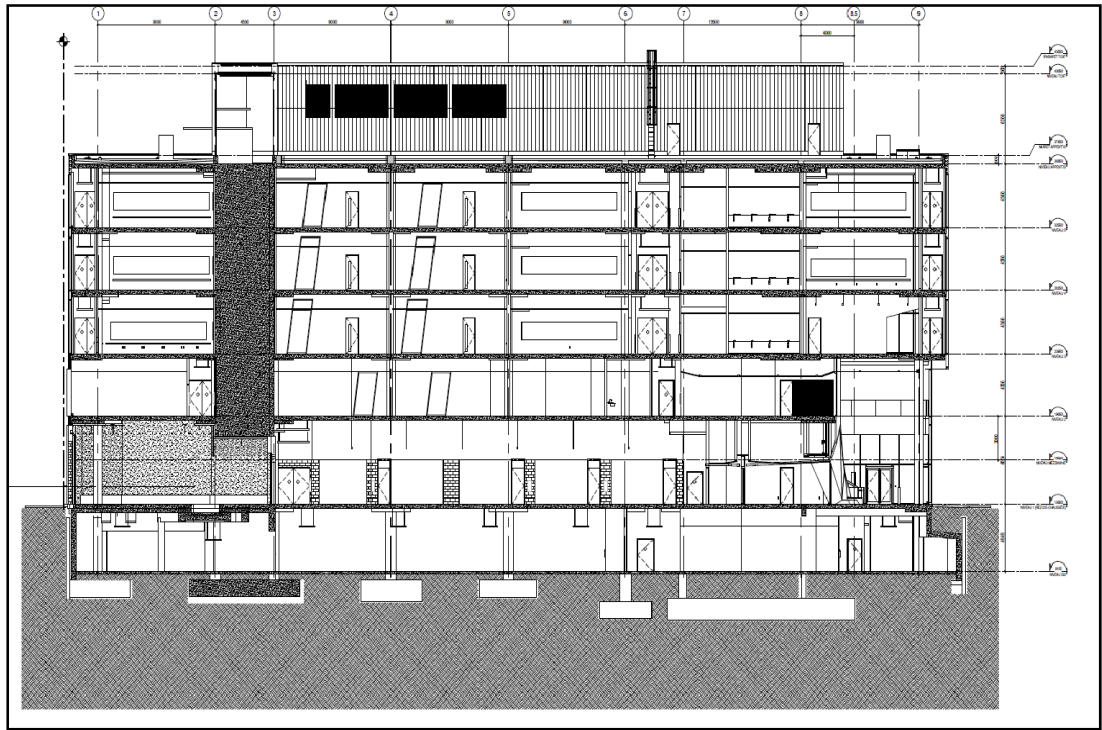


Figure 2.2 Elevation view of the MDE

The MDE is a reinforced concrete structure with a steel structure on the roof (mechanical room). The SCs in MDE consist of reinforced concrete slabs, beams, columns, rigid cores, and steel deck. The LFRS of the MDE is a conventional construction of reinforced concrete rigid cores (Figure 2.3). The building is located on a very dense soil known as site class C according to NBC 2015 (NRC, 2015). It was executed according to the requirements of the 2010 edition of the National Building Code of Canada, with a ductility force modification factor ($R_d = 1.5$), and an overstrength-related force modification factor ($R_o = 1.3$). A detailed description of materials and SCs is given in ANNEX I.

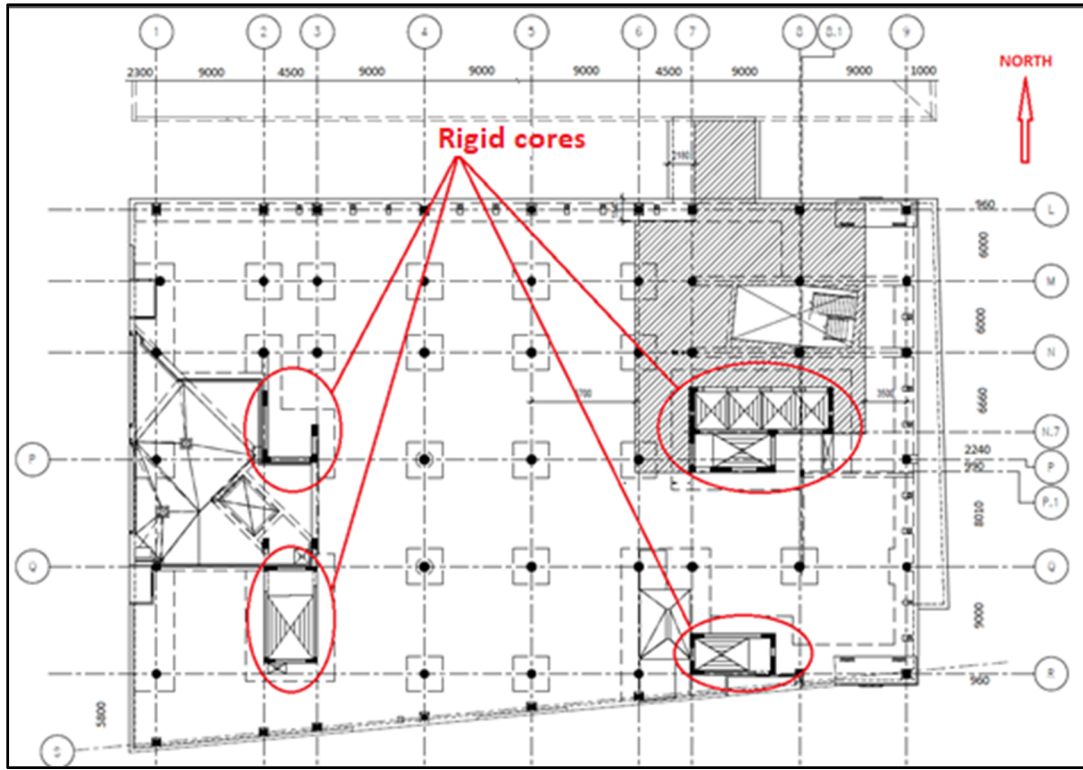


Figure 2.3 Plan view of the ground floor of the MDE

2.2 Description of NSWs selected in this study

The main NSCs studied in this research are the masonry infill walls and the curtain walls. The masonry infill walls are concrete block masonry (Figure 2.4) and have two different thicknesses with a compressive strength of 15 MPa. There is a gap of 10 mm between each infill wall and the structure, this gap is filled with an elastic material so that these elements are not in direct contact (Figure 2.5). On the other hand, the system of curtain walls used is a glazed system. These NSWs consist of mullions, transoms and aluminum rails with glazing made of tempered glass reinforced with heat. The gap between the glazing and the aluminum frame is 5 mm. The characteristics of the curtain walls are shown in Table 2.2 and Figure 2.6.

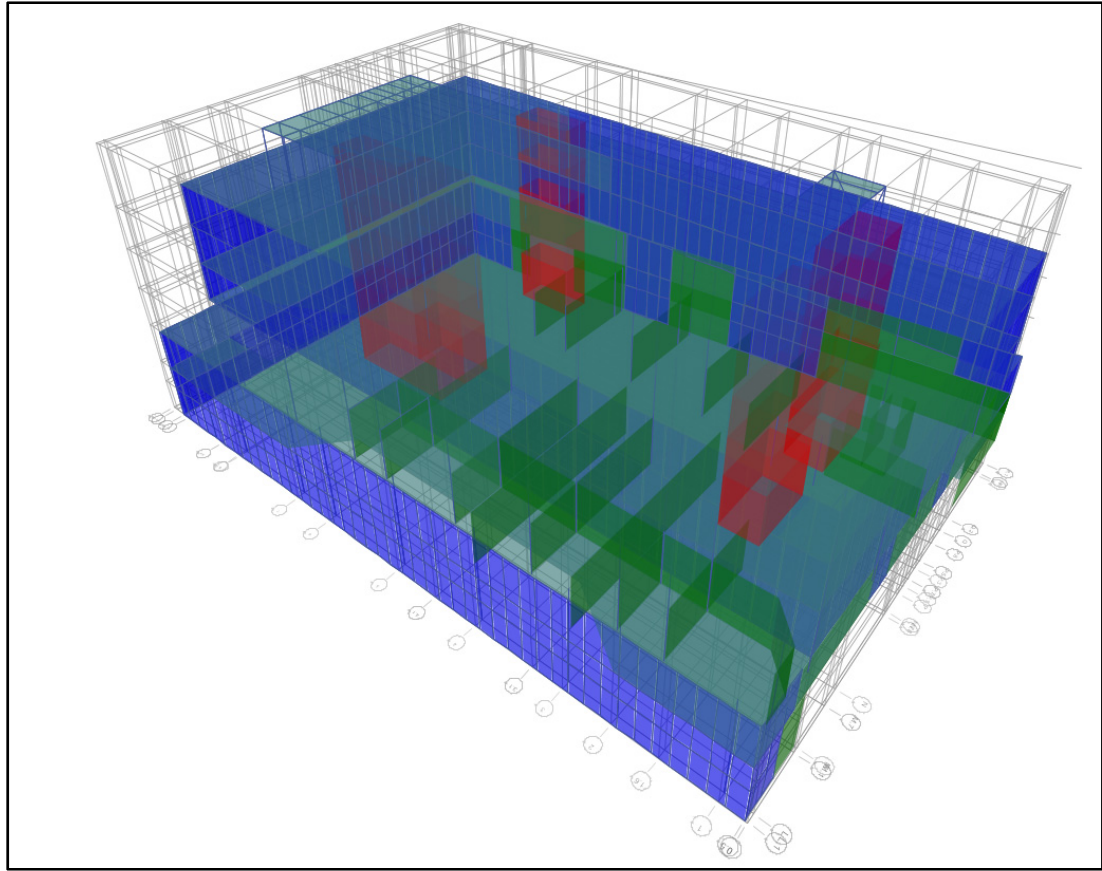


Figure 2.4 Masonry walls location on the ground floor

Table 2.1 provides the total surface of NSWs and floors.

Table 2.1 Total surface of NSWs and floors

Floor level	Surface (m ²)	Masonry walls (m ²)	Curtain walls (m ²)
Appentis	875	-	-
Roof	2537	-	-
5 th floor	2246	-	805
4 th floor	2367	-	805
3 rd floor	3031	-	805
2 nd floor	2574	291	591
Ground floor	3031	1740	720
Total	16661	2031	3726

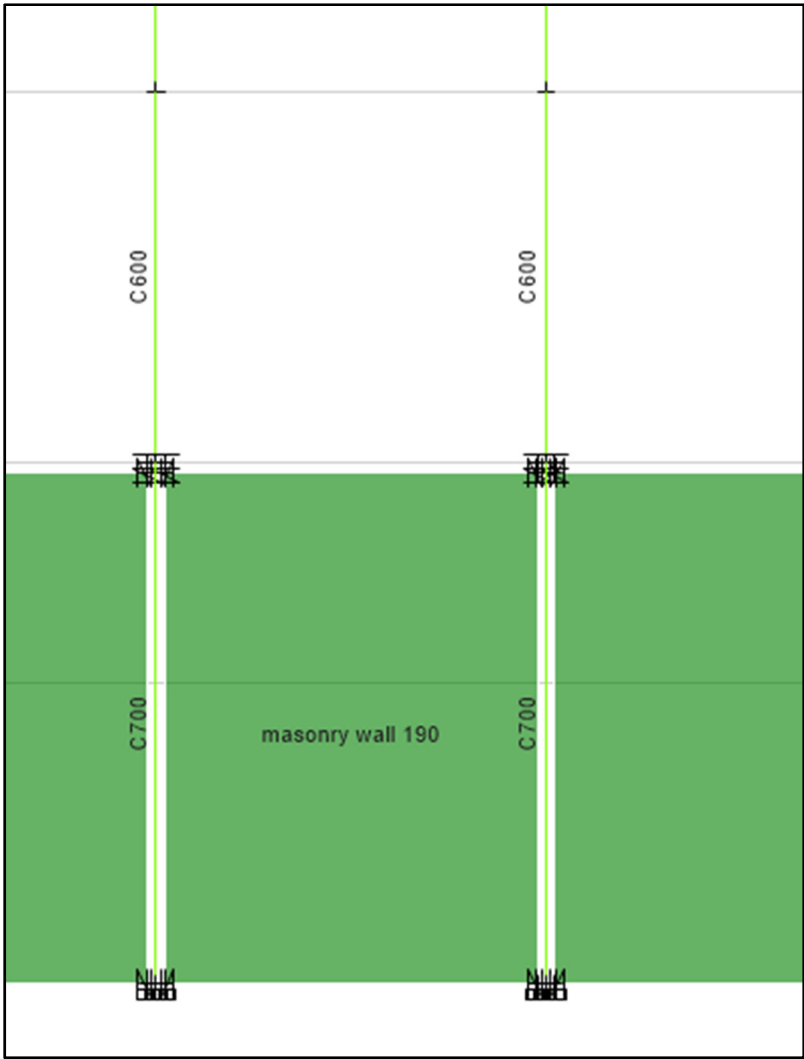


Figure 2.5 Masonry gap element

Table 2.2 Composition of the glass panels

Layer	Composition	Thickness (mm)
Exterior	Heat-strengthened glass	6
Intercalary	Argon gas	12
Interior	Heat-strengthened glass	6

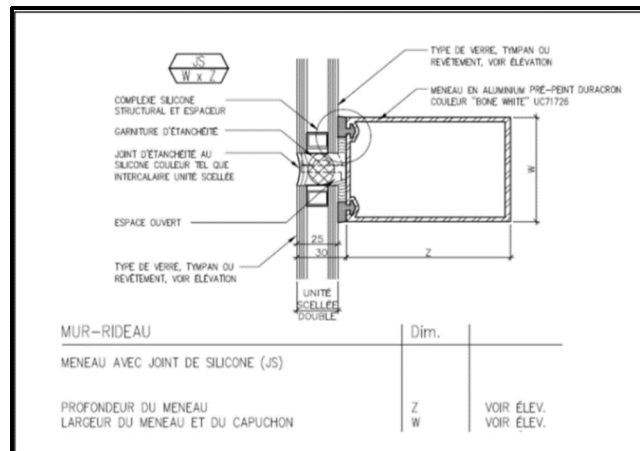


Figure 2.6 Details of the MDE curtain walls

A more detailed description of the components and materials is represented in ANNEX I.

2.3 Description of ambient vibration measurements (AVMs) of the MDE

To obtain modal properties of the MDE and calibrate its finite element models, AVMs were conducted in multi-floor levels. The principles of AVMs, the presentation of the experimental apparatus, the extraction and pretreatment of the data, and the acquisition of experimental data will be presented in the following sections.

2.3.1 Principles of AVMs

AVMs is considered an appropriate method for testing important civil structures (skyscrapers, hospitals, bridges, etc.) that are often difficult to excite using forced vibrations, or when the excitation of the structure is prohibited by the regulation, for example for civil protection buildings. Forced vibration measurements are impractical or prohibitively expensive for large-scale complex structures. As a result, ambient loading is relied on as the input excitations. Without detailed knowledge of the sources, output-only system identification techniques are required for the analysis of ambient vibration data.

This technique records the ambient excitations of the building, which are low-amplitude vibrations generated by ambient sources such as wind, mechanical equipment in operation, micro vibrations, traffic, loads due to use and occupancy, and other environmental loads (Brincker et Ventura, 2015). AVMs are used to:

- Provide necessary information on the dynamic properties of a building under real conditions in the elastic domain.
- Validate and refine finite element models since 3D mathematical models cannot capture all the details of a structure such as: - the interactions between the structure and the NSWs, the properties of the materials and the quality of the construction. Therefore, AVMs can complete and improve the assessment of the seismic vulnerability of an existing building.

The characteristics of the input forces governing the movement of the building are not known with this test, only the output data are collected by the operator, that's why it is also called operational modal analysis (OMA). The initial excitation is considered broadband white noise, which means that the excitation has a quantity of energy approximately equal to the frequency range used. Therefore, the dominant modal properties of the building are identified only from the measured response output. Assuming a constant input spectrum at each input DOF (white noise), the frequency response function is directly related to the output spectrum. Since the frequency response function with a DOF is described by peaks at the natural frequencies of the building, these frequencies can be detected directly from the output spectra.

In summary, the AVMs identify the dominant dynamic properties of the building including the lowest natural frequencies corresponding to the first modes of vibration, and the modal damping coefficients. In addition, they can identify floor accelerations, velocities, and displacements.

There are three different approaches for obtaining the modal parameters automatically using OMA: the Frequency Domain Decomposition (FDD), the Enhanced Frequency Domain Decomposition (EFDD), and the Stochastic Subspace Identification (SSI) technique.

1) Frequency Domain Decomposition (FDD)

The idea of the Frequency Domain Decomposition (FDD) technique is to perform an approximate decomposition of the system response into a set of independent single degree of freedom (SDOF) systems, one for each mode (Brincker et al., 2000). The decomposition is performed simply by decomposing each of the estimated spectral density matrices. In the above reference, it is shown that the singular values are estimates of the auto spectral density of the SDOF systems in modal coordinates, and the singular vectors are estimates of the mode shapes of the mode in the vicinity of the resonance peak (ARTEMIS Modal, 2018).

The FDD technique involves the main steps listed below:

- Estimating spectral density matrices from the raw time series data.
- Perform singular value decomposition of the spectral density functions.
- If multiple test setups are available, then average the first singular value of all test setups and average the second, etc.
- Peak pick of the average singular values. For well-separated modes, the first singular value is always picked. In case of close or replicated modes, pick the second singular value, the third singular value, etc. as well.
- Optionally, if multiple test setups are available, inspect the singular values of each test setup and pick the peaks manually if necessary.

2) Enhanced Frequency Domain Decomposition (EFDD)

The Enhanced Frequency Domain Decomposition (EFDD) is a refinement of the FDD since it makes possible to better decompose the modes and to calculate the damping ratio of each one. The modal parameters in EFDD are calculated using a range of frequencies in the neighbourhood of the peak point, known as a Single-Degree-of-Freedom (SDOF) spectral bell. The EFDD method uses a simple tool which allows comparing the similarity of 2 deformed

shapes through the square of the correlation between two mode shape vectors ϕ_1 and ϕ_2 called the Modal Assurance Criterion (MAC) (Equation 2.1):

$$\text{MAC}(\phi_1, \phi_2) = \frac{|\phi_1^H \phi_2|^2}{[\phi_1^H \phi_1][\phi_2^H \phi_2]} \quad (2.1)$$

Where H is the transposed conjugate vector. The MAC makes it possible to compare the evolution of a deformation over time, after damage for example, or to compare modes obtained in different ways (different recording or analysis methods). It can have a value between 0 and 1. A number near unity denotes the consistency (full orthogonality) of two mode shapes, whereas a value near zero indicates that the mode shapes are not consistent.

3) Stochastic Subspace Identification (SSI)

To extract structural dynamic properties of the building from the collected data, system identification techniques are used. The extracted properties can be used to assess the structure's condition. Among the many system identification techniques proposed for civil engineering structural monitoring applications, stochastic subspace identification (SSI) methods are regarded as a robust output-only identification technique when compared to other available methodologies (Peeters, 2000). Stochastic Subspace Identification (SSI) approaches fit a parametric model directly to raw time series data. A parametric model is a mathematical model that includes some parameters that may be changed to alter how the model fits to the data. In general, the aim is the collection of parameters that will minimize the difference between the model's projected and measured system responses (measurements). This is commonly referred to as a model calibration (ARTEMIS Modal, 2018).

The structure's stochastic state-space model is identified via SSI methods. The generated model may then be converted into a more convenient structural model format for engineering interpretation. The state-space model is compatible with both modal and Finite Element (FE) model formulations. Traditionally, the dynamic behaviour of civil engineering structural systems has been described using discrete Finite Element approximations. In this research, the

SSI method was used to determine modal parameters due to user-friendly implementations in the ARTeMIS Extractor software. Moreover, in the SSI method, the appearance of false system poles generally masks the underlying model order of the system. Stabilization diagrams can be used to distinguish between true or stable system poles and false poles (Figure 2.7).

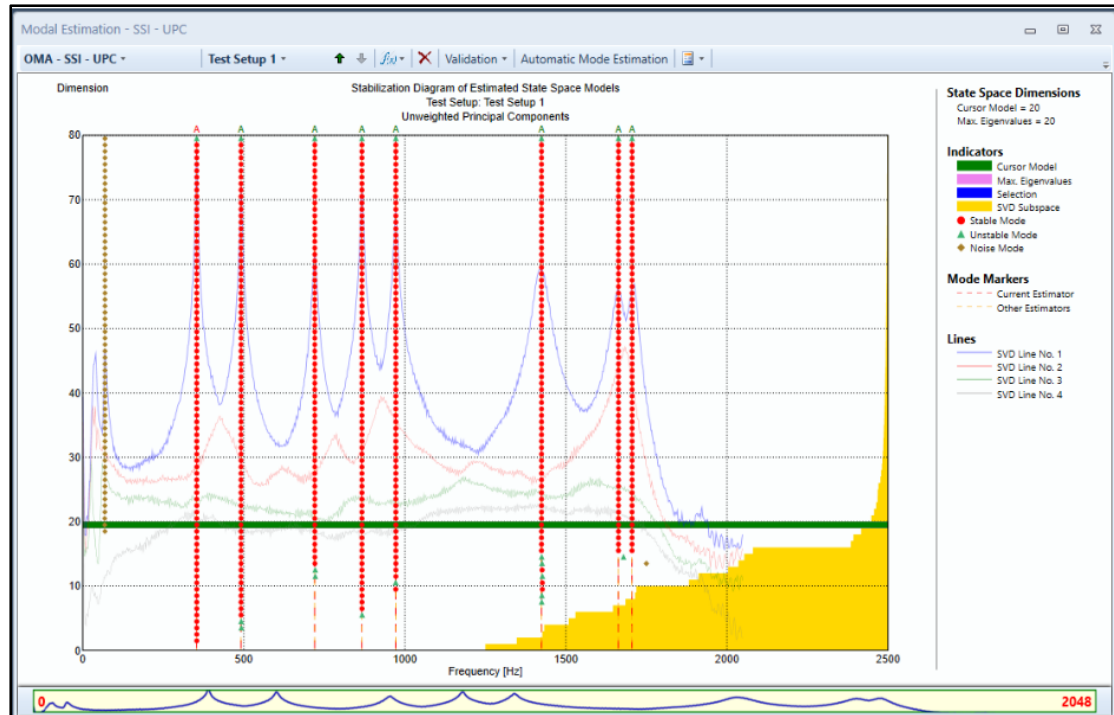


Figure 2.7 Stabilization diagram of estimated state space models
ARTeMIS Modal (2018)

2.3.2 Experimental apparatus and data acquisition

AVMs were performed using four Micromed Tromino ENGYN PLUS® sensors. They are portable, compact, and ultra-light sensors with a seismic noise acquisition system. Sensors with radio antennas and radio amplifiers are shown in Figure 2.8.



Figure 2.8 Trominos sensors a) with radio antennas b) with radio amplifiers

Before starting the recording of AVMs, it is imperative to define a north reference to be respected throughout the acquisitions and check that each sensor is levelled before each measurement (Brincker et Ventura, 2015). A measurement corresponds to the recording of the signals by all the sensors when they are positioned in a configuration in the building. A configuration corresponds to the position of the sensors in the building to capture its deformation modes. Therefore, it is necessary to perform different configurations to obtain a satisfactory measurement series. A measurement series corresponds to all the measurements made in a building grouping together several different configurations of the sensors.

During the recording of AVMs, at least one sensor is defined as the reference and must be fixed. It is usually placed at the top of the structure or at a sensible location (edge of the floor) to capture several modes of deformation; so that the modal deformations of the building can be deduced. As for the other sensors, they are placed at different positions to complete all the configurations. The set of sensors record the movement of the building and make it possible to establish, after a signal processing, the modal characteristics of the building. To facilitate the recording of the AVMs, a follow-up sheet (ANNEX II) is completed for each sensor with the following information: floor, location, sensor number, sensor chain number, and sensor trace.

The data acquisition was done at two stages of construction: bare frame and full frame. The details of AVMs recorded in the MDE are summarized in Table 2.3.

Table 2.3 Date and details of AVMs in the MDE

Stage of construction	Date	Number of sensors and setups
Bare frame	11/07/2018	3 sensors and amplifiers 1 setup with 1 reference sensor
Full frame	10/09/2020-12/09/2020	4 sensors and radio antennas 24 setups with 1 reference sensor

The acquisition time for each measurement lasts eight minutes and the signals are recorded at a frequency range of 0 to 128 Hz. Speeds between -0.04 mm / s and +0.04 mm / s and accelerations of 0 to 1.0 g are recorded by the sensors.

Figure 2.9 shows the configuration of the sensors on the 5th floor of the building at full-frame stage. The position of the sensors in this configuration makes it possible to obtain the translational deformation modes (translations in x and y and torsion).

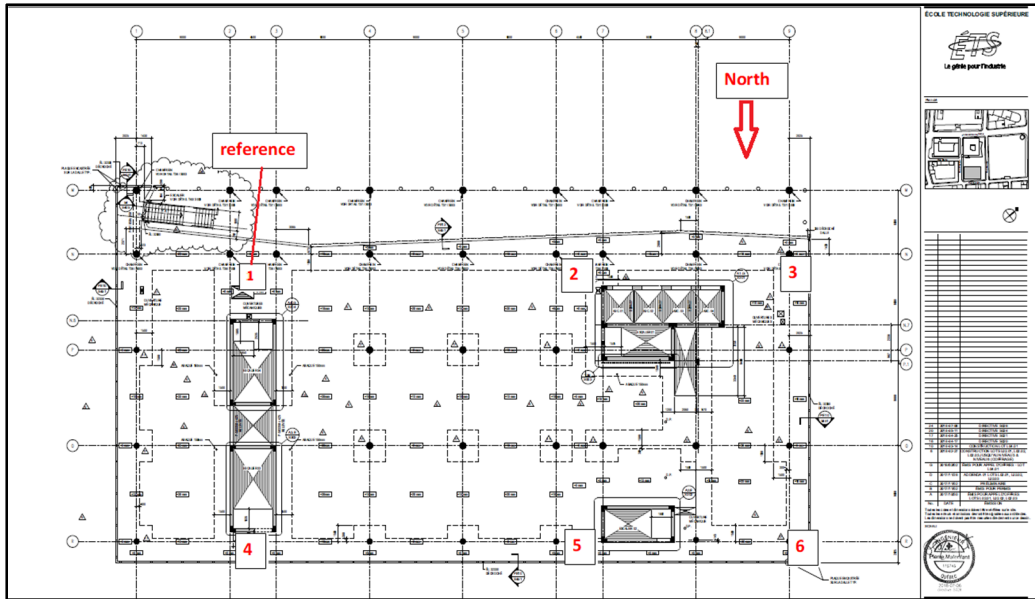


Figure 2.9 Configuration of the sensors on the 5th floor

2.3.3 Extraction and pretreatment of data

Signals recorded in the building are subjected to an extraction process using GRILLA® software (by MoHo s.r.l.), followed by preprocessing with MATLAB® (MatLab, 2020) code written by Tischer (2012). As the AVMs are carried out in the building, the operator sends the sensor recordings back to the computer with the GRILLA® (by MoHo s.r.l.) software, suitable for extracting the signals from each of the measurements for each sensor. A modal analysis of these signals is then carried out with the ARTeMIS Extactor® software (ARTeMIS Modal, 2018). The modal parameters were obtained by using two methods: Enhanced Frequency Domain Decomposition (EFDD), and Stochastic Subspace Identification (SSI). These two methods were used in order to validate the measurements.

Once the data has been extracted, each of the measurements undergoes signal preprocessing. The choice to use a MATLAB® (MatLab, 2020) procedure for the preprocessing of the signals comes from its simplicity of execution. Preprocessing consists of grouping all the signals of a measurement together to obtain a single signal. Before analyzing this signal, it is necessary to

identify the frequency peaks, remove the parasitic peaks and choose the direction of the signal to study. The signal preprocessing steps are presented in ANNEX II.

2.3.4 Experimental results and their validation

For the bare frame, one setup was recorded due to problems in connection between the trominos, and from this setup, it was possible to determine the dynamic properties of the first mode of vibration (Table 2.4).

Table 2.4 Modal parameters of the MDE at the bare frame stage

Measurement	AVMs			
Mode	Shape	F_i (Hz)	T_i (s)	ζ_i (%)
1	Transversal translation + torsion	1.9	0.53	1.98

For the full frame, the analysis was carried out from the AVMs recorded in the MDE (full frame). The MAC matrix between the EFDD and SSI methods are presented in Figure 2.10. The values of the frequencies obtained for the AVMs at this stage of construction are therefore validated since the MAC values at the diagonals are larger than 0.85.

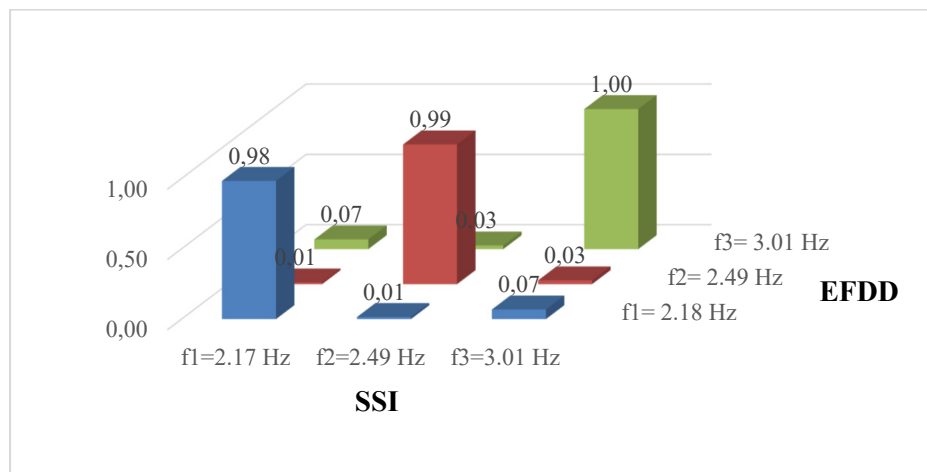


Figure 2.10 MAC matrix between SSI and EFDD methods

In this research, the SSI method was adopted to compute the frequencies used for the calibration of FEM, since this method determine whether the mode shape is stable or not, and the damping ratio of each mode. The modal parameters of the MDE (full frame) obtained using the SSI method are presented in Table 2.5.

Table 2.5 Modal parameters of the MDE at the full frame stage

Measurement	AVMs			
Mode	Shape	F_i (Hz)	T_i (s)	ζ_i (%)
1	Transversal translation + torsion	2.17	0.46	3.03
2	Longitudinal translation	2.49	0.4	2.08
3	Transversal translation + torsion	3.01	0.33	1.59

2.3.5 Comparison of periods and damping ratios between AVMs at different stages of construction

The recorded AVMs made it possible to determine the modal properties of the MDE of the first mode at different stages of construction. The periods obtained from these records are compared to assess the effect of NSWs on the building as shown in Table 2.6 where the bare frame properties are considered as the reference.

Table 2.6 Comparison of the periods obtained by AVMs at different stages of construction

Mode	Shape	Bare frame		Full frame		Difference	
		T (s)	ζ (%)	T (s)	ζ (%)	ΔT (%)	$\Delta \zeta$ (%)
1	Transversal Translation+torsion	0.53	1.98	0,46	3.03	-12.4	+53.3

The comparison of bare frame and full frame showed a -12.4% reduction in the building's fundamental period. The components added between these two stages are the masonry infill walls, the curtain walls, the mechanical equipment, and the content (partitions, furniture...).

Similar observations were found by Devin et al. (2015) and Middleton et Pavic (2013) where they compared the periods of building composed only of their structural components (bare frame) and once they were in service (full frame). They observed a larger decrease in the fundamental period ranging from -9.8% to -31.8% after adding the partitions and the claddings. This reduction shows that these NSWs (masonry infill walls and curtain walls) have contributed to rigidify the building.

Concerning damping ratios, It is worth noting that damping ratio measurements taken from AVMs exhibit high dispersion and are frequently judged unreliable. (Cremona et al., 2003; Tamura, 2006) found variation in damping ratios associated with various parameters such as structural materials, architectural finishing, types of NSWs, variation in damping evaluation techniques (proportional to vibration amplitude), and non-stationary excitations. The results achieved in this research for the full-frame stage (first mode) are within the predicted range since the damping ratio is very close to the damping ratio used in common practice for the linear analysis of new buildings ($\zeta=3\%$). In addition, the damping ratio obtained by AVMs is close to the damping ratio value of Tamura's (2006) proposed relationship between frequency and damping ratio (3.1%).

2.3.6 Comparison of fundamental periods using NBC equations and AVMs

Figure 2.11 illustrates a comparison between the fundamental periods of the MDE obtained with that proposed by the NBC equation, AVMs at bare frame and full frame stages, and the equation of Gilles et McClure (2012). The code estimates the fundamental period using a series of equations depending on the type of LFRS and the height of the building. The LFRS of the building consists of rigid cores. The equation of fundamental period for this type of LFRS is given in Equation (2.2).

$$T_a = 0.05h_n^{0.75} \quad (2.2)$$

Where h_n is the total height of the building (m).

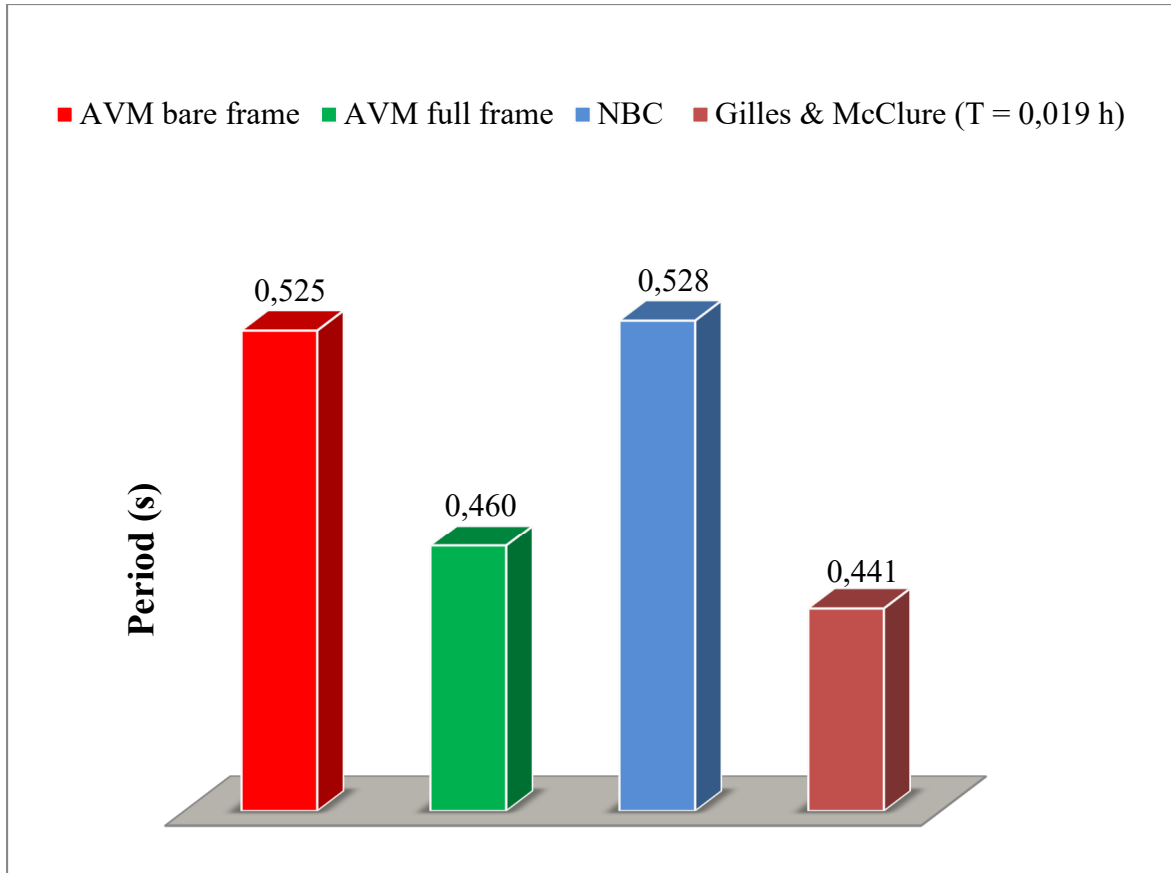


Figure 2.11 Fundamental periods of the MDE obtained by the NBC equation, AVMs (bare frame and full frame), and the equation of Gilles and McClure (2012)

Figure 2.11 shows that the NBC period exceeds those of the $AVM_{bare\ frame}$, $AVM_{full\ frame}$, and the equation of Gilles and McClure (2012) by +0.6%, +14.8%, and +19.7% respectively. These results affect the estimation of the spectral acceleration at short periods (Figure 2.12) and therefore an underestimation of the equivalent static force. For example, the MDE located in Montreal on a type C soil, $S(0.2) = 0.595g$ (used in the NBC for NSCs), $Sa(T_{AVM_{full\ frame}}) = 0.348g$ against $Sa(T_{NBC}) = 0.301g$, i.e., a decrease of 13.5% in the spectral acceleration when the equation of NBC is used. Researchers (Asgarian et McClure, 2014; Gilles et McClure, 2008) have obtained similar results. In their studies, the overestimation of the fundamental period by the NBC equation varies between +16% and +108% compared to AVMs and they claimed that the period used in design is overestimated.

The fundamental period obtained by the AVMs_{full frame} exceeds that of the equation of Gilles and McClure (2012) by +4.1%. In addition, the spectral acceleration deduced from the fundamental period equation of Gilles and McClure (2012) exceeds that of AVMs_{full frame} by 5.2%.

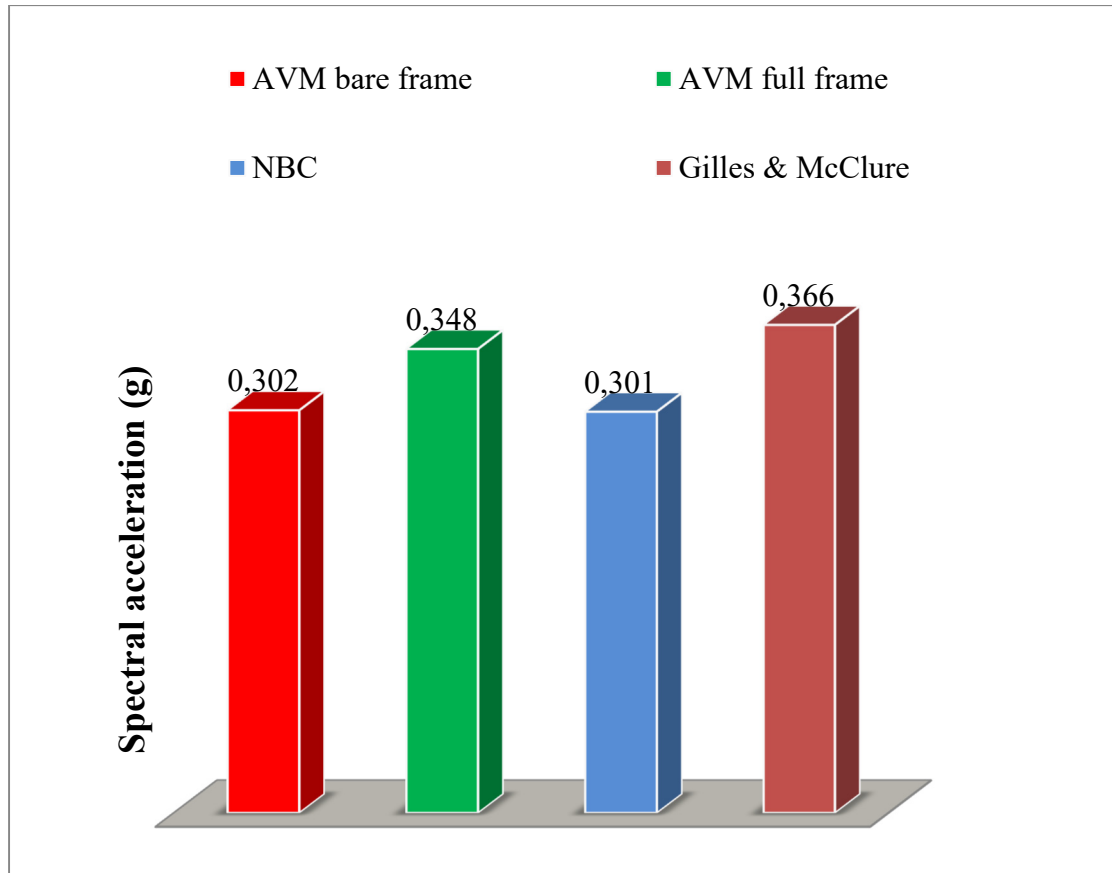


Figure 2.12 Spectral acceleration of the MDE according to different periods (the NBC equation, AVMs at both stages of construction, and the equation of Gilles and McClure 2012)

Therefore, the Gilles and McClure (2012) equation has a more realistic and conservative approach than that of NBC since the period deviations with the AVMs (full frame) are smaller. AVMs represent the actual behavior of the building considering the foundation, soil-structure interaction, actual mass, and the effect of NSWs.

2.4 Finite element Modelling and calibration of the MDE models

The calibration and simplifying assumptions of finite element modelling of structural and NSWs of the MDE at two construction stages are presented in the following section.

2.4.1 Modelling assumption of SCs

This building was modelled based on the structural and architectural plans using a finite element structural analysis software called ETABS 2017[®] (CSI, 2017). All the SCs sections and NSWs sections were considered as uncracked sections. According to the NBC 2015(NRC, 2015) clause 9.8.4.2, the moment of inertia of the gross concrete section can be used for sections that are uncracked at service loads and it is relatively new construction.

Several simplifying assumptions have been formulated such as considering the material properties as linear, elastic, and isotropic, in addition to assuming that the base of the structure is fixed and neglecting the soil-structure interactions. Moreover, the floor diaphragms were considered rigid.

At the bare frame stage, the MDE is modelled by representing all the components present during the first recordings of the AVMs, i.e., columns, slabs, rigid cores, beams, and secondary beams (Figure 2.13).

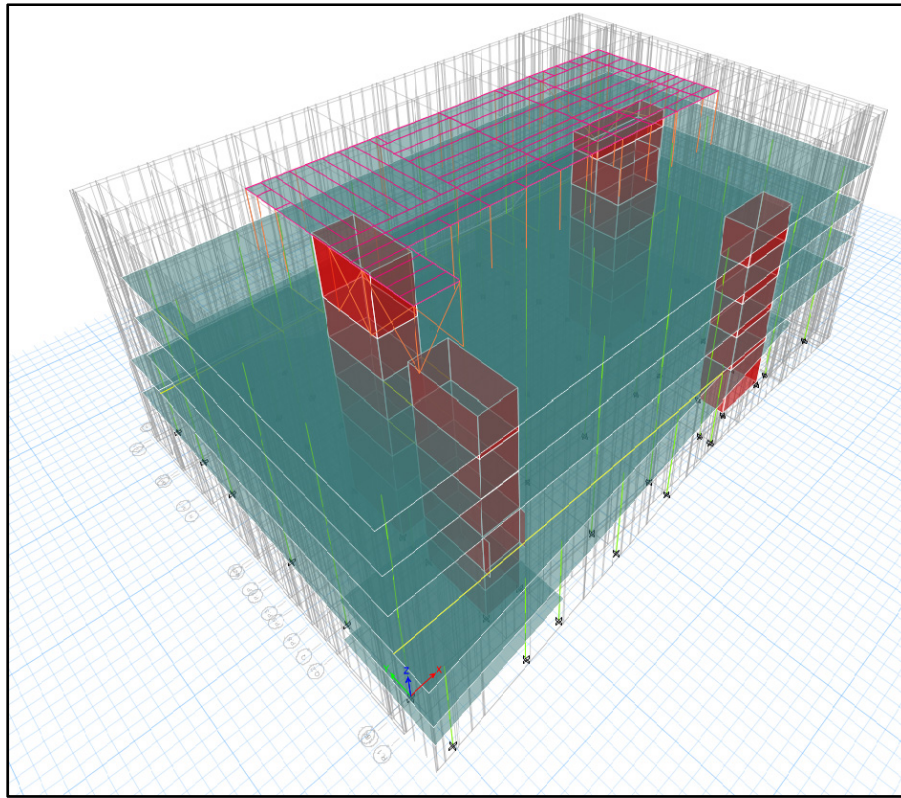


Figure 2.13 3-D FEM of the bare frame of MDE

Finally, the permanent loads (slope concrete, steel, deck, etc.) are added uniformly to the floors of the model. The calibration of the bare frame model is performed by comparing the modal parameter (fundamental period) obtained after the AVMs analysis (bare frame). At the full-frame stage, the curtain walls, masonry infill walls are added (Figure 2.14). Then, the permanent loads (mechanical system, ceiling, partitions, etc.) are added uniformly. All loads were adapted from the architectural plans (ANNEX III). Once the modelling is completed, the calibration of the full-frame model is performed by comparing the modal parameters (periods, and mode shapes) of the AVMs (full frame).

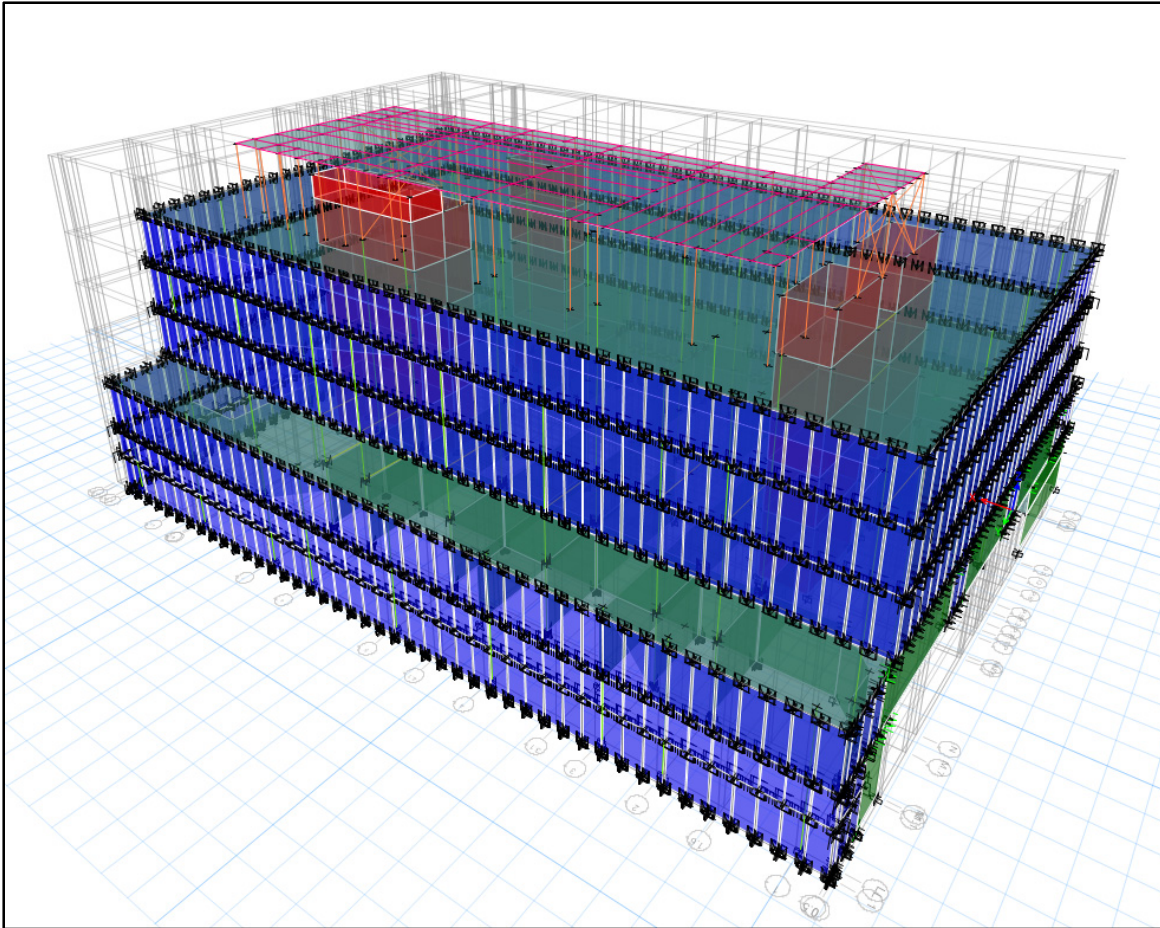


Figure 2.14 FEM of the full frame of MDE

The rigid cores and the slabs are modelled by using 4-nodes shell (mesh 500*500 mm) elements with 6 DOF (U_x , U_y , U_z , R_x , R_y , R_z) per node. Beams and columns are modelled by using 2-nodes beam elements with 6 DOF per node. Secondary beams are modelled by using 2-nodes beam elements with 6 DOF per node. The connections between beams-columns, beams-beams and slab walls are modelled by moment connections while the connections of the secondary beams are modelled as hinges.

2.4.2 Modelling assumption of NSWs

In this sub-section, the NSWs (masonry infill walls, and curtain walls) present in this building are modelled as well as the connections allowing linking the NSWs to the structure. The out-of-plane behavior of masonry infill walls, and curtain walls was not considered.

2.4.2.1 Modelling of masonry infill walls and connections with the surrounding reinforced concrete structure

The masonry infill walls are modelled by using 4-nodes shell (mesh 500) elements with 3 DOF (translations and rotation in the plane of masonry walls) per node. Then, the interface between the masonry infill wall and the surrounding structure is represented by a contact element called a *gap element*. The schematic form of a gap element is shown in Figure 2.15.

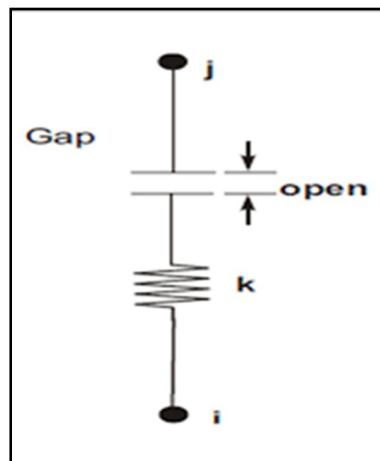


Figure 2.15 Gap element of the masonry wall

Caterino et al. (2017a)

This connection allows two surfaces to maintain or break physical contact and can have a tangential relative displacement with respect to each other. The gap element can support only compression in the normal direction to the surfaces and shear in the tangential direction. The advantage of using a gap element is its simplicity in modelling and the ability to transfer

stiffness from the masonry infill wall to the surrounding structure without taking loads. Chen have concluded that the quality of the interface and initial gaps between the masonry infill walls, and the surrounding structure may have a significant influence on the local and global behavior of the system and must be accounted for in design. A stiffness value assigned to this gap element was calculated according to Equations 1.9 and 1.10 developed by Dorji et Thambiratnam (2009) and presented in Table 2.7.

Table 2.7 Properties of the masonry infill walls gap element

Masonry infill walls	Thickness t (mm)	E_i (MPa)	$K_i = E_i \cdot t$ (N/mm)	$K_g = 0.0378 \cdot K_i + 347$ (N/mm)
M190	190	12750	2422500	91918
M330	330	12750	4207500	159391

2.4.2.2 Modelling of curtain walls and connections

The glass panels are modelled by using 4-nodes shell elements with 3 DOF (translations and rotation in the plane of curtain walls) per node. The aluminum mullions and transoms are modelled by using 2-nodes beam elements with 3 DOF per node. The connection between these elements is considered rigid. The interface between the glass panel and the aluminum frame is modelled by gap elements (Figure 2.16). These gap elements work in compression, in the plane of the glass panels and when the frame-glass space becomes zero. The space between the glass panel and the aluminum frame is simulated by these links. (Aiello et al., 2017; Casagrande et al., 2019) have performed non-linear analysis using gap elements to quantify the stiffness and strength of curtain walls.

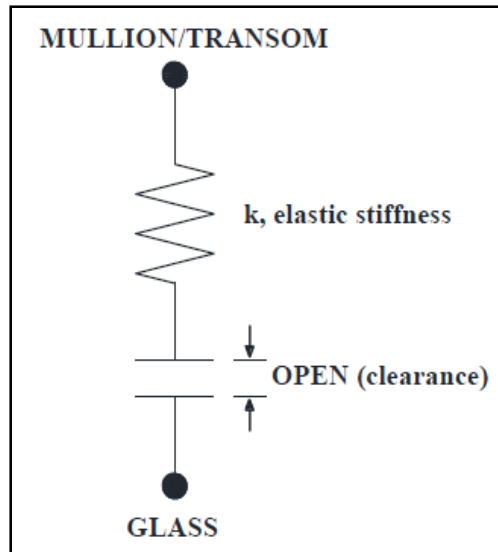


Figure 2.16 Connection between the aluminium frame and the glass panel

Caterino et al. (2017a)

Elastomeric gaskets are used to model the frictional behavior of the rubber gasket located between the glass panel and the aluminum frame (Caterino et al., 2017a). These elements are mainly subjected to shear deformations. The mechanical behavior of the joints is modelled by inserting nonlinear connections. These links are characterized by a behavior governed by the following parameters: elastic stiffness, yield force, post-yield stiffness ratio and yield exponent. The friction behavior of rubber is described with an elastoplastic Wen link. This connection is illustrated in Figure 2.17. In addition, this link is modelled in parallel with a gap element, which serves to simulate the gap between the glass panel and the frame. Characteristics of curtain wall connections are presented in ANNEX III.

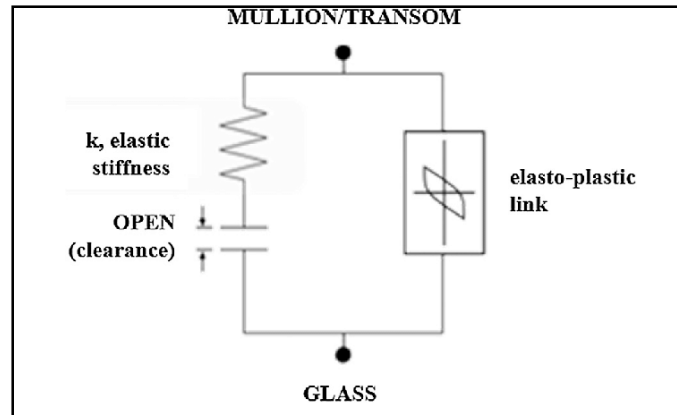


Figure 2.17 Elasto-plastic Wen link
Caterino et al. (2017a)

2.5 Calibration of FEM

The disparity between the numerical model and the structure is expected and can be explained by many factors, such as the fact that the numerical model is perfectly fixed at the base and at its connections, which is not the case in practice as the foundation has some flexibility (Farghaly et Ahmed, 2013; Stewart et al., 1999). Moreover, material defects and fabrication and construction tolerances can lead to disparities between the model and the structure. To account for differences between the model and reality, the finite element models must be calibrated with experimental tests such as AVMs (Brincker et Ventura, 2015). The references in this project are the modal parameters obtained with the AVMs at different stages of construction of the MDE. These measurements reflect the real dynamic behavior of the structure at low-excitation frequency and make it possible to validate the FEM.

2.5.1 Generalities concerning the calibration process

Before starting the calibration process of numerical models, it is instructive to have a good sense of what could be changed in a finite element model to perform meaningful calibration. Often a rather small uncertainty is present due to mass density and young's modulus, and a larger uncertainty is present due to incomplete information about connections and support

conditions. According to (Asgarian et McClure, 2014; A. Asgarian et McClure, 2012; Brincker et Ventura, 2015) the following parameters can have an effect on the calibration simulations:

- The material properties: the Poisson's ratio, the density, the modulus of elasticity, and the compressive strength.
- The dimension of SCs and NSWs

The objective of the calibration is to make the natural periods of the model coincide with those of the reference measurements, within an acceptable margin of $\pm 10\%$. As a guideline, Brincker et Ventura (2015) have underlined the uncertainty values that have been used by the authors for some important parameters influencing calibration studies. Table 2.8 indicates all the uncertainties on the parameters of a modelling.

Table 2.8 Uncertainties on the parameters of a numerical model
Adapted from (Brincker et Ventura, 2015)

Physical quantity	Level of uncertainty (%)
Modulus of elasticity and mass density of steel, and other metals	1-5
Modulus of elasticity and mass density of concrete, wood, and fiber reinforced materials	5-20
Total mass	1-5

Many techniques are available to achieve the calibration, such as manual calibration, automated calibration, and modifying the modulus of elasticity of materials to establish the best agreement between experimental results and numerical ones. In this research, the manual calibration was retained to calibrate the bare and full frame. The periods were calculated based on gross sections (i.e., uncracked sections) because the building was calibrated based on service loads. In addition, it is recently constructed.

2.5.2 Manual calibration

The manual updating technique begins with the identification of differences in experimental and analytical modal parameters, such as natural frequencies and mode shapes. Next, based on this inspection of results, the analyst must select parameters in the model to change and adjust them in a way that will improve the match between the model results and the experimental ones. This process may be repeated several times until the desired correspondence between experimental and analytical modal characteristics is achieved. There are significant limitations and difficulties in trying to obtain a good general correlation between experimental and analytical modal properties for a large civil engineering structure using this model updating technique. However, if the objective of the model updating process is just to obtain a model that matches one, two or three experimental modes, then manual updating may suffice (Brincker et Ventura, 2015).

2.5.3 Automated calibration

The automated calibration technique follows the same general procedures as in manual calibration except that the process is computer aided. The analyst can perform an in-depth inspection of the FE model using a sensitivity analysis. The computer program can determine the sensitivity of the dynamic characteristics of the model to parameters such as modulus of elasticity and mass density of materials, slab thickness, and applied loads, which can provide valuable information as to which parameters should be selected for calibration. Once the user has completed the parameter selection, the computer program runs several iterations to match the experimental and analytical modal properties by changing the selected model parameters. In this technique, the analyst can perform an in-depth inspection of the FE model using a sensitivity analysis. The computer program can determine the sensitivity of the dynamic characteristics of the model to many parameters, which can provide valuable information as to which parameters should be selected for calibration (Brincker et Ventura, 2015).

2.5.4 Modifying the modulus of elasticity

This technique consists in modifying the young's modulus E . By permitting independent variations in Young's modulus, E , for the different groups of structural elements, it is possible to have a sense how these affect the overall stiffness of the structure, as there is always a degree of uncertainty about the actual material properties of elements and the most realistic representation of stiffness in the model (Brincker et Ventura, 2015). From dynamics principles, it is known that:

$$f = \frac{\omega}{2\pi} = \frac{\sqrt{\frac{k}{m}}}{2\pi} = \frac{\sqrt{\frac{f(E)}{m}}}{2\pi} \quad (2.3)$$

Where:

f = the natural frequency of the structure (Hz)

ω = the angular frequency of the structure (rd/s)

k = the stiffness of the structure (N/m)

m = the mass of the structure (Kg)

E = the modulus of elasticity of the structure (N/m²).

By assuming that the moment of inertia and the length of elements is constant, the stiffness becomes only a function of E . In addition, keeping the mass as constant, the frequency only becomes function of the square root of E . Therefore, the adjustment of the modulus of elasticity E can be made according to Equation 2.4:

$$E_{adj} = E_i \left(\frac{f_m}{f_n} \right)^2 \quad (2.4)$$

Where:

E_{adj} = the adjusted modulus of elasticity (N/m²)

E_i = the initial modulus of elasticity (N/m²)

f_m = the natural frequency measured in situ (Hz)

f_n = the natural frequency initially found with the computer model (Hz)

2.5.5 Calibration of the bare frame

Due to insufficient ambient vibration measurements for the bare frame, it was calibrated by comparing the fundamental period of the model to that obtained in AVMs (Table 2.9).

Table 2.9 Comparison of the period obtained by AVMs at bare frame stage with that of calibrated and non-calibrated models

Mode	AVMs		Non calibrated model		Calibrated model	
	Shape	T (s)	T (s)	Difference	T (s)	Difference
1	Transversal translation + torsion	0.525	0,45	-14.29%	0.483	-8%

Before calibration, the difference of the fundamental period between the AVMs and the non-calibrated model reached -14.29%, which is unacceptable since greater than 10%. Therefore, the model was updated by modifying the properties of concrete and the applied loads (Table 2.10). Once the calibration has been carried out, the period difference obtained is -8%. Therefore, the calibrated model reflects the behavior of the MDE at the bare frame stage.

Table 2.10 Calibration of the bare frame model

Parameters	Modification
Weight of concrete	+4%
Elasticity modulus of concrete	-10%
Applied loads	+3%

The new values of the material properties after calibration are presented in ANNEX IV.

2.5.6 Calibration of the full-frame model

The first two vibration periods of AVMs were used to calibrate the full frame finite element model (Table 2.11).

Table 2.11 Comparison of the period obtained by AVMs at full-frame stage with that of calibrated and non-calibrated models

Mode	AVMs		Non calibrated model		Calibrated model	
	Shape	T (s)	T (s)	Diff	T (s)	Diff
1	Transversal translation + torsion	0.46	0.475	3.26%	0.472	2.61%
2	Longitudinal translation	0.401	0.452	12.71%	0.403	0.5%

Before calibration, the difference of the periods between the AVMs and the non-calibrated model reached +3.26% and +12.71%, which is unacceptable for the second period since it is greater than 10%. Therefore, the model was updated by modifying the properties of NSWs and the applied loads (Table 2.12). Once the calibration has been carried out, the differences in the periods become +2.61% and +0.5%.

Table 2.12 Calibration of the full frame model

Parameters	Modification
Weight of glass panels	-20%
Weight of aluminum frames	-5%
Weight of masonry infill walls	-20%
Elasticity modulus of glass panels	+20%
Elasticity modulus of aluminum frames	+5%
Elasticity modulus of masonry infill walls	+20%
Applied loads	-5%

The adjusted values of the material properties after calibration are presented in ANNEX IV. The mode shape correlation coefficient presented in Equation (2.5) (Ewins, 2009) was used to validate the calibration (Table 2.13).

$$r = \frac{\sum (x_i - \bar{x})(y_i - \bar{y})}{\sqrt{\sum (x_i - \bar{x})^2 \sum (y_i - \bar{y})^2}} \quad (2.5)$$

Where r is the correlation coefficient, x_i is the value of the displacement of the joint representing the tromino in the numerical model, \bar{x} is the mean of the values of the x-variables, y_i is the displacement of the tromino in ARTeMIS, \bar{y} is the mean of the values of the y-variables.

Table 2.13 Correlation between the mode shapes obtained by AVMs at full-frame stage and that of calibrated and non-calibrated models

	AVMs	Non calibrated model	Calibrated model	
Mode	Shape	correlation	correlation	Diff
1	Transversal translation + torsion	0.902	0.916	1.55%
2	Longitudinal translation	0.895	0.894	-0.11%

Concerning the correlation between the mode shapes obtained by AVMs and that of the calibrated model, the correlation is acceptable because it is more than 85% (91.6% for mode 1 and 89.4% for mode 2).

Therefore, the calibrated model reflects the behavior of the MDE at the full-frame stage.

2.5.7 Comparison of mode shapes of calibrated FE models

Mode shapes were generated through numerical models; they remained unchanged in both stages. This is explained by the presence of masonry infill walls only on the ground floor. Figure 2.18 illustrates the comparison of mode shapes for the calibrated bare frame and full frame.

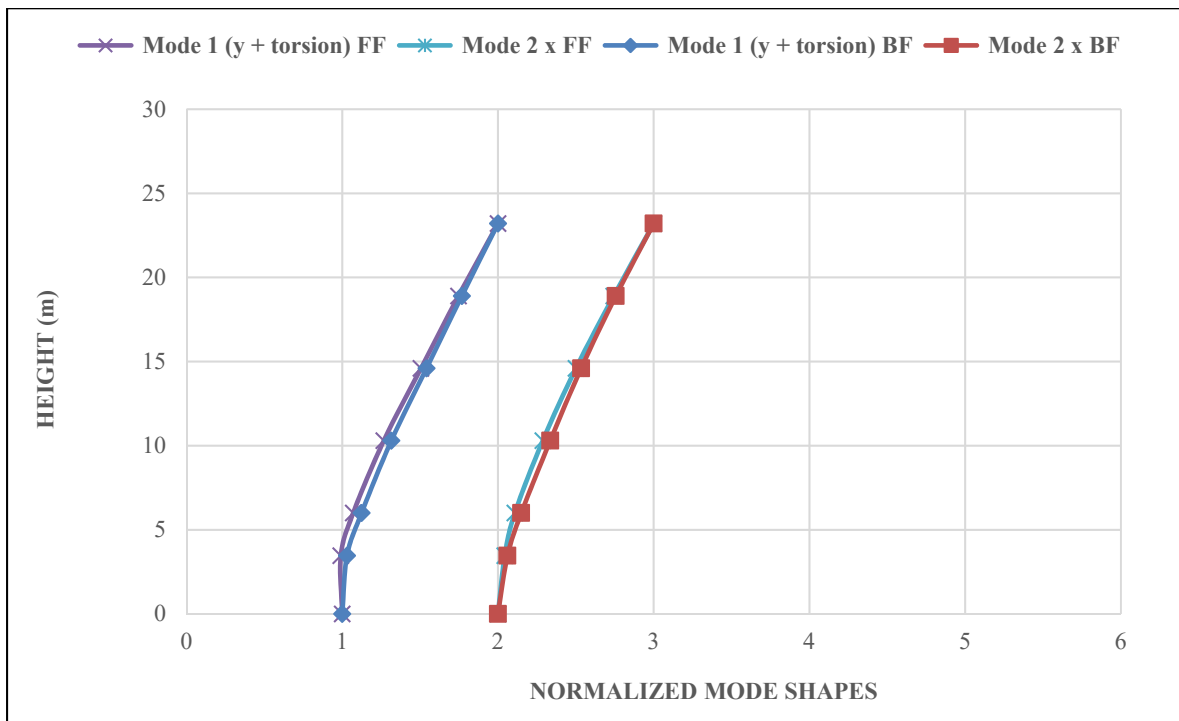


Figure 2.18 Normalized mode shapes for the MDE (modes 1 and 2)

2.6 Conclusion

A description of the MDE buildings is provided in this chapter. The brief description of SCs and NSWs, and the connections between these components are presented.

The modal parameters of the MDE are obtained for the bare frame (mode 1), and the full frame (modes 1 and 2). A comparison of the AVMs is carried out at the different stages of construction, namely in the bare frame, and full frame of the MDE. Then, a comparison of the

periods is also carried out between the NBC and the AVMs. In addition, the simplifying assumptions used, the modelling and the calibration of the FE models for the MDE building are presented in chapter 2.

In the next chapter, the stiffness and mass contribution of masonry infill walls and curtain walls will be presented and discussed. In addition, a parametric study will be conducted to assess the effect of masonry infill walls on the fundamental period, and mass and stiffness contribution.

CHAPTER 3

EVALUATION OF THE STIFFNESS AND MASS CONTRIBUTION OF NSWs

In this chapter, the relative contribution of stiffness and mass of masonry infill walls and curtain walls will be presented. In addition, a parametric study will be conducted to assess the effect of masonry infill walls on the fundamental period, and mass and stiffness.

3.1 Stiffness and mass contribution of NSWs

Once the numerical model has been calibrated at the full-frame stage, it is possible to estimate the stiffness and mass contribution of masonry infill walls relative to the full-frame building. It is adequate to use Equation 3.1 with the characteristics of the full-frame model and Equation 3.2 with the characteristics of the full-frame model without masonry walls or curtain walls (it depends on which NSC is considered for assessing its relative contribution). The full frame was used as a reference since it was calibrated with reliable AVMs.

$$\omega_1 = 2\pi f_1 \quad (3.1)$$

$$\omega_2 = 2\pi f_2 \quad (3.2)$$

Knowing the ratios of frequency and mass at the two stages of construction, it is possible to obtain the stiffness ratio which results in Equation 3.3.

$$\frac{k_1}{k_2} = \left(\frac{f_1}{f_2}\right)^2 \frac{m_1}{m_2} \quad (3.3)$$

The stiffness and mass contribution of masonry infill walls and curtain walls are represented in Tables 3.1 to 3.4.

Table 3.1 Stiffness and mass contribution of masonry infill walls in the transversal direction

m₁ (Kg)	15 241 590
f₁ (Hz)	2.12
T₁ (s)	0.472
m₂ (Kg)	14 275 535
f₂ (Hz)	2.00
T₂ (s)	0.5
m₁/m₂	1.068
T₁/T₂	0.94
k₁/k₂	1.20
% Mass	+6.8%
% Period	-5.6%
% Stiffness	+20%

Table 3.2 Stiffness and mass contribution of masonry infill walls in the longitudinal direction

m₁ (Kg)	15 241 590
f₁ (Hz)	2.48
T₁ (s)	0.403
m₂ (Kg)	14 275 535
f₂ (Hz)	2.38
T₂ (s)	0.42
m₁/m₂	1.068
T₁/T₂	0.96
k₁/k₂	1.16
% Mass	+6.8%
% Period	-4.05%
% Stiffness	+16%

Tables 3.1 and 3.2 show that the stiffness ratio is equal to 1.2 and 1.16 between the full-frame stage and the full frame without masonry infill walls in the transversal and longitudinal direction respectively, which corresponds to a stiffness contribution of +20% and +16% for the masonry infill walls of the MDE. This contribution is explained by the important presence of masonry infill walls on the ground floor in both directions. The mass contribution is +6.8% over the entire building. This result is comparable to the results of several studies (Bonne, 2018; Chaker et Cherifati, 1999; Negro et Verzeletti, 1996; Su et al., 2005), who determined ratios varying from 1.2 to 11.7 for low-rise buildings. This ratio is explained by the presence of masonry infill wall only on the ground floor of the MDE.

Finally, since these NSWs increase the stiffness and the mass, they therefore decrease the fundamental period of the structure by -5.6%. This value remains lower than the percentage of 15% recommended by the NBC Sentence 4.1.8.3.(7) (NRC, 2015). Therefore, the modified period cannot be used to determine the design forces although they provide an additional stiffness of +20% and +16%. Hence, the NBC should consider the mass and the stiffness in the calculation of the fundamental period, not only the height of the building.

Table 3.3 Stiffness and mass contribution of curtain walls in the transversal direction

m₁ (Kg)	15 241 590
f₁ (Hz)	2.12
T₁ (s)	0.472
m₂ (Kg)	15 132 416
f₂ (Hz)	2.08
T₂ (s)	0.481
m₁/m₂	1.0072
T₁/T₂	0.98
k₁/k₂	1.05
% Mass	+0.72%
% Period	-1.9%
% Stiffness	+5%

Table 3.4 Stiffness and mass contribution of curtain walls in the longitudinal direction

m₁ (Kg)	15 241 590
f₁ (Hz)	2.48
T₁ (s)	0.403
m₂ (Kg)	15 132 416
f₂ (Hz)	2.54
T₂ (s)	0.393
m₁/m₂	1.0072
T₁/T₂	1.025
k₁/k₂	0.96
% Mass	+0.72%
% Period	+2.54%
% Stiffness	-4%

Tables 3.3 and 3.4 show that the stiffness ratio is equal to 1.05 and 0.96 between the full-frame stage and the full frame without curtain walls in the transversal and longitudinal direction respectively, which corresponds to a stiffness contribution of +5% for the curtain walls in the transversal direction, and -4% in the longitudinal direction. However, Li et al. (2011) found a stiffness contribution of at least +12% for the curtain walls. This difference in contribution is explained by a presence of curtain walls on all the faces and floors of the building in east and west sides (transversal direction) and disconnection from upper floors in the north side (longitudinal direction). The mass contribution is +0.72% over the entire building.

As previously seen with masonry infill walls, curtain walls decrease the period of the structure by -1.9%. This value is always lower than the 15% recommended by NBC 2015.

By comparing the full frame with masonry walls and curtain walls to the bare frame, these NSWs contribute to the stiffness of the building by +24% and +5.6% in the transversal and longitudinal directions respectively. Therefore, it can be concluded that masonry walls contribute more to the stiffness of the building than curtain walls.

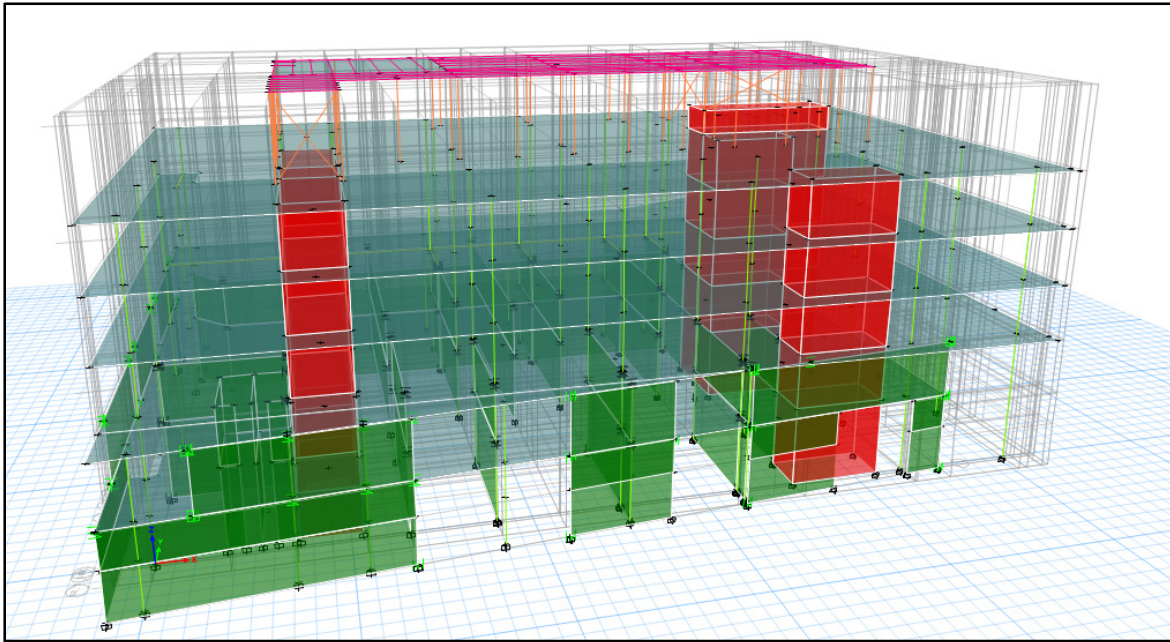
3.2 Parametric study of the effect of masonry infill walls on the fundamental period, and mass and stiffness contribution

In this section, a parametric study is conducted to assess the effect of masonry infill walls on the fundamental period, and mass and stiffness. The parametric study consists of three cases: the presence of masonry infill walls in the ground and 2nd floors, the presence of masonry infill walls in the ground, 2nd and 3rd floors, and the presence of masonry infill walls in all floors (the plans of distribution of masonry walls are represented in ANNEX III). Figures 3.1 to 3.3 illustrate the arrangement of the masonry walls for the three cases.

Table 3.5 provides a summary of the surface of masonry walls in each floor for the three cases. The model of the full frame without curtain walls was taken as a reference. The results of this parametric study are represented in Tables 3.6, 3.7, and 3.8.

Table 3.5 The surface of masonry walls in each floor for each case

Floor level	Surface (m ²)			
	Floor surface	Masonry walls in GF and 2nd floor	Masonry walls in GF, 2nd, and 3rd floor	Masonry walls in all floors
Appentis	875	-	-	-
Roof	2537	-	-	-
5 th floor	2246	-	-	1303
4 th floor	2367	-	-	1303
3 rd floor	3031	-	1303	1303
2 nd floor	2574	1714	1714	1714
Ground floor	3031	1740	1740	1740
Total	16661	3454	4757	7363

Figure 3.1 Masonry walls in the ground and 2nd floors

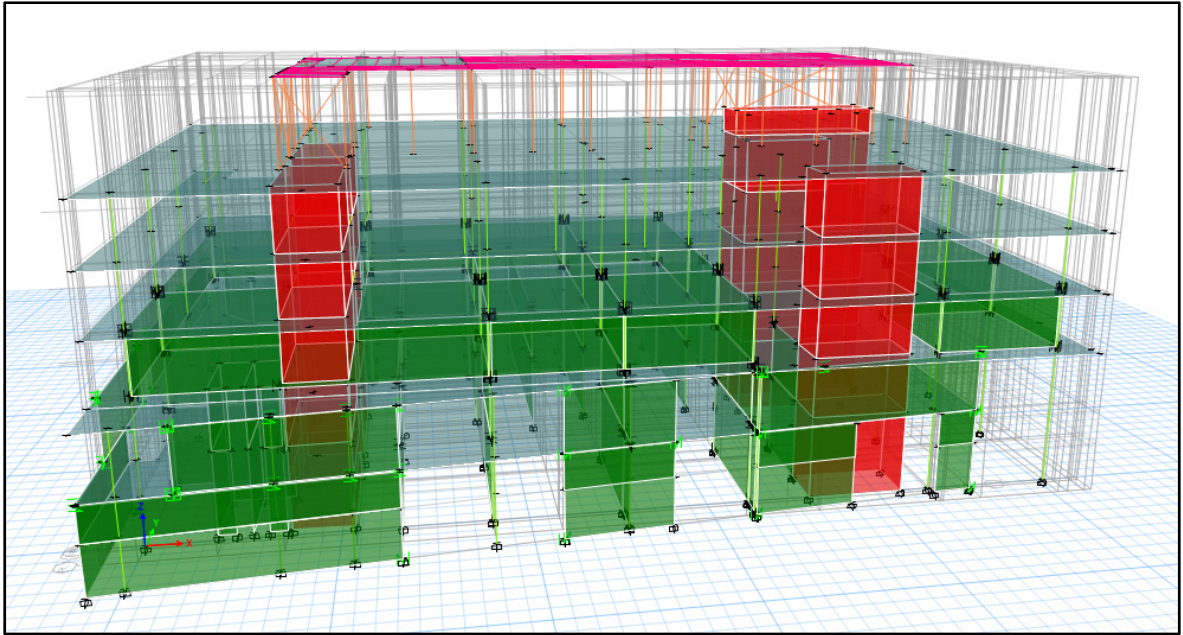


Figure 3.2 Masonry walls in the ground, 2nd, and 3rd floors

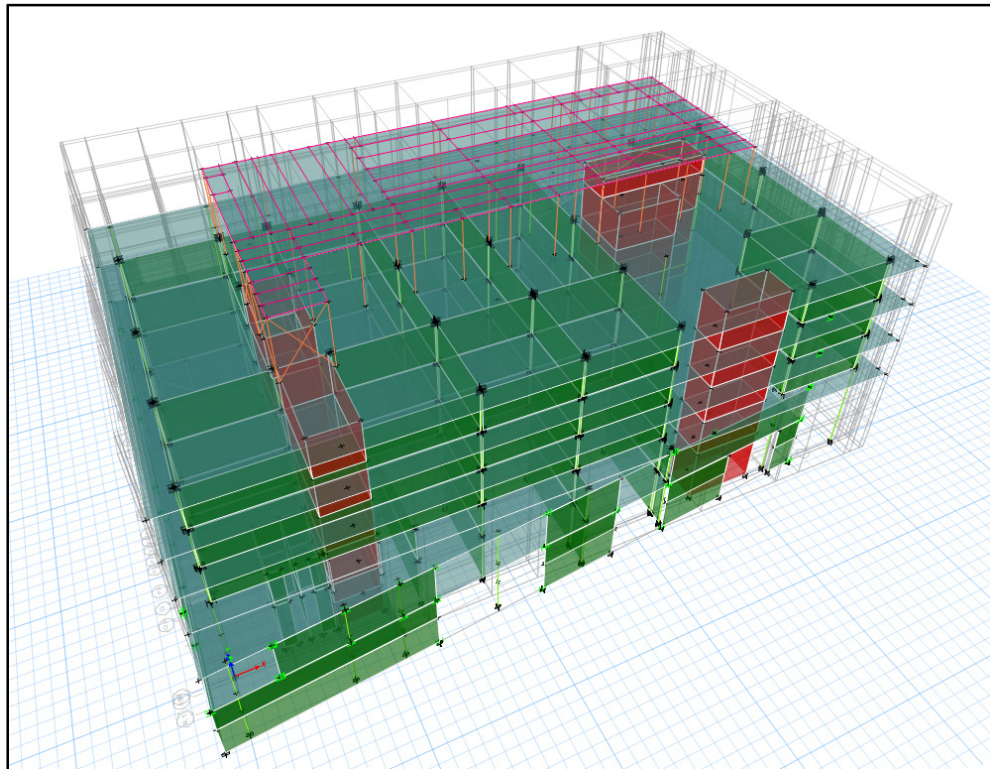


Figure 3.3 Masonry walls in all floors

Table 3.6 Results of the parametric study of masonry walls in the ground and second floors

m₁ (Kg)	15 308 155
f₁ (Hz)	2.227
T₁ (s)	0.449
m₂ (Kg)	15 132 416
f₂ (Hz)	2.08
T₂ (s)	0.481
m₁/m₂	1.012
T₁/T₂	0.93
k₁/k₂	1.16
% Mass	+1.2%
% Period	-6.7%
% Stiffness	+16.1%

Table 3.7 Results of the parametric study of masonry walls in the ground, second, and third floors

m₁ (Kg)	15 647 706
f₁ (Hz)	2.381
T₁ (s)	0.420
m₂ (Kg)	15 132 416
f₂ (Hz)	2.08
T₂ (s)	0.481
m₁/m₂	1.03
T₁/T₂	0.87
k₁/k₂	1.36
% Mass	+3.4%
% Period	-12.7%
% Stiffness	+35.6%

Table 3.8 Results of the parametric study of masonry walls in all floors

m_1 (Kg)	16 636 493
f_1 (Hz)	2.463
T_1 (s)	0.406
m_2 (Kg)	15 132 416
f_2 (Hz)	2.08
T_2 (s)	0.481
m_1/m_2	1.10
T_1/T_2	0.84
k_1/k_2	1.54
% Mass	+10%
% Period	-15.6%
% Stiffness	+54.3%

Tables 3.5 to 3.7 show that by adding masonry infill walls to the building, the stiffness increased in a range between +16.1 and +54.3%, and the mass increased in range between +1.2 and +10%. Therefore, adding masonry infill walls to the building, contributes more to stiffness than in mass. Su et al. (2005) found that adding masonry infill walls to all floors rigidify the building by more than +60%. Hence, the results of this parametric study can be considered as reliable. In addition, adding masonry infill walls has decreased the fundamental period in a range between -6.7 and -15.6%. The NBC 2015 recommends neglecting the difference between periods if it is less than 15%. Therefore, it is good to consider the masonry infill walls in calculating the fundamental period when they are presented at all levels of the building.

3.3 Conclusion

The stiffness and mass contribution of masonry infill walls and curtain walls was presented for each individually in the transversal and longitudinal directions. It was found that masonry walls contribute more to the stiffness of the building than to an addition of mass in both directions. In Curtain walls contribute more to the stiffness of the building than to an addition of mass in

the transversal direction, but in the longitudinal direction, they contribute to mass more than stiffness because of the disconnection from upper floors in the north side.

In addition, a parametric study was conducted to assess the effect of masonry infill walls on the fundamental period, mass, and stiffness. It was found that adding masonry infill walls to the building adds stiffness more than mass to the building. furthermore, it decreases the fundamental period by an important percentage that should be considered while calculating the fundamental period of buildings.

The next chapter assessed the effect of NSWs of the MDE on engineering demand parameters (absolute floor accelerations and inter-story drifts) used for the design of NSWs.

CHAPTER 4

PEAK FLOOR ACCELERATIONS AND INTER-STORY DRIFTS OF THE MDE WHEN SUBJECTED TO EARTHQUAKES COMPATIBLE WITH THE UHS FOR MONTREAL

In this chapter, the effect of NSWs of the MDE on engineering demand parameters (absolute floor accelerations and inter-story drifts) used for the design of NSWs was assessed. For time history analysis of the buildings at both construction stages, the selection and scaling of synthetic ground motions compatible with Montreal uniform hazard spectrum with a return period of 2500 years are also described.

4.1 Selection and scaling of earthquakes

Using time history data of seismic accelerations compatible with the seismicity of the region makes it possible to obtain the history of the responses of the building and can be applied as much in the linear domain as nonlinear (Tremblay et al., 2015). In this project, the building under study is analyzed with linear time history analysis. Due to lack of recorded ground motions from earthquakes in eastern Canada, seismic analysis was performed using synthetic earthquakes (Atkinson, 2009). These earthquakes must be selected and scaled to match the Montreal target spectra with 2% probability of exceedance per 50 years.

Two methods, A and B, are proposed in NBC commentary – Part J (NRC, 2015) to select and scale ground motions. The method A was adopted in this research.

This section presents the earthquake scaling process. This process is divided into three steps:

- 1- Determining the period range for the scaling,
- 2- Selecting earthquakes,
- 3- Calculating the scaling factors.

4.1.1 Period range

According to the appendix of commentary J (NRCC, 2017) section 2.2, when the analysis is performed on a three-dimensional structural model, either with ground motion components in only one horizontal direction or with pairs of orthogonal horizontal ground motion components, the upper-bound period should be based on the longest first-mode period in the two orthogonal directions and the lower-bound period should be established to include the periods of the modes necessary to achieve 90% mass participation in each orthogonal direction, without exceeding 0.15 times the shortest first-mode period in the two orthogonal directions. The lower and upper limits of the period range, T_{min} and T_{max} , are determined using Equations 4.1 and 4.2, respectively. Where $T_{90\%}$ is the period of the mode corresponding to a cumulative modal participation of 90% of the mass of the building. The periods were calculated based on gross sections (i.e., uncracked sections) according to the method A. The values of T_{Bldg1} and $T_{90\%}$ used for the selection and scaling ground motion are represented in Table 4.1.

$$T_{min} = \min [0.15 T_{Bldg1}, T_{90\%}] \quad (4.1)$$

$$T_{max} = \max [2 T_{Bldg1}, 1.5s] \quad (4.2)$$

The synthetic ground motions database in Atkinson (2009) was obtained for two scenarios. The first scenario includes the events with moment magnitude $M = 6.0$ at a fault distance R , ranging between 10 and 30 km. These events are at a period range T_{R1} , which varies from T_{min} to 1.0 s. The second scenario includes events with $M = 7.0$ at larger distances between 20 and 70 km. These events are at a period range T_{R2} , which varies from 0.5 s to T_{max} .

Table 4.1 Modal periods and ranges for ground motion scaling for the MDE

T_{Bldg1}	$T_{90\%}$	T_{R1}	T_{R2}
0.472s	0.077s	[0.071s, 1s]	[0.5s, 1.5s]

4.1.2 Selection of earthquake records

The accelerograms used in this project were derived based on a point source stochastic method and the obtained accelerograms are available at www.seismotoolbox.ca. The site also contains the response spectra for each earthquake evaluated with a 5% damping.

In this research, the seismic simulations were performed in both horizontal directions separately. The same procedure was done for both directions since according to equations (4.1) and (4.2), the period range was the same (i.e., $0.15 T_{Bldg1} \approx 0.15 T_{Bldg2} < T_{90\%}$). Each scenario therefore has 45 earthquakes from which 3 earthquakes will be chosen for a total of 12 earthquakes for the 2 scenarios (Table 4.2). Also, the vertical components of earthquakes are ignored in the analysis given that the study of vertical accelerations of floors and NSWs is not part of the objectives of this research.

The process of selecting earthquakes is explained in the following steps:

- For each period located in the scaling range, carry out the geometric mean between the spectral accelerations of the two horizontal components (separately) of the earthquake to obtain an average spectrum.
- For each period, calculate the ratio between the acceleration of the target spectrum and the acceleration of the average spectrum obtained in the previous step.
- Calculate the mean and standard deviation of the ratios obtained.
- Select the earthquakes whose mean of ratios is between 0.5 and 2 and which have the lowest standard of deviations.

The site also contains the response spectra for each earthquake evaluated with a 5% damping. For Eastern Canada, 4 earthquake scenarios were generated depending on the magnitude and distance from the source of the earthquake. Table 4.2 summarizes these different scenarios.

Table 4.2 Selected earthquakes

Scenario	Magnitude	R (Km)	Records	Scaling factors
1	6	15	East6C1_7	0.676
			East6C1_26	0.999
			East6C1_31	0.854
		30	East6C2_5	1.432
			East6C2_8	0.987
			East6C2_10	1.259
2	7	25	East7C1_25	0.529
			East7C1_28	0.669
			East7C1_30	0.539
		100	East7C2_1	1.234
			East7C2_3	1.193
			East7C2_11	1.646

The nomenclature of the record means that the record is in the east of Canada, with a magnitude of 6 or 7, soil type C and 1 or 2 refers to the proximity to the source of the earthquake (1 for near and 2 for far). The last number (after the _) is the number of the record.

The calculation of scaling factors will be represented in the next subsection.

4.1.3 Calculation of the scaling factors

According to the NBC Guidelines, each ground motion must be scaled such that its response spectrum $S_g(T)$ generally equals or exceeds the target spectrum $S_T(T)$ over the appropriate period range which is the spectrum of Montreal (downtown Montreal). The process of calculating the scaling factor for each earthquake involves the following steps (Atkinson, 2009; Tremblay et al., 2015):

- The mean of the ratios obtained in the selected earthquakes is the scaling factor.
- For each selected earthquake, apply the scaling factor to the seismic accelerations to obtain the calibrated earthquake.
- Check that the mean spectrum of the earthquakes calibrated for each magnitude scenario (magnitudes 6 and 7) is not less than 10% of the target spectrum. If necessary, apply a second scaling factor to the earthquakes. This second factor is determined incrementally by increasing the spectra concerned to obtain a difference of 10% or less between the target spectrum and the average of the spectra concerned.

The scaling factor of the selected earthquakes are represented in Table 4.2.

Figures 4.1 and 4.2 respectively show an illustration of the mean spectra and an illustration of the difference between the mean of the calibrated spectra and the target spectrum.

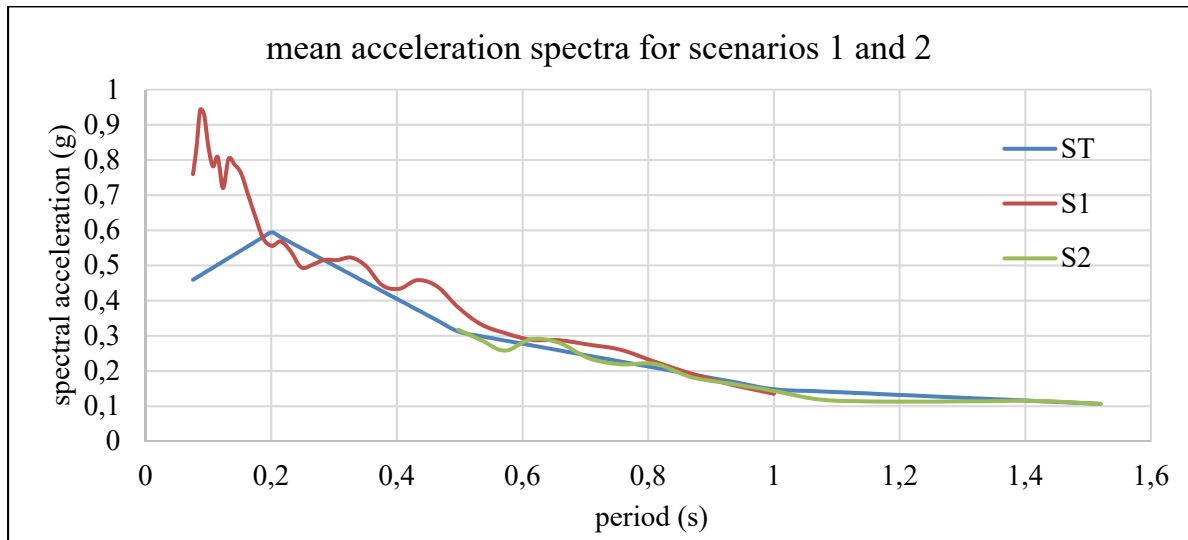


Figure 4.1 Mean acceleration spectra for scenarios 1 et 2

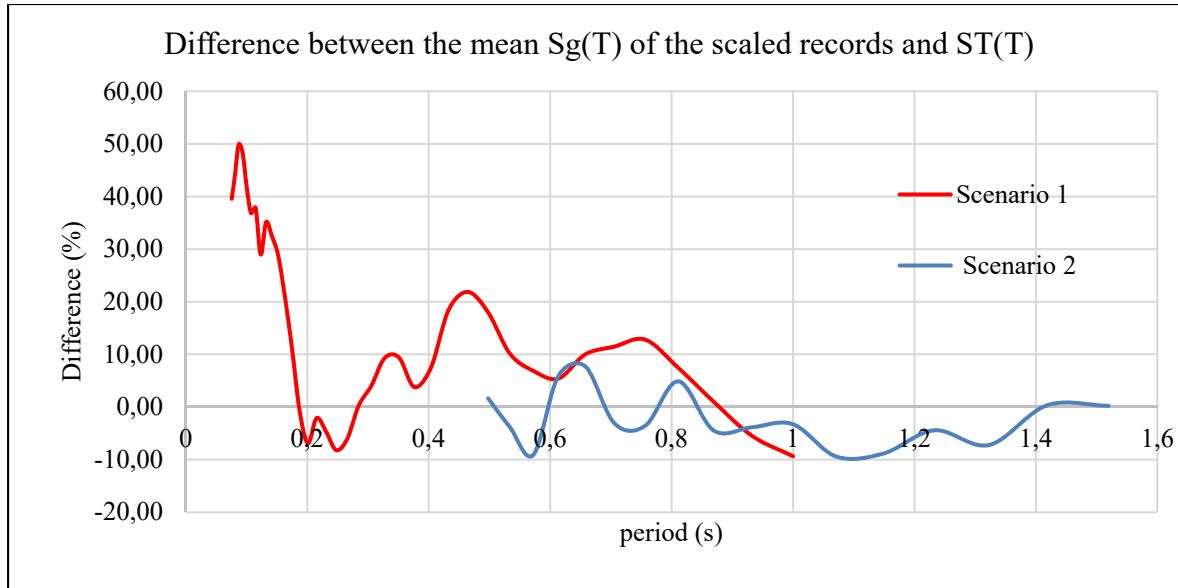


Figure 4.2 Difference between the mean $S_g(T)$ of the scaled records and $ST(T)$

4.2 Seismic response of the MDE

In this subsection, the engineering demand parameters (inter-story drift, and floor acceleration amplification) of the bare frame and full frame will be discussed. The seismic response was calculated based on cracked sections. According to the NBC 2015 (NRC, 2015), the moment of inertia for cracked sections is $0.75 I_g$ for shear walls, $0.4 I_g$ for beams, and $0.7 I_g$ for columns. Where I_g is the moment of inertia of the gross section.

4.2.1 Inter-story drift computed with finite element models

The FE models of the building made it possible to determine the inter-story drift of each floor. The inter-story displacement of the mechanical room located on the roof of the building is neglected since it is not part of the structural system of the building.

Tables 4.3 and 4.4 compare the inter-story drift in longitudinal and transversal direction respectively of each floor of the building in two cases: with and without NSWs in the building and with the FEMA 356 limits for immediate occupancy (IO).

Table 4.3 Comparison of the inter-story drifts in longitudinal direction in both stages of construction

Storey	Longitudinal direction		Difference	FEMA 356
	Without NSWs (%)	With NSWs (%)		
Roof	0.33	0.27	-19.5%	1%
5	0.33	0.27	-18.4%	1%
4	0.30	0.25	-17.5%	1%
3	0.26	0.17	-35.7%	1%
2	0.20	0.12	-38.8%	1%
Mezzanine	0.12	0.07	-44.3%	1%

Table 4.3 shows that there is a decrease in the inter-story drift for all stories between the two cases (with and without NSWs). This decrease varied from -17.5% to -44.3% and it is explained by the important presence of curtain walls in floors and masonry walls on the ground floor. Figure 4.3 shows the vertical distribution of the inter-story drift ratio along the height of the buildings in the longitudinal direction.

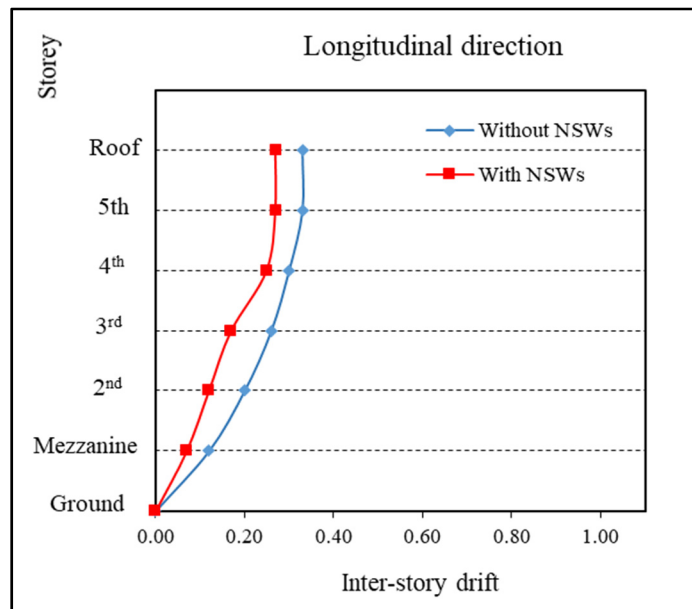


Figure 4.3 Inter-story drifts in the longitudinal direction at both stages of construction

Table 4.4 Comparison of the inter-story drifts in transversal direction in both stages of construction

Storey	Transversal direction		Difference	FEMA 356
	Without NSWs (%)	With NSWs (%)		
Roof	0.43	0.34	-19.7%	1%
5	0.43	0.35	-18.1%	1%
4	0.38	0.33	-14.6%	1%
3	0.36	0.27	-24.7%	1%
2	0.42	0.12	-72.3%	1%
Mezzanine	0.11	0.08	-27.5%	1%

In the transversal direction, Table 4.4 shows a decrease in the inter-story drift for all stories between the two cases (with and without NSWs). This decrease varied from -14.6% to -72.3% and it is explained by the important presence of curtain walls in floors and masonry walls on the ground floor. Figure 4.4 shows the vertical distribution of the inter-story drift ratio along the height of the buildings in the transversal direction.

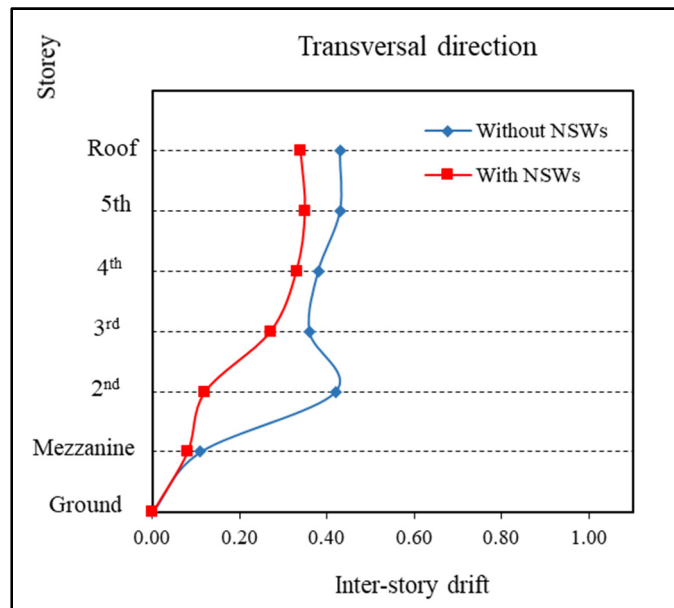


Figure 4.4 Inter-story drifts in the transversal direction in both stages of construction

By comparing the inter-story drift in both directions, we can notice that the NSWs decrease the inter-story drift by an equal percentage in both directions for almost all floors, except for the 2nd floor, where the decrease is -72.3% in the transversal direction and -38.8% in the longitudinal direction. This is explained by the importance presence of masonry panels in the south side of the MDE.

It can be noted that the inter-story drift ratios obtained from numerical models are less than the FEMA 356 IO limit of 1% for both directions.

4.3 Floor acceleration amplification (FAA)

In this section, the variation of PFA/PGA along the building height is compared with the height modification factor A_x proposed in NBC 2015 (NRC, 2015). In addition, a comparison between the FAA of the bare frame and the full frame is made.

4.3.1 At full frame stage using AVMs and FEM in the transversal direction

Figure 4.5 illustrates the comparison between the FAA resulting from the first mode of vibration for AVMs, 3 values (median, 16th percentile, and 84th percentile) of the FAA in the FEM full frame, and NBC 2015 in the transversal direction. The NBC 2015 recommends the same linear variation of PFA/PGA from 1 at ground level to 3 at roof level.

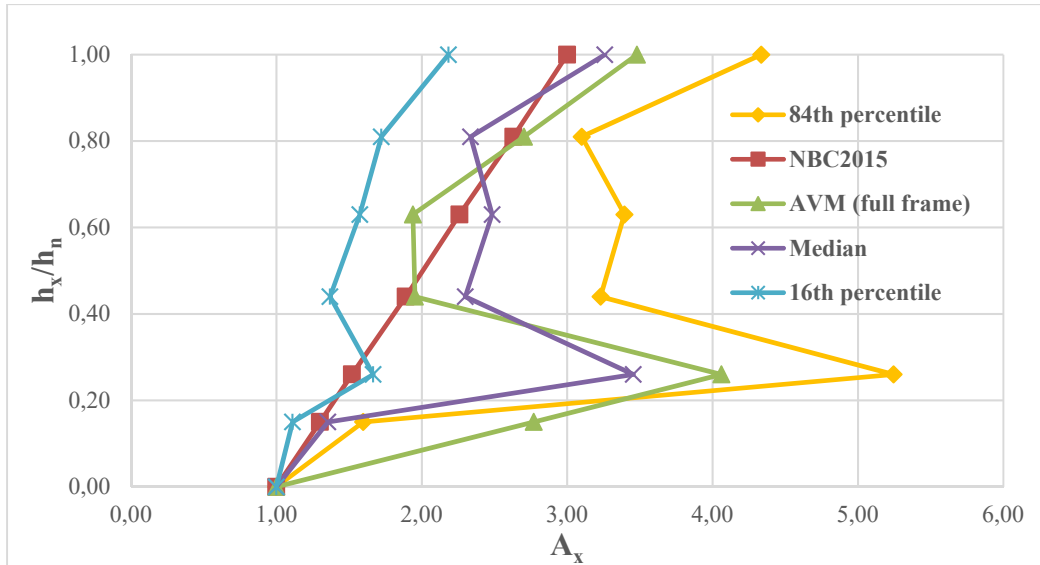


Figure 4.5 FAA of the full frame based on AVMs, the numerical model and NBC 2015 provisions in the transversal direction

A first observation is that the A_x factor are underestimated by NBC 2015 at almost every floor and roof. The values of FAA are presented in ANNEX V. Considering the 84th percentile value of the responses, the roof-FAA is 4.33 for the FEM full frame, 3.48 for the AVMs_{full frame}, and 3 for the NBC 2015. Similar results were found by Asgarian et McClure (2020), where they conducted linear seismic analysis on 27 reinforced concrete buildings with 2 types of LFRS (reinforced concrete shear walls system and reinforced concrete moment-resisting frame system) located in Montreal, for which AVMs are used to determine their in situ 3D dynamic characteristics. They observed that the amplification factors vary between 2.3 and 4.1 for medium-rises buildings.

A second observation relates to the trends of the variation of PFA/PGA along the building height. The assumption of linear variation is not accurate for medium-rises buildings. This is because the first mode is not totally lateral (transversal translation + torsion), and the effect of higher modes especially in lower floors.

4.3.2 Comparison of the FAA at full frame stage using AVMs and FEM in the longitudinal direction

Figure 4.6 illustrates the comparison between the FAA resulting from the first mode of vibration for AVMs, 3 values (median, 16th percentile, and 84th percentile) of the FAA in the FEM full frame, and NBC 2015 in the longitudinal direction. However, in this case study, the 1st mode of vibration is not dominant. There is an effect of higher modes (see modal participation mass ratio in ANNEX IV). The FAA of AVMs were calculated by taking the peak floor acceleration registered at each story.

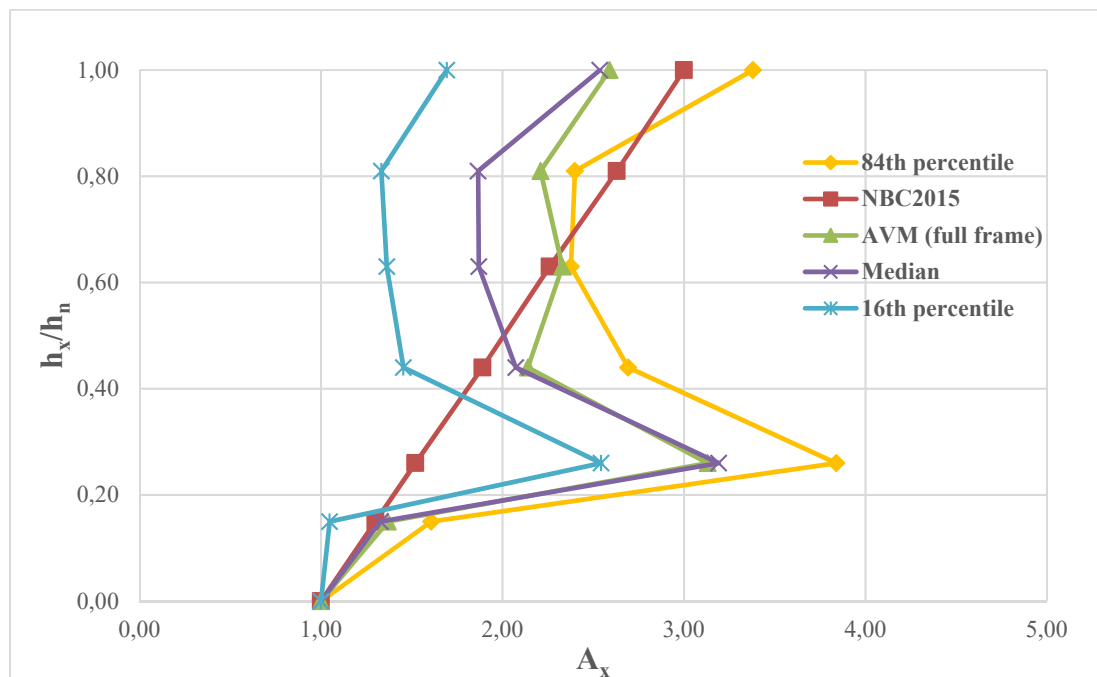


Figure 4.6 FAA of the full frame based on AVMs, the numerical model and NBC 2015 provisions in the longitudinal direction

Figure 4.6 shows that the A_x ratios are underestimated by NBC 2015 at almost all floors, especially in lower floor level (between $0.2h$ and $0.6h$). The FAA values computed from AVMs_{full frame} are almost equal to those of the median values of the numerical models in the lower floors. However, they yield higher values in the upper floors. Considering the 84th percentile value of the responses, the roof-FAA is 3.38 for the FEM full frame, 2.59 for the

$AVM_{full\ frame}$, and 3 for the NBC 2015. In addition, it is observed that the linear variation assumption is not accurate especially in lower floors which are affected by higher modes. Therefore, considering only first mode of vibration can lead to underestimations of peak floor acceleration demands (Taghavi et Miranda, 2005).

4.3.3 Comparison of FAA of bare frame and full frame using FEM

The objective of this section is to compare the FAA of the bare frame and the full frame to study the influence of the NSWs on the accelerations of the floors.

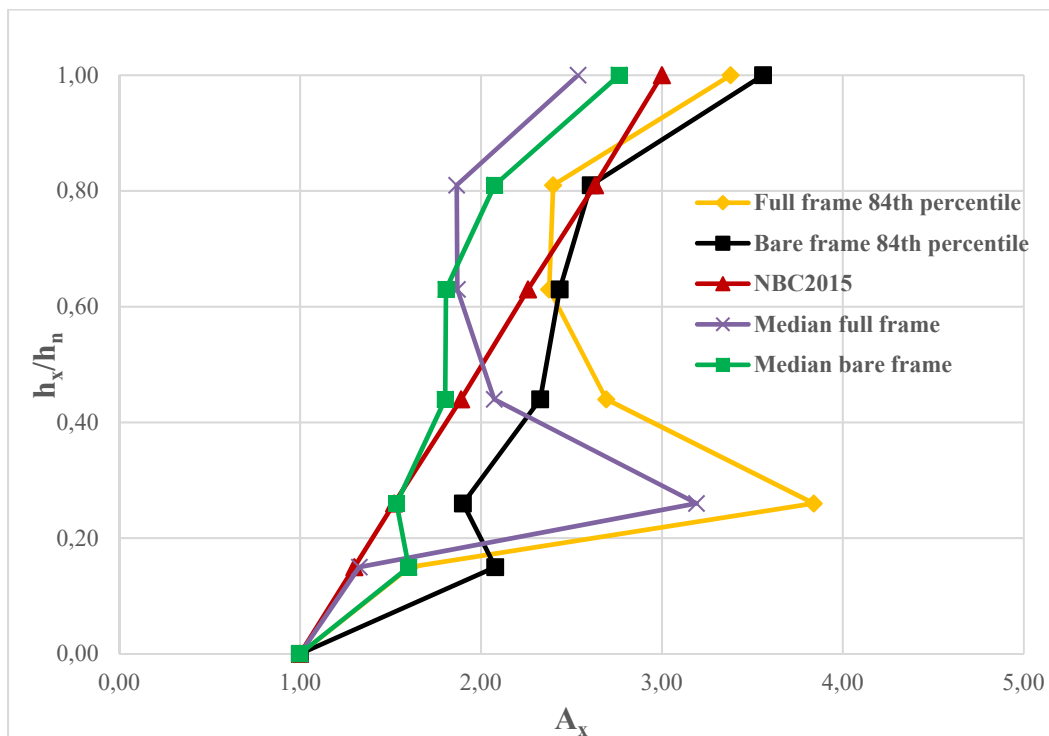


Figure 4.7 Comparison of the FAA of bare frame and full frame in the longitudinal direction

Figure 4.7 shows that the 84th percentile of the FAA of the full frame is higher than those of bare frame in intermediate floors (2nd, and 3rd). This is due to the presence of NSWs and the full connection with SCs from all sides. For the mezzanine, and the upper floors (4th, 5th, and roof), the FAA of the bare frame are higher than those of the full frame. This is due to the

disconnection between the curtain walls and the SCs in the north side of the upper floors, and the effect of higher modes on the mezzanine. In addition, the FAA deduced from AVMs, show that the FAA at the bare frame roof (2.77) is higher than that of the full frame (2.59). The values of the FAA are represented in ANNEX V. Moreover, the FAA are much higher at intermediate floor levels especially in the 2nd floor where the FAA is 3.84. This value leads to a high floor acceleration which will affect the acceleration sensitive components such as ceilings, mechanical pipes and machinery.

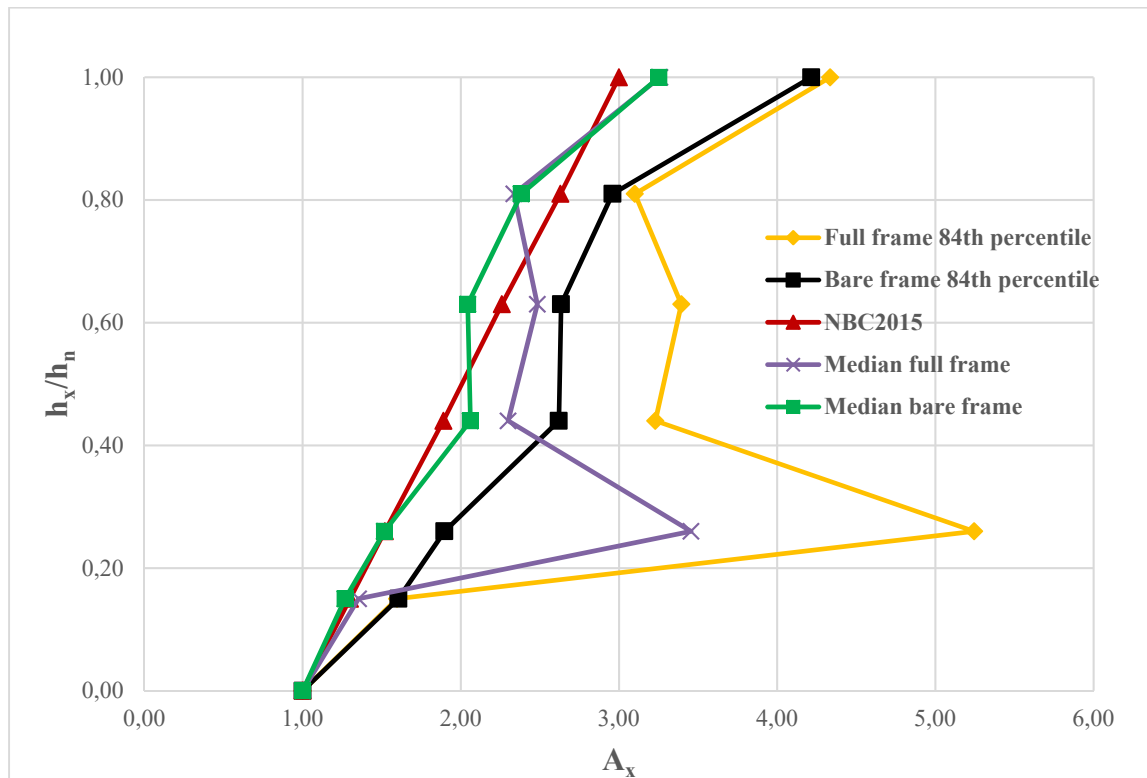


Figure 4.8 Comparison of the FAA of bare frame and full frame in the transversal direction

Figure 4.8 shows that the 84th percentile of the FAA of the full frame is higher than those of bare frame in almost all floors, and close at the rooftop. This is due to the presence of NSWs and the full connection with SCs from all sides. In addition, the FAA are much higher at intermediate floor levels especially in the 2nd floor where the FAA is 5.25. This value leads to

a high floor acceleration which will affect the acceleration sensitive components such as ceilings, mechanical pipes and machinery.

It should be noted that the addition of the NSWs led to a decrease in the fundamental period of the building by 2.3% according to the FEM. In addition, the FAA deduced from AVMs, show that the FAA at full frame roof (3.48) is higher than that of the bare frame (2.95). Perrone et Filiatrault (2018) have found similar results where the FAA at bare frame roof was around 2.85 and 3.6 at full frame roof.

Based on these results, the conclusion would be that a reduction of the fundamental period, and the interaction between NSWs and SCs may affect the absolute floor acceleration.

4.4 Conclusion

The floor acceleration amplifications and inter-story drifts under the effect earthquake records compatible with the UHS for Montreal were assessed. It was observed that NSWs have contribute to the reduction of inter-story drift at all floors in both directions, and to rigidify the building as a result. In addition, it was demonstrated that the NBC 2015 equation underestimates the floor acceleration amplification along the height, which may affect the absolute floor acceleration.

CONCLUSION

The main objective of this research is the evaluation of the effects of the curtain walls and masonry walls, on the dynamic properties (mode shapes, fundamental period, damping ratios, and lateral stiffness), and engineering demand parameters (absolute floor accelerations, and inter-story drifts) of a case study building located on the campus of École de Technologie Supérieure (ÉTS) in Montreal by using numerical models and AVMs. While detailed conclusions have been made at the end of each chapter, an overall conclusion is made here, and the study led to the following conclusions:

As part of this research, a literature review is carried out on NSWs in chapter 1. It appeared that:

- These components could affect the fundamental period.
- Damping ratio could be significantly underestimated during the design stage, and the only way to accurately estimate damping is to consider additional factors such as NSWs.
- Masonry infill walls, and curtain walls are NSWs that help to rigidify the structure depending on their quantity in the building.
- NSWs affect the engineering demand parameters (accelerations and inter-story drifts) of a building.

Chapter 2 presents a description of the MDE, recorded AVMs at different stages of construction (bare frame and full frame) were analyzed and validated with different techniques (EFDD and SSI). The modal parameters of the MDE were obtained at both stages of construction. Then, two 3D finite element models of the studied building were developed in both stages of construction (bare frame, and full frame) and calibrated with AVMs. The analysis of these results leads to the following conclusions:

- The comparison of periods between AVMs at different stages of construction shows a reduction in the building's fundamental period by -12.4%. The components added

between these two periods are the masonry infill walls, the curtain walls, and the content.

- The overall results confirm that the design period of the MDE is overestimated by the NBC by +14.8%, which implies an underestimation of the spectral acceleration by -13.5% and therefore an underestimation of the equivalent static force. In addition, the equation developed by Gilles and McClure (2012) yields more realistic and conservative values than that of the NBC since it exceeds the period of the $AVM_{sfull\ frame}$ by +4.1%. It would be better to use this equation for buildings with rigid cores rather than the NBC equation.
- The mode shapes remained similar in both stages. This is explained by the presence of masonry infill walls only on the ground floor.

Chapter 3 discusses the relative contribution of the mass and stiffness of NSWs (masonry infill walls, and curtain walls), and their effect on the fundamental period of the MDE. In addition, a parametric study was conducted to assess the effect of masonry infill walls on these dynamic properties. The analysis of these results leads to the following conclusions:

- The masonry walls contribute to the stiffness of the building in both directions (+20% in transversal direction, and +16% in longitudinal direction).
- The curtain walls contribute to the stiffness of the building by +5% in the transversal direction. However, in the longitudinal direction, curtain walls decrease the stiffness of the building by -4% because of their disconnection from upper floors in the north side.
- The parametric study shows that adding masonry infill walls to the building adds more stiffness than mass to the building. In addition, it decreases the fundamental period by a percentage varying from -6.7% to -15.6% that should be considered while calculating the fundamental period of buildings. Moreover, they increase the stiffness contribution by an important percentage varying from +16.1% to +54.3%.

In chapter 4, the effect of NSWs of the MDE on engineering demand parameters (absolute floor accelerations and inter-story drifts) is assessed under the effect of selected and scaled earthquake records matching Montreal's uniform hazard spectrum (5% damping) with a return period of 2500 years. It was concluded that:

- NSWs contribute to the reduction of inter-story drift in both directions (from -20.5% to -41.6% in the longitudinal direction, and from -25.8% to -67.6% in the transversal direction).
- NSWs can affect the absolute floor acceleration. The FAA of the full frame are higher than those of bare frame in almost all floors in the transversal direction. In the longitudinal direction, the FAA of the full frame are higher than those of bare frame in intermediate floors (2nd, and 3rd), and less than those of the bare frame in the mezzanine, and the upper floors (4th, 5th, and roof). This is due to the disconnection between the curtain walls and the SCs in the north side of the upper floors, and the effect of higher modes on the mezzanine. Moreover, it was deduced that the FAA are not linear, and they are underestimated by the NBC at almost all levels.

RECOMMENDATIONS

While this thesis has enabled some questions to be answered related to the effect of NSWs on dynamic properties and EDPs of a case study building, others remain unresolved and some of the proposed conclusions should be validated with subsequent studies.

It was found that the conventional methods of evaluation of the fundamental period proposed by the NBC 2015 led to an overestimation of values compared to the AVMs recorded in the MDE. These results may lead to an underestimation of the design spectral acceleration and therefore an underestimation of the equivalent static force of the building studied. It would be good in the future to come up with an equation that considers the stiffness and mass of SCs and NSWs of the building, instead of an equation that depends only on the height of the building or just consider only the mass of NSCs. In addition, it was shown that stiffness contribution is related to the quantity of masonry walls in the building (i.e., the relative stiffness contribution has increased when adding masonry walls to different floors).

Regarding the effect of NSWs (masonry infill walls, and curtain walls) on the building, it has been shown that these elements provide a significant amount of stiffness to the structure.

Research should be continued in the following areas:

1. Modelling the SCs and NSWs in the nonlinear domain to draw conclusions as to their seismic performance.
2. Optimizing the calibration by performing an automatic calibration instead of a manual calibration. The use of FEMTools[®] software would facilitate the studies of finite element models since it makes it possible to automatically calibrate the numerical models on the experimental tests

3. Considering the effect of soils on all SCs and NSWs of the MDE.
4. Leaving sensors in the MDE throughout its construction to directly record the evolution of the effect of NSWs on the modal properties of the building.
5. Studying the effect of NSWs on buildings with different characteristics such as skyscrapers, buildings with different type of LFRS and also different materials (steel structure, masonry structure, etc.).

ANNEX I

DEFINITION OF MATERIALS, STRUCTURAL COMPONENTS, AND NON-STRUCTURAL WALLS

Table-A I-1 Characteristics of concrete

Standards	CSA A23.3
Characteristics	Concrete C30/37
Weight (Kg/m³)	2400
E (Mpa)	24648
Poisson ratio	0.2
f_c (Mpa)	30

Table-A I-2 Characteristics of steel

Standards	CSA G40.21M grade 300W	CSA G40.21M grade 350W	ASTM A500 grade C	ASTM A653- SS grade 230
Characteristics	Steel	Steel	Steel hardened	Steel
Weight (Kg/m³)	7850	7850	7850	7850
E (Mpa)	200000	200000	200000	200000
Poisson ratio	0.3	0.3	0.3	0.3
F_y (Mpa)	300	350	318	230
F_u (Mpa)	450	450	428	310
F_{ye} (Mpa)	330	385		253
F_{ue} (Mpa)	495	495		341

Table-A I-3 Characteristics of NSWs materials

Standards	CSA A440.2	CAN/CSA-S157	CSA A-371
Characteristics	Glass	Aluminium	Masonry
Weight (Kg/m3)	2390	2714	2000
E (Mpa)	70000	69637	12750
Poisson ratio	0.25	0.33	0.2
f_c (Mpa)		241.32	15

Table-A I-4 Characteristics of steel beams and columns

Component	Materials	Type	Section (mm*mm)	Standard
Beam	Steel	W	200x15	CSA G40.21M GRADE 350 W
			200x19	
			200x27	
			250x18	
			360x33	
			360x39	
			360x45	
			410x39	
			410x46	
			410x54	
			460x52	
			530x66	
			530x82	
			610x113	
Column	Steel	HSS square	76x76x6.4	ASTM A500 GRADE C
			102x102x4.8	
			127x76x6.4	
			152x152x4.8	
			152x152x6.4	
			203x203x6.4	
		HSS circular	273x13	
			324x6.4	
			324x13	

Table-A I-5 Characteristics of concrete beams and columns

Component	Materials	Type	Section	Class of resistance	Standard
Beam	Concrete	Rectangular	250x425	C30/37	CSA A23.3
			285x560	C30/37	
			300x560	C30/37	
			300x800	C30/37	
			300x1000	C30/37	
			350x425	C30/37	
			400x700	C30/37	
			400x1000	C30/37	
			400x1915	C30/37	
			400x2210	C30/37	
			500x850	C30/37	
			500x1000	C30/37	
			500x1800	C30/37	
			600x700	C30/37	
			650x700	C30/37	
			700x2210	C30/37	
			800x700	C30/37	
			800x2210	C30/37	
			1020x670	C30/37	
		Square	500x500	C30/37	
			650x650	C30/37	
			700x700	C30/37	
Column	Concrete	Rectangular	300x600	C30/37	
			450x650	C30/37	
			500x800	C30/37	
			500x900	C30/37	
			500x1255	C30/37	

		Square	600x1370	C30/37	
			750x900	C30/37	
			750x750	C30/37	
		Circular	500Ø	C30/37	
			600Ø	C30/37	
			650Ø	C30/37	
			700Ø	C30/37	
			800Ø	C30/37	

Where C30/37 is the class of concrete ($f'_c = 30$ MPa).

Table-A I-6 Characteristics of rigid floors, floor slabs, and steel deck

Components	Materials	Thickness (mm)	Class of resistance	Standard
Rigid cores	Concrete	300	C30/37	CSA A23.3
		350	C30/37	
		425	C30/37	
		500	C30/37	
Floor slab	Concrete	275	C25/30	CSA A23.3
		275	C30/37	
Steel deck	Steel	38		ASTM A653-SS-Gr230

Table-A I-7 Characteristics of NSWs

Component	Materials	Section	Thickness (mm)	Compression resistance (MPa)	Standard
Infill walls	Masonry		190 330	15 15	CSA A-371
Curtain wall Mullion / Rail	Aluminium	165x64 133x64	3.2 3.2		CAN/CSA- S157
Glazing	Glass		12		CSA A440.2

ANNEX II

AMBIENT VIBRATION MEASUREMENTS

Table-A II-1 Follow-up sheet of records

[illegible]

Signal pre-processing steps (Tischer, 2012)

Step 1: Grouping of signals captured using MATLAB® software.

- suppression of spurious peaks using the CROP SIGNAL tool.
- choice of direction to study east-west/north-south or both.
- choice of the measure studied.
- changing the sample frequency.

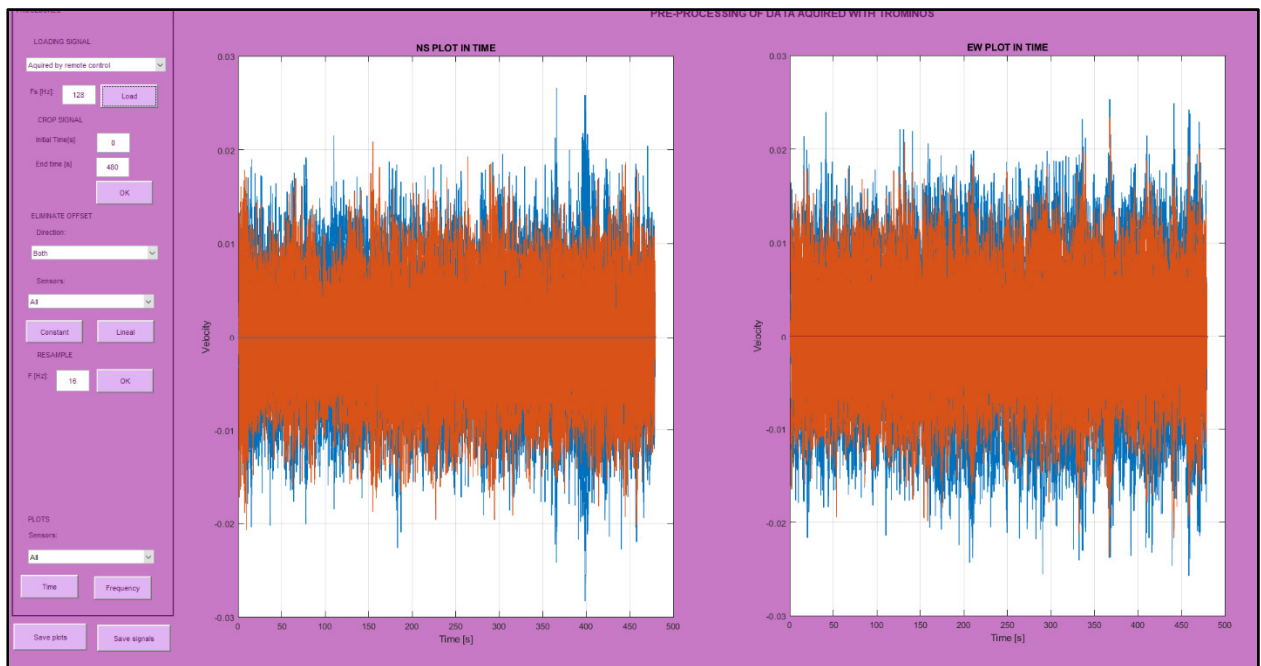
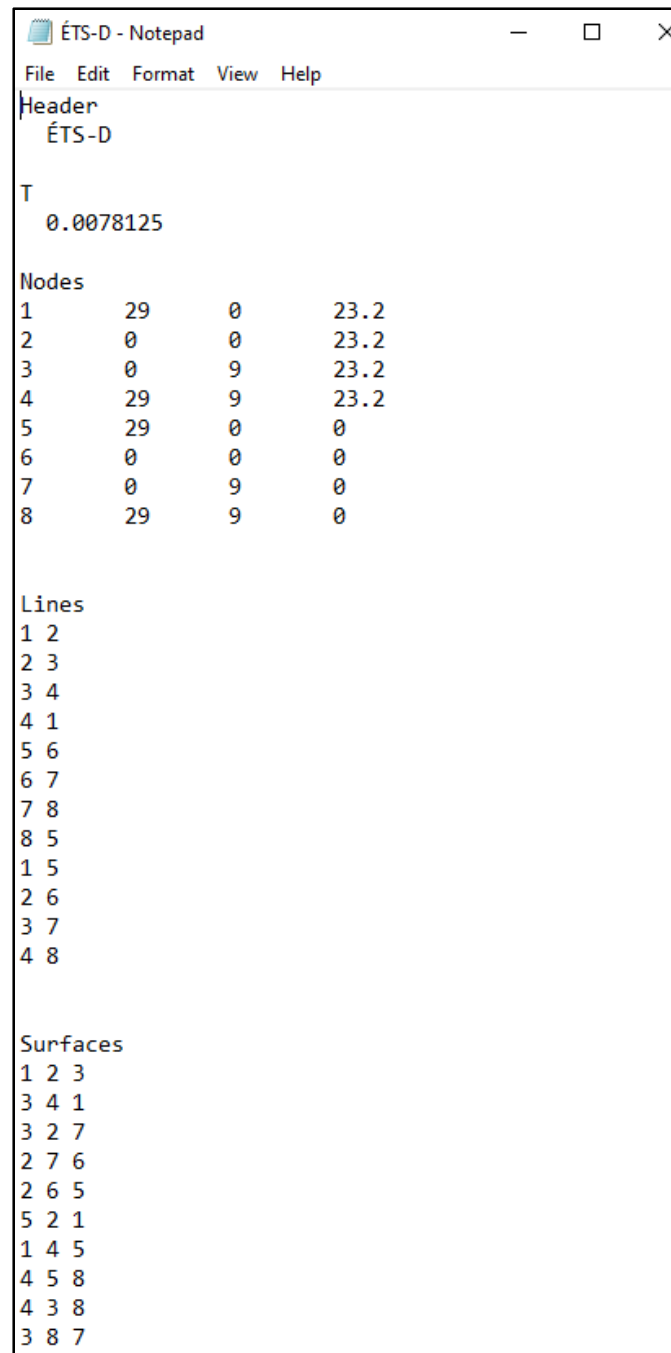


Figure-A II-1 Output signal after preprocessing using MATLAB®

Step 2: Creation of a cfg file reproducing the geometry of the measurement points linked to the .txt files for building modelling (nodes, lines, surfaces)



```
ÉTS-D - Notepad
File Edit Format View Help
Header
ÉTS-D

T
0.0078125

Nodes
1      29      0      23.2
2      0       0      23.2
3      0       9      23.2
4      29      9      23.2
5      29      0       0
6      0       0       0
7      0       9       0
8      29      9       0

Lines
1 2
2 3
3 4
4 1
5 6
6 7
7 8
8 5
1 5
2 6
3 7
4 8

Surfaces
1 2 3
3 4 1
3 2 7
2 7 6
2 6 5
5 2 1
1 4 5
4 5 8
4 3 8
3 8 7
```

Figure-A II-1 Cfg file

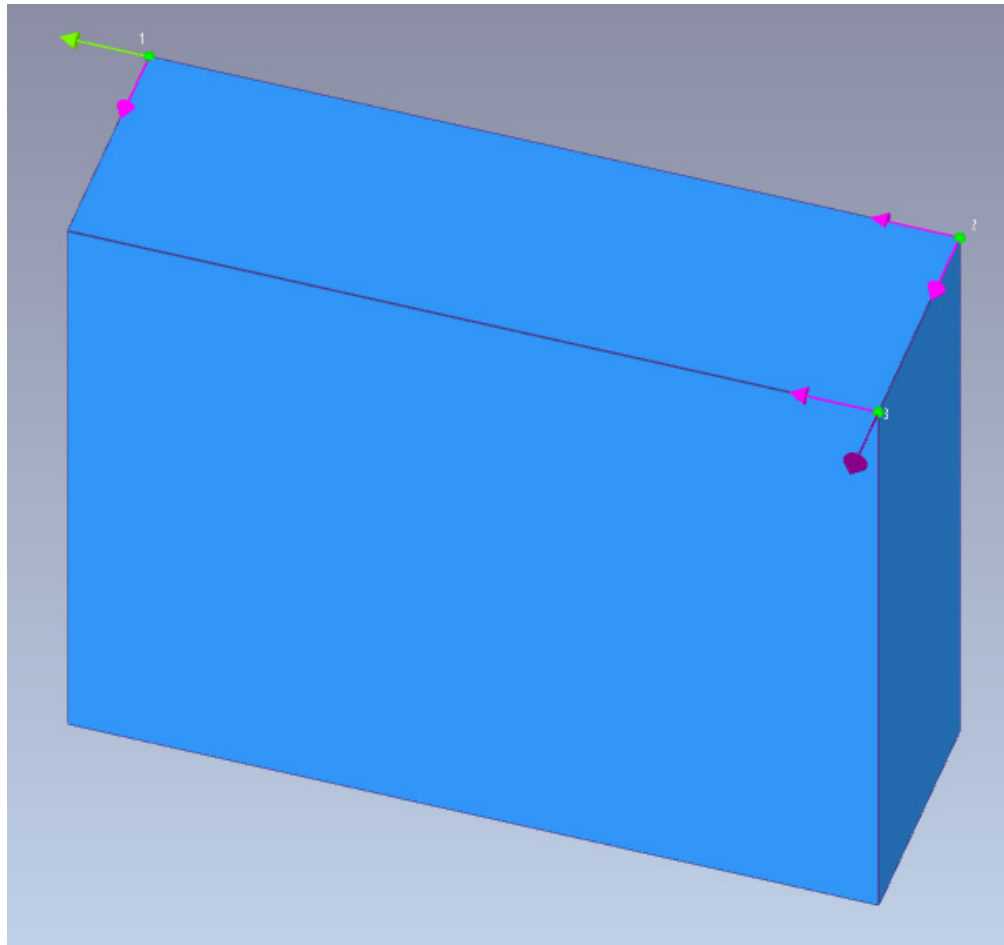


Figure-A II-2 Configuration of the AVMs for the bare frame

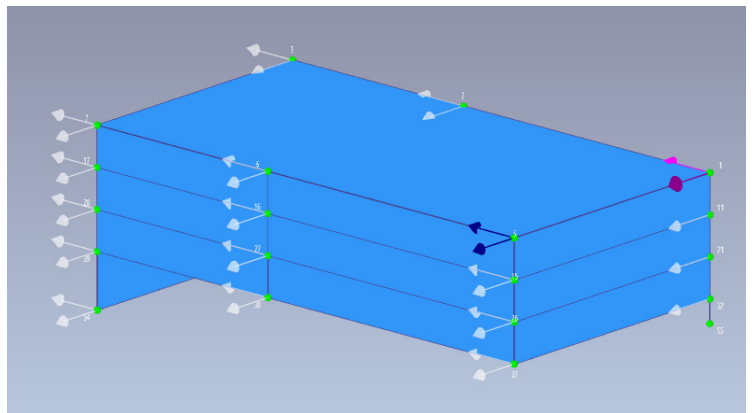
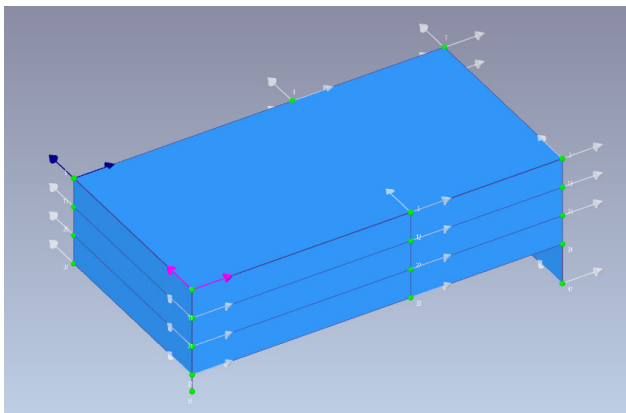
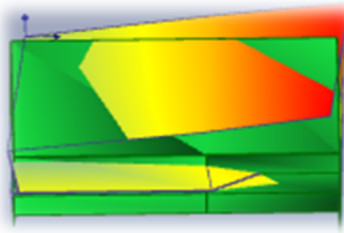
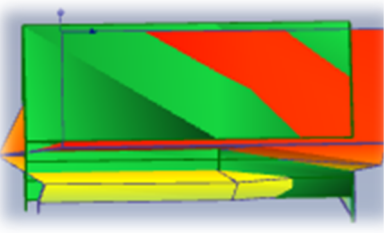
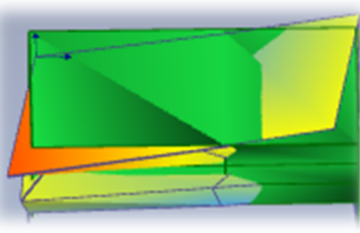


Figure-A II-3 Configuration of the AVMs for the full frame

Table-A II-4 Results of modal analysis of the full frame using an SSI method

		
Mode 1 Transversal translation + torsion	Mode 2 Longitudinal translation	Mode 3 Transversal translation + torsion
$f_1 = 2.17 \text{ Hz}$	$f_2 = 2.49 \text{ Hz}$	$f_3 = 3.01 \text{ Hz}$

ANNEX III

FINITE ELEMENT MODELLING

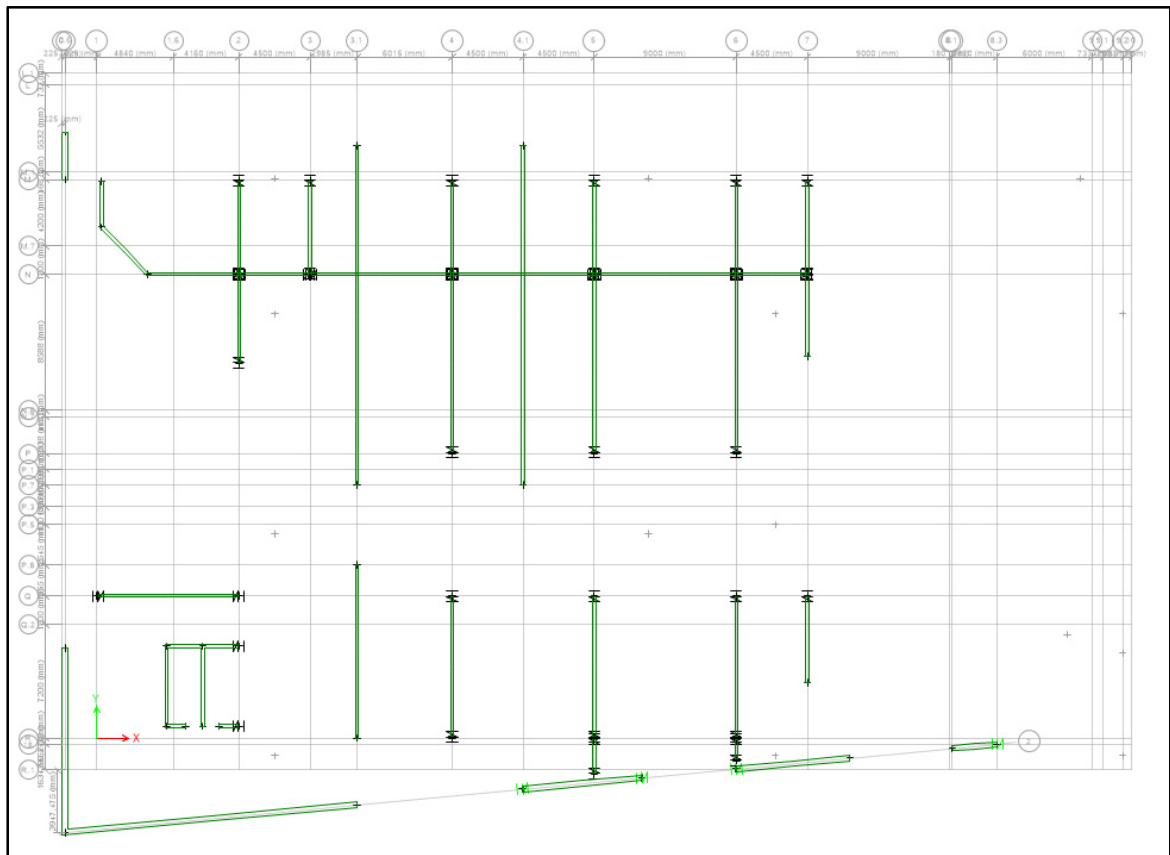


Figure-A III-1 Plan view of masonry walls in the ground floor floor

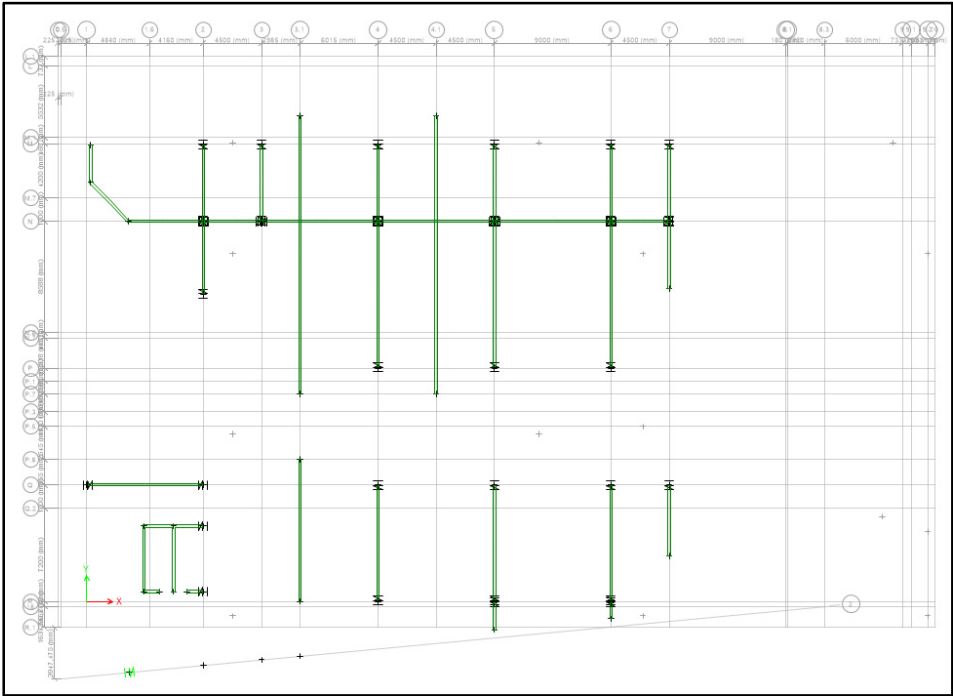


Figure-A III-2 Plan view of masonry walls in the 2nd floor

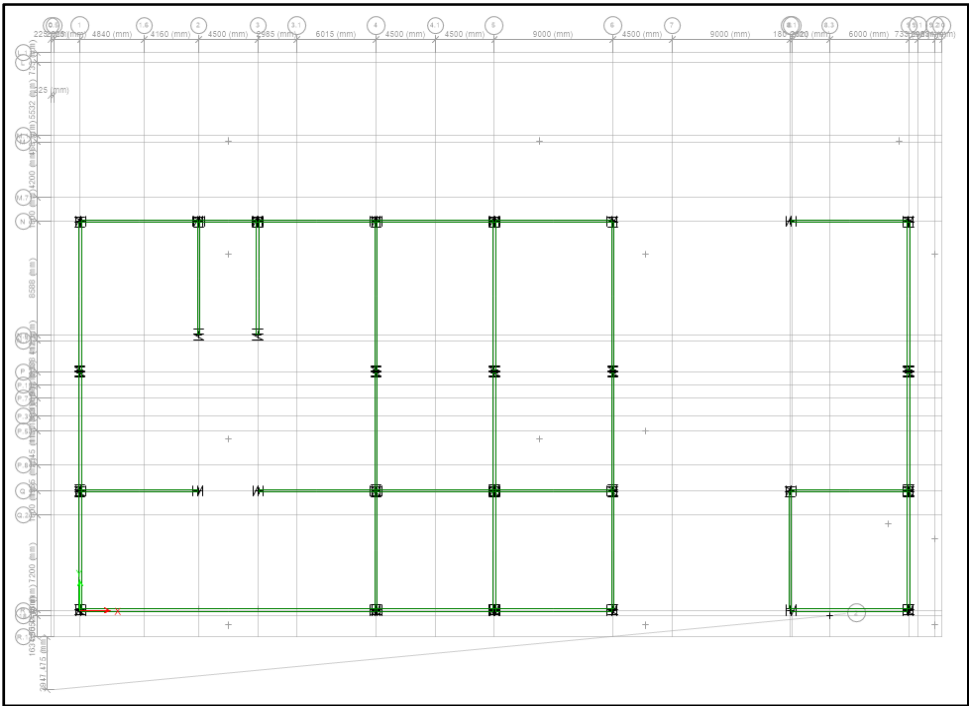


Figure-A III-3 Plan view of masonry walls in the (3rd, 4th, and 5th floor)

Table-A III-1 Characteristics of curtain wall connections
Adapted from (Caterino et al., 2017b)

Curtain walls connection		Details
Gap element	Space frame-glass	5 mm
	Local stiffness induced in the frame-glass contact	0.5 KN/mm
Link elasto-plastique Wen	Elastic stiffness	0.7 KN/mm
	Yield force	0.1 KN
	Post-yield stiffness ratio	0
	Yield exponent	1

Table-A III-2 Permanent loads of bare frame

Building level		Loads	
Appentis		Roof & apron	0.5 KPa
Roof		Slope concrete	3.5 KPa
5th floor		Absent	0 KPa
4th floor		Absent	0 KPa
3rd floor	Floor	Absent	0 KPa
	North terrace	Paving	1.4 KPa
		Slope concrete	2.4 KPa
		Total	3.8 KPa
	South terrace	Slope concrete	3.2 KPa
2nd floor		Absent	0 KPa
Mezzanine		Absent	0 KPa

Table-A III-3 Permanent loads of full frame

Building level		Loads	
Appentis		BF	0.5 KPa
		Mechanical	0.5 KPa
		Total	1 KPa
Roof		BF	3.5 KPa
		Roof	0.7 KPa
		Total	4.2 KPa
5th floor		BF	0 KPa
		Partitions	0.4 KPa
		Mechanical/ceilings	0.1 KPa
		Total	0.5 KPa
4th floor		BF	0 KPa
		Partitions	0.4 KPa
		Mechanical/ceilings	0.1 KPa
		Total	0.5 KPa
3rd floor	Inside floor	BF	0 KPa
		Partitions	0.4 KPa
		Mechanical/ceilings	0.1 KPa
		Total	0.5 KPa
	North terrace	BF	3.8 KPa
		Roof	0.7 KPa
		Total	4.5 KPa
	South terrace	BF	3.2 KPa
		Roof	0.7 KPa
		Total	3.9 KPa
2nd floor		BF	0 KPa
		Partitions	0.4 KPa
		Mechanical/ceilings	0.1 KPa
		Total	0.5 KPa
Mezzanine		BF	0 KPa
		Partitions	0.4 KPa
		Mechanical/ceilings	0.1 KPa
		Total	0.5 KPa

ANNEX IV

CALIBRATION OF FINITE ELEMENT MODELS OF THE MDE

Bare frame

Table-A IV-1 New values of
the parameters of calibrated materials

Materials Parameters	Concrete C30/37
Density (kg/m ³)	2400
Calibrated density	2500
Diff %	4%
Young modulus (MPa)	24648
Calibrated Young modulus (MPa)	22183
Diff %	-10%

Table-A IV-2 Uncertainties and new values of
permanent loads

Loads	Floors				3rd floor			2nd floor	Mezzanine
	Appentis	Roof	5th floor	4th floor	North terrace	Building	South terrace		
Load (kg/m ²)	50	350	Absent	Absent	380	Absent	320	Absent	Absent
Calibrated load (kg/m ²)	51.5	360	Absent	Absent	391	Absent	330	Absent	Absent
Diff %	3%	3%			3%		3%		

Full frame

Table-A IV-3 Uncertainties and new values of the properties of calibrated materials

Materials Parameters	Glass	Aluminium	Masonry walls
Density (kg/m ³)	2390	2714	2000
Calibrated density	1912	2578	1600
Diff %	-20%	-5%	-20%
Young modulus (MPa)	70000	69637	12750
Calibrated Young modulus (Mpa)	84000	73119	15300
Diff %	20%	5%	20%

Table-A IV-4 Uncertainties and new values of Permanent loads

Floors Loads	Appentis	Roof	5th floor	4th floor	3rd floor			2nd floor	Mezzanine
					North terrace	Building	South terrace		
Load (kg/m ²)	101.5	430	50	50	461	50	400	50	50
Calibrated load (kg/m ²)	99	426.5	47.5	47.5	457.5	47.5	396.5	47.5	47.5
Diff %	-5%	-5%	-5%	-5%	-5%	-5%	-5%	-5%	-5%

Table-A IV-5 Properties of the masonry infill walls *gap element* after calibration

Masonry infill walls	Thickness t (mm)	E _i (MPa)	K _i = E _i *t (N/mm)	K _g = 0.0378*K _i + 347 (N/mm)
M190	190	15300	2907000	110232
M330	330	15300	5049000	191199

Table-A IV-6 Modal participation mass ratio (MPMR) of the bare frame

Mode	Period	UX	UY	RZ	Sum UX	Sum UY	Sum RZ
1	0.483	0.046	0.431	0.271	0.046	0.431	0.271
2	0.38	0.603	0.113	0.009	0.649	0.544	0.280
3	0.363	0.077	0.172	0.469	0.726	0.716	0.749
4	0.233	0.002	0.033	0.001	0.728	0.749	0.750
5	0.128	0.040	0.038	0.101	0.767	0.787	0.851
6	0.112	0.087	0.052	0.001	0.854	0.839	0.852
7	0.096	0.009	0.105	0.089	0.863	0.943	0.941
8	0.08	0.087	0.000	0.003	0.950	0.943	0.944
9	0.056	0.000	0.011	0.012	0.950	0.954	0.956

Table-A IV-7 Modal participation mass ratio (MPMR) of the full frame

Mode	Period	UX	UY	RZ	Sum UX	Sum UY	Sum RZ
1	0.472	0.098	0.263	0.174	0.098	0.263	0.174
2	0.403	0.262	0.072	0.002	0.360	0.334	0.175
3	0.369	0.000	0.000	0.000	0.360	0.334	0.175
4	0.356	0.000	0.000	0.000	0.360	0.334	0.175
5	0.35	0.000	0.113	0.123	0.361	0.447	0.298
6	0.311	0.243	0.028	0.152	0.604	0.475	0.450
7	0.288	0.063	0.198	0.195	0.667	0.673	0.645
8	0.239	0.043	0.005	0.031	0.710	0.679	0.676
9	0.162	0.000	0.000	0.000	0.710	0.679	0.676
10	0.129	0.000	0.000	0.000	0.710	0.679	0.676
11	0.122	0.000	0.000	0.000	0.710	0.679	0.676
12	0.117	0.034	0.054	0.119	0.744	0.732	0.795
13	0.093	0.000	0.000	0.000	0.744	0.732	0.796
14	0.087	0.114	0.101	0.003	0.859	0.834	0.799
15	0.077	0.065	0.069	0.109	0.923	0.902	0.908

ANNEX V

FLOOR ACCELERATION AMPLIFICATION

Table-A V-1 Absolute floor acceleration of bare frame (longitudinal direction)
under selected and scaled earthquakes

Acceleration (m/sec ²)						
Story	East6c1_7	East6c1_26	East6c1_31	East6c2_5	East6c2_8	East6c2_10
Roof	6,31	4,55	5,34	6,11	4,96	7,76
Story5	4,33	3,22	4,10	4,62	3,61	5,15
Story4	2,55	3,91	3,49	4,99	2,83	2,96
Story3	3,41	4,17	2,99	5,55	2,43	3,29
Story2	3,60	3,00	2,25	4,96	3,07	3,00
Mezzanine	3,88	3,48	3,65	5,17	3,73	1,99
Ground floor	2,94	1,41	1,59	2,33	2,39	1,84
Acceleration (m/sec ²)						
Story	East7c1_25	East7c1_28	East7c1_30	East7c2_1	East7c2_3	East7c2_11
Roof	3,50	6,15	4,46	6,82	3,45	4,67
Story5	3,00	5,24	3,65	5,15	2,65	3,47
Story4	2,43	4,84	3,08	4,99	3,01	2,27
Story3	3,32	4,12	3,40	3,73	2,84	2,39
Story2	3,98	3,29	2,58	2,53	1,96	2,04
Mezzanine	3,55	3,23	3,05	2,11	2,01	1,94
Ground floor	1,98	2,20	2,54	1,81	1,53	1,47
Acceleration (m/sec ²)						
Story	hx/hn	Median	16th percentile	84th percentile	AVM	
Roof	1,00	5,34	4,23	6,43	0,053	
Story5	0,81	4,02	3,17	5,15		
Story4	0,63	3,45	2,52	4,88		
Story3	0,44	3,47	2,74	4,14		
Story2	0,26	3,02	2,20	3,69		
Mezzanine	0,15	3,15	2,01	3,76		
Ground floor	0,00	2,00	1,51	2,42	0,019	

Table-A V-2 Absolute floor acceleration of bare frame (transversal direction)
under selected and scaled earthquakes

Acceleration (m/sec ²)						
Story	East6c1_7	East6c1_26	East6c1_31	East6c2_5	East6c2_8	East6c2_10
Roof	6,97	7,42	4,71	9,01	4,93	6,86
Story5	4,69	4,65	4,86	5,48	5,12	4,76
Story4	3,22	4,07	4,59	4,96	5,89	3,00
Story3	3,51	4,56	4,17	4,88	4,89	3,84
Story2	3,30	3,43	2,27	3,82	2,74	2,51
Mezzanine	3,28	2,52	1,16	3,37	2,98	1,73
Ground floor	2,94	1,41	1,59	2,33	2,39	1,84
Acceleration (m/sec ²)						
Story	East7c1_25	East7c1_28	East7c1_30	East7c2_1	East7c2_3	East7c2_11
Roof	5,89	7,30	5,32	6,45	3,78	6,38
Story5	3,74	5,50	3,88	4,47	3,10	4,60
Story4	2,50	4,86	3,57	4,31	3,10	3,15
Story3	2,85	4,71	3,68	4,58	2,96	2,85
Story2	3,46	4,15	2,85	2,91	2,10	1,96
Mezzanine	3,72	2,70	2,38	2,06	2,10	2,04
Ground floor	1,98	2,20	2,54	1,81	1,53	1,47
Acceleration (m/sec ²)						
Story	hx/hn	Median	16th percentile	84th percentile	AVM	
Roof	1,00	6,25	4,88	7,33	0,044	
Story5	0,81	4,57	3,84	5,20		
Story4	0,63	3,93	3,08	4,88		
Story3	0,44	3,96	2,94	4,75		
Story2	0,26	2,96	2,23	3,54		
Mezzanine	0,15	2,50	1,96	3,30		
Ground floor	0,00	2,00	1,51	2,42	0,015	

Table-A V-3 Absolute floor acceleration of full frame (longitudinal direction)

under selected and scaled earthquakes

Acceleration (m/sec ²)						
Story	East6c1_7	East6c1_26	East6c1_31	East6c2_5	East6c2_8	East6c2_10
Roof	5,34	6,13	4,87	4,79	3,54	6,55
Story5	4,05	4,71	3,51	3,51	3,61	3,73
Story4	5,18	4,71	2,57	4,91	3,62	3,48
Story3	5,41	5,31	3,96	5,61	3,83	2,91
Story2	5,03	5,63	6,09	7,13	5,37	5,64
Mezzanine	2,96	2,68	2,51	3,78	3,05	1,85
Ground floor	2,94	1,41	1,59	2,33	2,39	1,84
Acceleration (m/sec ²)						
Story	East7c1_25	East7c1_28	East7c1_30	East7c2_1	East7c2_3	East7c2_11
Roof	4,28	7,07	4,71	3,61	3,84	3,48
Story5	3,59	4,52	3,78	2,89	2,39	2,78
Story4	3,59	4,35	3,51	2,92	2,40	2,72
Story3	4,44	4,22	5,19	2,92	2,48	2,56
Story2	6,83	7,50	8,64	6,73	5,09	4,51
Mezzanine	2,92	2,28	3,22	2,08	1,79	2,13
Ground floor	1,98	2,20	2,54	1,81	1,53	1,47
Acceleration (m/sec ²)						
Story	hx/hn	Median	16th percentile	84th percentile	AVM	
Roof	1,00	4,85	3,59	6,23	0,050	
Story5	0,81	3,59	2,87	4,16	0,043	
Story4	0,63	3,66	2,68	4,76	0,045	
Story3	0,44	4,07	2,83	5,33	0,041	
Story2	0,26	6,18	5,07	7,22	0,060	
Mezzanine	0,15	2,60	2,02	3,09	0,026	
Ground floor	0,00	2,00	1,51	2,42	0,019	

Table-A V-4 Absolute floor acceleration of full frame (transversal direction)
under selected and scaled earthquakes

Acceleration (m/sec ²)						
Story	East6c1_7	East6c1_26	East6c1_31	East6c2_5	East6c2_8	East6c2_10
Roof	6,46	8,42	6,92	5,17	6,19	6,81
Story5	5,69	4,71	4,85	4,18	4,28	5,10
Story4	5,70	7,19	4,37	5,99	4,69	4,44
Story3	5,57	7,23	2,56	6,00	4,71	4,43
Story2	7,01	10,43	6,13	4,49	10,65	3,60
Mezzanine	2,94	2,02	1,91	3,25	3,13	2,27
Ground floor	2,94	1,41	1,59	2,33	2,39	1,84
Acceleration (m/sec ²)						
Story	East7c1_25	East7c1_28	East7c1_30	East7c2_1	East7c2_3	East7c2_11
Roof	6,09	7,92	5,79	5,06	4,67	4,80
Story5	4,90	4,80	3,76	3,80	2,93	4,68
Story4	4,90	5,23	3,68	3,80	2,89	4,09
Story3	3,92	5,23	4,93	3,37	2,89	2,86
Story2	3,68	13,88	6,55	6,06	3,74	4,31
Mezzanine	3,18	3,02	4,79	2,30	2,28	1,53
Ground floor	1,98	2,20	2,54	1,81	1,53	1,47
Acceleration (m/sec ²)						
Story	hx/hn	Median	16th percentile	84th percentile	AVM	
Roof	1,00	6,19	5,00	7,16	0,052	
Story5	0,81	4,47	3,79	4,95	0,040	
Story4	0,63	4,75	3,77	5,77	0,029	
Story3	0,44	4,47	2,88	5,67	0,029	
Story2	0,26	6,71	3,72	10,49	0,060	
Mezzanine	0,15	2,72	2,00	3,20	0,041	
Ground floor	0,00	2,00	1,51	2,42	0,015	

Table-A V-5 FAA of bare frame (longitudinal direction) under selected and scaled earthquakes

FAA						
Story	East6c1_7	East6c1_26	East6c1_31	East6c2_5	East6c2_8	East6c2_10
Roof	2,15	3,23	3,35	2,62	2,08	4,22
Story5	1,47	2,28	2,57	1,98	1,51	2,80
Story4	0,87	2,77	2,19	2,14	1,19	1,61
Story3	1,16	2,96	1,88	2,38	1,02	1,79
Story2	1,22	2,12	1,41	2,13	1,29	1,63
Mezzanine	1,32	2,47	2,29	2,22	1,56	1,08
Ground floor	1,00	1,00	1,00	1,00	1,00	1,00
FAA						
Story	East7c1_25	East7c1_28	East7c1_30	East7c2_1	East7c2_3	East7c2_11
Roof	1,77	2,80	1,76	3,77	2,26	3,17
Story5	1,52	2,38	1,44	2,85	1,74	2,36
Story4	1,23	2,20	1,21	2,76	1,97	1,54
Story3	1,68	1,88	1,34	2,06	1,86	1,62
Story2	2,01	1,50	1,02	1,40	1,29	1,39
Mezzanine	1,80	1,47	1,20	1,16	1,32	1,31
Ground floor	1,00	1,00	1,00	1,00	1,00	1,00
FAA						
Story	hx/hn	Median	16th percentile	84th percentile	NBC2015	AVM
Roof	1,00	2,76	1,97	3,56	3,00	2,77
Story5	0,81	2,08	1,54	2,61	2,63	
Story4	0,63	1,81	1,18	2,44	2,26	
Story3	0,44	1,80	1,28	2,33	1,89	
Story2	0,26	1,53	1,17	1,90	1,52	
Mezzanine	0,15	1,60	1,12	2,08	1,30	
Ground floor	0,00	1,00	1,00	1,00	1,00	

Table-A V-6 FAA of bare frame (transversal direction) under selected and scaled earthquakes

FAA						
Story	East6c1_7	East6c1_26	East6c1_31	East6c2_5	East6c2_8	East6c2_10
Roof	2,37	5,26	2,96	3,87	2,07	3,73
Story5	1,60	3,30	3,05	2,35	2,14	2,59
Story4	1,10	2,89	2,88	2,13	2,47	1,63
Story3	1,20	3,23	2,61	2,09	2,05	2,09
Story2	1,12	2,43	1,43	1,64	1,15	1,36
Mezzanine	1,12	1,79	0,73	1,45	1,25	0,94
Ground floor	1,00	1,00	1,00	1,00	1,00	1,00
FAA						
Story	East7c1_25	East7c1_28	East7c1_30	East7c2_1	East7c2_3	East7c2_11
Roof	2,98	3,32	2,10	3,57	2,48	4,33
Story5	1,89	2,51	1,53	2,47	2,03	3,12
Story4	1,26	2,21	1,41	2,38	2,03	2,14
Story3	1,45	2,15	1,45	2,53	1,94	1,94
Story2	1,75	1,89	1,12	1,61	1,38	1,33
Mezzanine	1,88	1,23	0,94	1,14	1,38	1,38
Ground floor	1,00	1,00	1,00	1,00	1,00	1,00
FAA						
Story	hx/hn	Median	16th percentile	84th percentile	NBC2015	AVM
Roof	1,00	3,25	2,29	4,22	3,00	2,95
Story5	0,81	2,38	1,80	2,96	2,63	
Story4	0,63	2,04	1,45	2,63	2,26	
Story3	0,44	2,06	1,50	2,62	1,89	
Story2	0,26	1,52	1,14	1,90	1,52	
Mezzanine	0,15	1,27	0,93	1,61	1,3	
Ground floor	0,00	1,00	1,00	1,00	1,00	

Table-A V-7 FAA of full frame (longitudinal direction) under selected and scaled earthquakes

FAA						
Story	East6c1_7	East6c1_26	East6c1_31	East6c2_5	East6c2_8	East6c2_10
Roof	1,82	4,34	3,06	2,06	1,49	3,56
Story5	1,38	3,33	2,20	1,51	1,51	2,03
Story4	1,76	3,34	1,61	2,11	1,52	1,89
Story3	1,84	3,76	2,49	2,41	1,61	1,58
Story2	1,71	3,99	3,82	3,06	2,25	3,06
Mezzanine	1,01	1,90	1,57	1,62	1,28	1,00
Ground floor	1,00	1,00	1,00	1,00	1,00	1,00
FAA						
Story	East7c1_25	East7c1_28	East7c1_30	East7c2_1	East7c2_3	East7c2_11
Roof	2,17	3,22	1,85	1,99	2,51	2,37
Story5	1,82	2,06	1,49	1,60	1,57	1,89
Story4	1,82	1,98	1,38	1,61	1,57	1,84
Story3	2,25	1,92	2,04	1,62	1,63	1,74
Story2	3,46	3,42	3,40	3,72	3,34	3,06
Mezzanine	1,48	1,04	1,27	1,15	1,17	1,44
Ground floor	1,00	1,00	1,00	1,00	1,00	1,00
FAA						
Story	hx/hn	Median	16th percentile	84th percentile	NBC2015	AVM
Roof	1,00	2,54	1,69	3,38	3,00	2,59
Story5	0,81	1,87	1,33	2,40	2,63	2,21
Story4	0,63	1,87	1,36	2,38	2,26	2,33
Story3	0,44	2,07	1,45	2,69	1,89	2,14
Story2	0,26	3,19	2,54	3,84	1,52	3,13
Mezzanine	0,15	1,33	1,05	1,61	1,3	1,37
Ground floor	0,00	1,00	1,00	1,00	1,00	1,00

Table-A V-8 FAA of full frame (transversal direction) under selected and scaled earthquakes

FAA						
Story	East6c1_7	East6c1_26	East6c1_31	East6c2_5	East6c2_8	East6c2_10
Roof	2,20	5,97	4,34	2,22	2,59	3,70
Story5	1,94	3,34	3,04	1,80	1,80	2,77
Story4	1,94	5,09	2,74	2,57	1,97	2,42
Story3	1,90	5,12	1,61	2,57	1,97	2,41
Story2	2,39	7,39	3,84	1,93	4,47	1,96
Mezzanine	1,00	1,43	1,20	1,40	1,31	1,23
Ground floor	1,00	1,00	1,00	1,00	1,00	1,00
FAA						
Story	East7c1_25	East7c1_28	East7c1_30	East7c2_1	East7c2_3	East7c2_11
Roof	3,08	3,61	2,28	2,80	3,06	3,26
Story5	2,48	2,19	1,48	2,10	1,92	3,18
Story4	2,48	2,38	1,45	2,10	1,89	2,78
Story3	1,98	2,38	1,94	1,86	1,89	1,94
Story2	1,86	6,32	2,58	3,35	2,45	2,92
Mezzanine	1,61	1,37	1,89	1,27	1,49	1,04
Ground floor	1,00	1,00	1,00	1,00	1,00	1,00
FAA						
Story	hx/hn	Median	16th percentile	84th percentile	NBC2015	AVM
Roof	1,00	3,26	2,18	4,33	3,00	3,48
Story5	0,81	2,34	1,72	3,10	2,63	2,70
Story4	0,63	2,48	1,57	3,39	2,26	1,94
Story3	0,44	2,30	1,37	3,23	1,89	1,95
Story2	0,26	3,46	1,67	5,25	1,52	4,06
Mezzanine	0,15	1,35	1,11	1,60	1,3	2,77
Ground floor	0,00	1,00	1,00	1,00	1,00	1,00

ANNEX VI

SELECTION AND SCALING OF GROUND MOTION TIME HISTORIES

Table-A VI-1 FAA Scaling factors for earthquakes (scenario 1)

Scenario 1							
TRS1 min	0.071						
TRS1 max	1						
				Selected	F1	F2	F final
East 6c1	M 6.0	R (KM)	15	east6c1_7	5.95E-01	1.14	0.68
				east6c1_26	8.79E-01	1.14	1.00
				east6c1_31	7.52E-01	1.14	0.85
East 6c2	M 6.0	R (KM)	30	east6c2_5	1.26E+00	1.14	1.43
				east6c2_8	8.69E-01	1.14	0.99
				east6c2_10	1.11E+00	1.14	1.26

Table-A VI-2 FAA Scaling factors for earthquakes (scenario 2)

scenario 2							
TRS2 min	0.5						
TRS2 max	1.5						
				Selected	F1	F2	F final
East 7c1	M 7.0	R (KM)	25	east7c1_25	5.27E-01	1.004	0.53
				east7c1_28	6.67E-01	1.004	0.67
				east7c1_30	5.37E-01	1.004	0.54
East 7c2	M 7.0	R (KM)	100	east7c2_1	1.23E+00	1.004	1.23
				east7c2_3	1.19E+00	1.004	1.19
				east7c2_11	1.64E+00	1.004	1.65

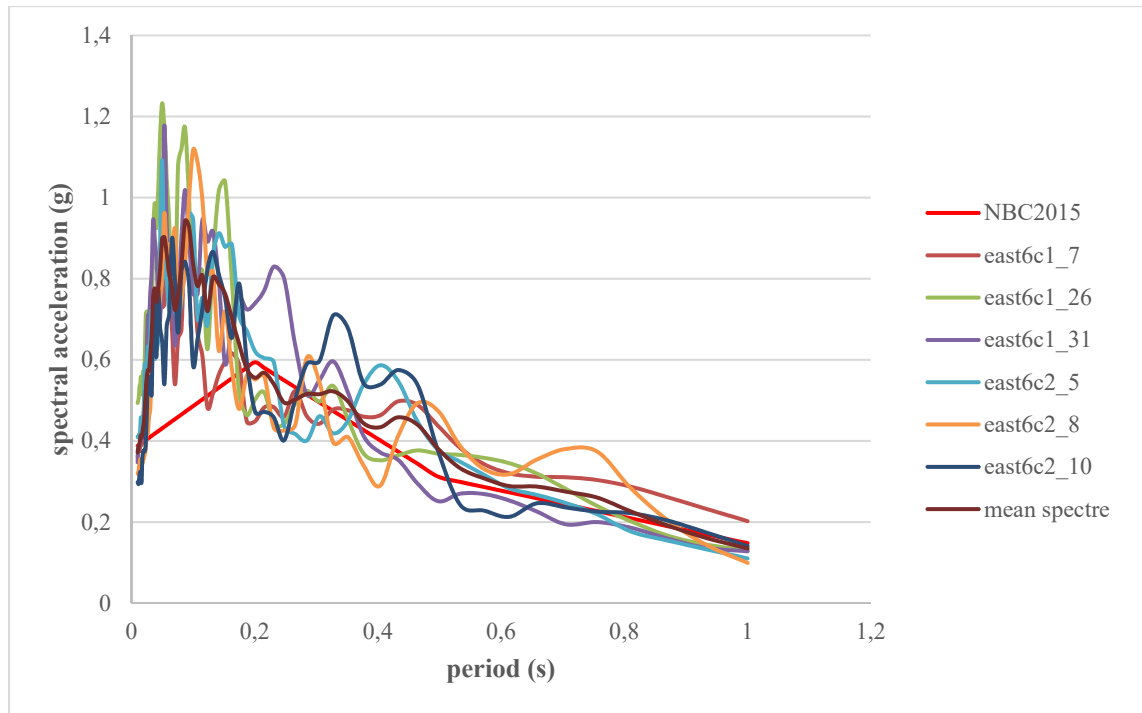


Figure-A VI-1 Acceleration spectra of the selected and scaled individual ground motion time histories from scenario 1

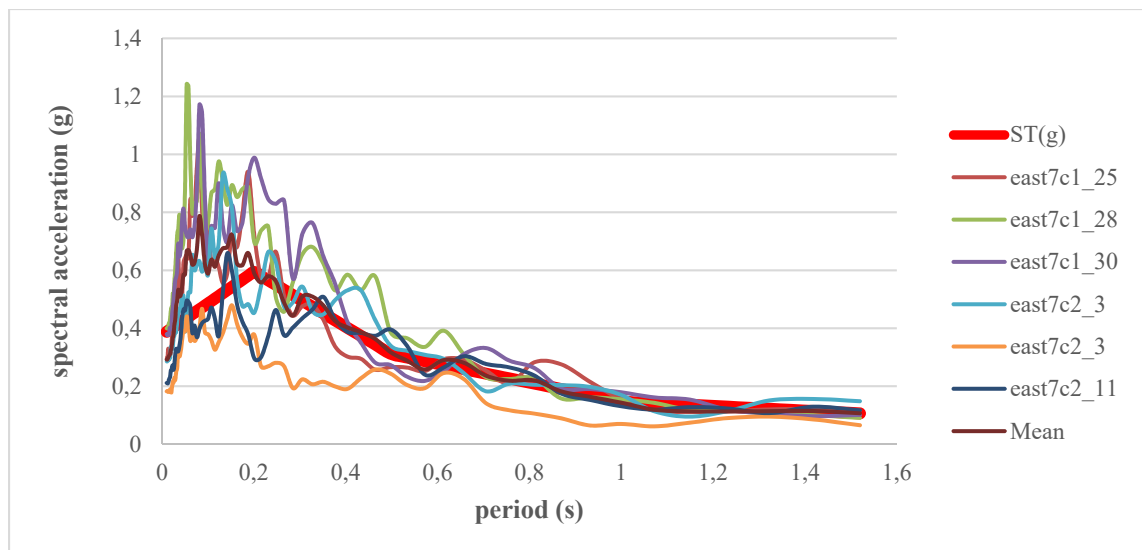


Figure-A VI-2 Acceleration spectra of the selected and scaled individual ground motion time histories from scenario 2

REFERENCES

- Aiello, C., Caterino, N., Maddaloni, G., Bonati, A., & Occhiuzzi, A. (2017). Experimental comparison of in-plane mechanical response of glazed curtain walls. *Experimental comparison of in-plane mechanical response of glazed curtain walls*, 59-68.
- Al-Chaar, G. K. (2002). Evaluating strength and stiffness of unreinforced masonry infill structures. Construction Engineering Research Laboratory (ERDC/CERL TR-02-1). <https://erdc-library.erdcdren.mil/jspui/bitstream/11681/19773/1/CERL-TR-02-1.pdf>.
- Aldeka, A. B., Chan, A. H., & Dirar, S. (2014). Response of non-structural components mounted on irregular RC buildings: comparison between FE and EC8 predictions. *Earthquakes and Structures*, 6(4), 351-373.
- Amanat, K. M., & Hoque, E. (2006). A rationale for determining the natural period of RC building frames having infill. *Engineering Structures*, 28(4), 495-502.
- ARTEMIS Modal, S. (2018). Structural Vibration Solutions A: S.
- Asgarian, A. (2012). Impact of seismic retrofit and presence of terra cotta masonry walls on the dynamic properties of a hospital building in Montreal, Canada (Master's thesis, McGill University).
- Asgarian, A., & McClure, G. (2014). Impact of seismic rehabilitation and presence of unreinforced masonry (URM) infill walls on the dynamic characteristics of a hospital building in Montreal. *Canadian Journal of Civil Engineering*, 41(8), 748-760.
- Asgarian, A., & McClure, G. (2017). Using ambient vibration measurements to generate experimental floor response spectra and inter-story drift curves of reinforced concrete (RC) buildings. *Procedia engineering*, 199, 92-97.
- Asgarian, A., & McClure, G. (2020). Direct generation of floor design spectra (FDS) from uniform hazard spectra (UHS) Part I: formulation of the method. *Canadian Journal of Civil Engineering*, 47(12), 1372-1386.
- Asgarian, A., & McClure, G. (2012). Impact of seismic retrofit and presence of terra cotta masonry walls on the dynamic properties of a hospital building in Montreal, Canada. *Masters Abstracts International (Vol. 51)*.
- Atkinson, G. M. (2009). Earthquake time histories compatible with the 2005 National building code of Canada uniform hazard spectrum. *Canadian Journal of Civil Engineering*, 36(6), 991-1000.

- Bonne, A. (2018). Caractérisation de l'effet des composants non structuraux sur les propriétés dynamiques des bâtiments (Master's thesis, École de technologie supérieure).
- Brincker, R., & Ventura, C. (2015). *Introduction to operational modal analysis*. John Wiley & Sons.
- Brincker, R., Zhang, L., & Andersen, P. (2000). Modal identification from ambient responses using frequency domain decomposition. Proceeding of the 18th International Modal Analysis Conference (IMAC), San Antonio, Texas.
- Casagrande, L., Bonati, A., Occhiuzzi, A., Caterino, N., & Auricchio, F. (2019). Numerical investigation on the seismic dissipation of glazed curtain wall equipped on high-rise buildings. *Engineering Structures*, 179, 225-245.
- Caterino, N., Del Zoppo, M., Maddaloni, G., Bonati, A., Cavanna, G., & Occhiuzzi, A. (2017a). Seismic assessment and finite element modelling of glazed curtain walls. *Structural Engineering and Mechanics*, 61(1), 77-90.
- Caterino, N., Del Zoppo, M., Maddaloni, G., Bonati, A., Cavanna, G., & Occhiuzzi, A. (2017b). Seismic assessment and finite element modelling of glazed curtain walls. *Structural Engineering and Mechanics*, 61(1), 77-90.
- Chaker, A. A., & Cherifati, A. (1999). Influence of masonry infill panels on the vibration and stiffness characteristics of R/C frame buildings. *Earthquake engineering & structural dynamics*, 28(9), 1061-1065.
- Cremona, C., de Souza Barbosa, F., & Alvandi, A. (2003). Identification modale sous excitation ambiante: *Application à la surveillance des ponts*. *Mécanique & industries*, 4(3), 259-271.
- CSA-S832-14. (2014). S832-14: Seismic Risk Reduction of Operational and Functional Components (OFCs) of Buildings: Canadian Standard Association, CSA Group.
- Devin, A., & Fanning, P. (2012a). The evolving dynamic response of a four storey reinforced concrete structure during construction. *Shock and Vibration*, 19(5), 1051-1059.
- Devin, A., & Fanning, P. (2012b). Impact of nonstructural components on modal response and structural damping. *Topics on the Dynamics of Civil Structures, Volume (1)*, (pp. 415-421). Springer.
- Devin, A., Fanning, P., & Pavic, A. (2015). Modelling effect of non-structural partitions on floor modal properties. *Engineering Structures, Volume (91)*, 58-69.

- Dorji, J., & Thambiratnam, D. P. (2009). Modelling and analysis of infilled frame structures under seismic loads. *The open construction and building technology journal*, 3(1), 119-126.
- Doudoumis, I., Mitsopoulou, E., & Charalambakis, N. (1995). *The influence of the friction coefficients on the uniqueness of the solution of the unilateral contact problem*, (pp. 79-86). Springer.
- Durrani, A. J., & Luo, Y. (1994). Seismic retrofit of flat-slab buildings with masonry infills. *Proceedings from the NCEER workshop on seismic response of masonry infills*, (pp. 1-8).
- El-Dakhakhni, W. W., Elgaaly, M., & Hamid, A. A. (2003). Three-strut model for concrete masonry-infilled steel frames. *Journal of Structural Engineering*, 129(2), 177-185.
- Ewins, D. J. (2009). *Modal testing: theory, practice and application* (pp.415-446). John Wiley & Sons (edition 2).
- Farghaly, A. A., & Ahmed, H. H. (2013). Contribution of soil-structure interaction to seismic response of buildings. *KSCE Journal of Civil Engineering*, 17(5), 959-971.
- FEMA 356, (2000). *Prestandard and commentary for the seismic rehabilitation of buildings*: Washington, DC.
- Fiorino, L., Bucciero, B., & Landolfo, R. (2019). Evaluation of seismic dynamic behaviour of drywall partitions, façades and ceilings through shake table testing. *Engineering Structures, Volume* (180), 103-123.
- Gilles, D., & McClure, G. (2008). Development of a period database for buildings in Montreal using ambient vibrations. *Proceedings of the 14th world conference on earthquake engineering*. Beijing, China.
- Gilles, D., & McClure, G. (2012). Measured natural periods of concrete shear wall buildings: insights for the design of Canadian buildings. *Canadian Journal of Civil Engineering*, 39(8), 867-877.
- Holmes, M. (1961). Steel frames with brickwork and concrete infilling. *proceedings of the Institution of civil Engineers*, 19(4), 473-478.
- Kechidi, S., & Bourahla, N. (2014). Effective use of ambient vibration measurement for modal updating. *Proceedings of the 1st National Meeting of Civil Engineering*, Bejaia, Algeria (pp. 22-23).

- Kim, Y.-M., & You, K.-P. (2002). Dynamic responses of a tapered tall building to wind loads. *Journal of wind engineering and industrial aerodynamics, Volume (90)*, (12-15), 1771-1782.
- Lefebvre, K. (2012). Étude du comportement sous charges latérales des ossatures de béton armé avec murs de remplissage de maçonnerie, construites avant les années 1960 (PhD thesis, École de technologie supérieure).
- Li, B., Duffield, C. F., & Hutchinson, G. L. (2009). The influence of non-structural components on the serviceability performance of high-rise buildings. *Australian Journal of Structural Engineering*, 10(1), 53-62.
- Li, B., Hutchinson, G. L., & Duffield, C. F. (2010). Contribution of typical non-structural components to the performance of high-rise buildings based on field reconnaissance. *Journal of Building Appraisal*, 6(2), 129-151.
- Li, B., Hutchinson, G. L., & Duffield, C. F. (2011). The influence of non-structural components on tall building stiffness. *The Structural Design of Tall and Special Buildings*, 20(7), 853-870.
- MatLab, P. (2020). 9.9. 0.1495850 (R2020b). The MathWorks Inc.: Natick, MA, USA.
- Memari, A. M., Shirazi, A., Kremer, P. A., & Behr, R. A. (2011). Development of finite-element modeling approach for lateral load analysis of dry-glazed curtain walls. *Journal of architectural engineering*, 17(1), 24-33.
- Middleton, C., & Pavic, A. (2013). The dynamic stiffening effects of non-structural partitions in building floors. *Topics in Dynamics of Civil Structures, Volume 4* (pp. 513-519). Springer.
- Negro, P., & Verzeletti, G. (1996). Effect of infills on the global behaviour of R/C frames: energy considerations from pseudodynamic tests. *Earthquake engineering & structural dynamics*, 25(8), 753-773.
- NRC. (2015). *National Building Code of Canada 2015*. National Research Council of Canada, Ottawa, Ontario.
- NRCC. (2017). Structural Commentaries (User's Guide–NBC 2015: Part 4 of Division B.
- Orumiyehi, A., Kohrangi, M., & Bazzurro, P. (2017). Seismic Performance of 3-D Infilled and Bare Frame RC Building Models using Average Spectral Acceleration. *Procedia engineering, Volume (199)*, 3558-3563.
- Peeters, B. (2000). System identification and damage detection in civil engineering (PhD thesis, KU Leuven university).

- Perrone, D., & Filiatrault, A. (2018). Seismic demand on non-structural elements: Influence of masonry infills on floor response spectra. 16th European Conference on Earthquake Engineering, Thessaloniki, Greece.
- Petrone, C., Magliulo, G., & Manfredi, G. (2015). Seismic demand on light acceleration-sensitive nonstructural components in European reinforced concrete buildings. *Earthquake engineering & structural dynamics*, 44(8), 1203-1217.
- Polyakov, S. (1960). On the interaction between masonry filler walls and enclosing frame when loaded in the plane of the wall. *Translations in earthquake engineering*, 2(3), 36-42.
- Qu, B., Goel, R., & Chadwell, C. (2014). Evaluation of ASCE/SEI 7 provisions for determination of seismic demands on nonstructural components. 10th US National Conference on Earthquake Engineering. Anchorage, Alaska.
- Shirazi, A. (2005). Development of a seismic vulnerability evaluation procedure for architectural glass curtain walls. (PhD thesis, The Pennsylvania State University).
- Singh, M., Moreschi, L., Suarez, L., & Matheu, E. (2006). Seismic design forces. I: Rigid nonstructural components. *Journal of Structural Engineering*, 132(10), 1524-1532.
- Smith, B. S. (1967). Methods for predicting the lateral stiffness and strength of multi-storey infilled frames. *Building Science*, 2(3), 247-257.
- Sofi, M., Lumantarna, E., Duffield, C., & Mendis, P. (2017). Effects of Interior Partition Walls on Natural Period of High-Rise Buildings. *International Journal of Structural Stability and Dynamics*, 17(06), 1771006.
- Stewart, J. P., Seed, R. B., & Fenves, G. L. (1999). Seismic soil-structure interaction in buildings. II: Empirical findings. *Journal of Geotechnical and Geoenvironmental Engineering*, 125(1), 38-48.
- Su, R., Chandler, A. M., Sheikh, M. N., & Lam, N. (2005). Influence of non-structural components on lateral stiffness of tall buildings. *The Structural Design of Tall and Special Buildings*, 14(2), 143-164.
- Surana, M., Singh, Y., & Lang, D. H. (2017). Effect of Response Reduction Factor on Peak Floor Acceleration Demand in Mid-Rise RC Buildings. *Journal of The Institution of Engineers (India): Series A*, 98(1), 53-65.
- Taghavi, S., & Miranda, E. (2005). Approximate floor acceleration demands in multistory buildings. II: Applications. *Journal of Structural Engineering*, 131(2), 212-220.

- Tamura, Y. (2006). Damping in buildings. Tokyo Polytechnic University, The 21st Century Center of Excellence Program, Lecture, 10.
- Tischer, H. (2012). Rapid seismic vulnerability assessment of school buildings in Québec. (PhD thesis, McGill University).
- Tremblay, R., Atkinson, G. M., Bouaanani, N., Daneshvar, P., Léger, P., & Koboevic, S. (2015). Selection and scaling of ground motion time histories for seismic analysis using NBCC 2015. 11th Canadian Conference on Earthquake Engineering (11CCEE), Victoria, BC, Canada (Vol. 99060).